Department of Electrical and Computer Engineering

Reliability Improvement of Autonomous Microgrids through Interconnection and Storage

Megha Goyal

This thesis is presented for the Degree of
Doctor of Philosophy
of
Curtin University

January 2016

Dedicated to the lotus feet of

'Sai'

ABSTRACT

A microgrid may contain a large number of distributed generators (DGs) and loads. These DGs can be inertial or non-inertial, dispatchable or non- dispatchable. The combination of these various types of DGs makes the microgrid control a challenging task, especially when the microgrid operates in an autonomous (islanded) mode. The response rates of inertial DGs are slower than non-inertial DGs due to their inertia, which can cause large transients in the system. A pseudo inertia concept is introduced for non-inertial DGs (converter interfaced DG) in order to match their response rate with inertial DGs which facilitates stable operation of the microgrid.

Moreover, some of the non-dispatchable DGs can come online or go offline in plug and play fashion. A new algorithm is designed for synchronization of DGs to integrate them smoothly with an islanded microgrid which operates in a frequency droop. In this algorithm, no explicit frequency measurement is required – it relies only on the measurement of instantaneous PCC bus voltage.

To improve reliability of an islanded microgrid, it must be equipped with some distributed storage units that can quickly come online when peak load exceeds the total generation of DGs. Battery energy storage systems (BESSs) are considered in this thesis, which must operate in a fashion such that only the amount of overload power is supplied. When there are several BESSs distributed throughout a microgrid, they must supply power according to their present rating (state of charge). An algorithm based on the modification of angle droop control is proposed to facilitate this even when a microgrid contains rotary generators and operates in frequency droop.

A distribution static compensator (DSTATCOM) can be used in a microgrid for power quality improvement. However the DSTATCOM must operate at the microgrid frequency. A modification of the frequency droop control is proposed to include an isochronous controller such that the microgrid frequency can be brought back to 50 Hz despite any change in load or generation.

Two microgrids that are in close proximity can be interconnected for mutual support during any contingency. To maintain the integrity of the operation of these two microgrids, they must be connected by an interlinking back to back converter

system. An overall power flow control algorithm is developed for the interconnection of two microgrids which operates under different droop control regimes.

A cluster of microgrids can be interconnected through common ac feeder, which is termed in this thesis as a power exchange highway (PEH). In this connection, a microgrid can get support during any sudden power shortfall. Each microgrid in such a cluster must be connected through an interlinking converter to the power exchange highway such that each microgrid can operate independent of all other microgrids. A double layered droop control algorithm is proposed for a cluster of microgrids such that it can prevent a collapse in any of the microgrids in the cluster due to the lack of available generation.

All the proposed methods are verified through extensive digital computer simulation using PSCAD software.

ACKNOWLEDGEMENT

With a deep sense of gratitude, I acknowledge the invaluable guidance received from my thesis advisor Prof. Arindam Ghosh. I am deeply grateful for his inspiration, supervision, constant encouragement and active participation in carrying out this work. It was a great honour for me to pursue my research under his supervision.

I would like to thank Australia for giving me the opportunity of doctoral research here. I thank Queensland University of Technology, Curtin University and Australia Research Council (ARC) for the financial support.

I thank all my friends Nimsiri, Yuthika, Elayarajah, Emma, Florian, Dilruksi, Sumit, Lakmali, Lakini, Sree, Rishu, Priyanka, Shaini and many others who made my stay in Australia. My brother Sachin gave me a warm welcome to Australia and without his presence, this PhD would not have started.

With many other staff in QUT and Curtin, I would like to thank our HDR (High degree by research) office (Elaine, Robyn, Mark and their team) for all support and help.

Achievements in life do not come alone by one's own efforts but by the blessings of God, parents and siblings (Leena, Sachin). I express my deep sense of reverence and profound gratitude to my parents and my family members for the pains and sufferings they have undergone to bring me up to this stage. I acknowledge with utmost warmth their sacrifice, patience, guidance, unconditional support and love.

CONTENTS

LIST OF FIGURES

LIST OF TABLES

KEYWORDS

Microgrid

Microgrids Cluster

Distributed Generators

Frequency Droop

Voltage Droop

Angle Droop

Dynamic Droop

Microturbine

Diesel Generator

Voltage Source Converter

Battery Energy Storage System

State of Charge

Distribution Static Compensator

Wind Energy Conversion System

PV Array

Back to Back Converter

Synchronization

ABBREVIATIONS

AVR	Automatic voltage regulator
BESS	Battery energy storage system
BTB	Back to Back
DER	Distributed energy resource
DFIG	Double fed induction generator
DLQR	Discrete time linear quadratic regulator
DG	Distributed generator
DGEN	Diesel generator
DSTATCOM	Distribution static compensator
DSU	Distributed storage unit
ESS	Electrical energy storage
IC	Internal combustion
IGBT	Insulated gate bipolar transistor
KE	Kinetic energy
MPPT	Maximum power point tracking
NI	Non inertial
OPC	Optimal power control
OTC	Optimal torque control
PCC	Point of common coupling
PEC	Power exchange converter
PEH	Power exchange highway
PMSG	Permanent magnet synchronous generator
PV	Photovoltaic solar cells
SiC	Silicon carbide
SG	Synchronous generator
SOC	State of charge
UPS	Uninterruptible power supply
VSC	Voltage source converter
WECS	Wind energy conversion system
ZOH	Zero order hold

LIST OF SYMBOLS

P_i , Q_i	Real, reactive power supplied by i^{th} DG respectively
P_L , Q_L	Real, reactive power of the load respectively
ω_g	Mechanical rotational speed
ω_e	Electrical speed
T_m	Mechanical torque
T_e	Electromagnetic torque
J_{rl}	Combined inertia of load and rotor
B	Combined viscous friction of load and rotor
F_L	Fuel rate
P_m	Mechanical power
$\dot{m}_a$	Fuel mass flow rate
P_{eg}	Electrical power generated by PMSG
R_f	Transformer and converter losses
L_f	Filter inductance
C_f	Filter capacitance
L_i	Output inductance of the i^{th} converter
m_{ai}	Angle droop coefficient of i^{th} DG
n_{ai}	Voltage droop coefficient of i^{th} DG
P_i^*	Real rated power of i^{th} DG
Q_i^*	Reactive rated power of i^{th} DG
δ_{gi}^*	Rated voltage angle of i^{th} DG
V_{gri}	Rated voltage magnitude of i^{th} DG
δ_{gi}	Actual voltage angle of i^{th} DG
V_{gi}	Actual voltage magnitude of i^{th} DG
ω	Operating frequency
m_f	Frequency droop coefficient
f_d	Frequency deviation limit
ω^*, ω_r	Rated frequency of the system
n_f	Voltage droop coefficient
H	Inertia constant
K_D	Damping ratio

ω_{DG}	DG frequency output from swing
δ	Angle of DG output voltage
ρ	Air density
A	Cross-sectional area
C_P	Power coefficient of the blade
λ	Tip speed ratio
v_m	Mean wind speed
v_w	Wind speed
k	Ramp speed of wind
R_{f1} , R_{f2}	Line resistances
L_{f1} , L_{f2}	Line reactances
V_{dc}	Actual DC capacitor voltage
V_{dcref}	DC capacitor reference voltage
V_m	Magnitude of PCC voltage
$\mathbf{v}_{m0}$	Zero sequence component of the instantaneous voltages
$\mathbf{v}_{m1}$	Positive sequence component of the instantaneous voltages
$\mathbf{v}_{m2}$	Negative sequence component of the instantaneous voltages
P_{MPPT}	Maximum available power from PV
f_m	Minimum frequency limit of the system
P_b^*	Rated power of the BESS
P_b	Power injected from BESS
f_{th}	Frequency threshold
P_{DGENi}	Power supplied by i^{th} diesel generator
P_{dstat}	Power supplied by DSTATCOM
P_{ov}	Overload power
P_{surpAi}	Surplus power of i^{th} DG of MG-A
P_{surpBi}	Surplus power of i^{th} DG of MG-B
P_{surpA}	Surplus power of MG-A
Trg_{ovA}	Trigger signal of overload in MG-A
Trg_{ovB}	Trigger signal of overload in MG-B
m_H	Dynamic droop coefficient
f_H	Power exchange highway frequency
f_{Hmax}	Maximum frequency limit of dynamic droop

f_{Hmin}	Minimum frequency limit of dynamic droop
P_H^*	Reference real power of dynamic droop in PEH
P_H	Actual real power in PEH
P_M^*	Total generation capacity of microgrid
f_{Hd}	Dynamic droop frequency deviation limit
P_{ee}	Surplus power of a microgrid
T_{rg}	Triggering signal
i_f	Filter inductor current
i_{fHPF}	High frequency components of i_f
u_c	Converter switching signal
h	Hysteresis band
v_{tri}	Triangular carrier waveform

CHAPTER 1

INTRODUCTION

A microgrid is a small grid consisting of loads and small generators distributed along its feeders. Small size, cheaper and efficient new generation technologies interconnected to distribution systems form a microgrid. The growing pressure, primarily driven by environmental concern, for generating more electricity from renewable and improving energy efficiency have promoted applications of the distributed energy resources (DERs), which include both distributed generators (DGs) and storage, in the energy system [1-3]. A microgrid can be connected to grid or can be electrically isolated from the power grid, similar to physical islands [4-5].

For islanded mode of operation, control of real and reactive power is essential to maintain a stable operation and total load demand plus losses should not exceed the combined available power of all DG units [6]. The voltage and frequency should also be controlled to remain within specified limits. Table 1.1 lists various advantages of microgrid.

Table 1.1. Advantages of microgrid [7].

Value Proposition	Description
Reduced Cost	Reducing the cost of energy and managing price volatility
Reliability	Improving reliability and power quality
Security	Increasing the resiliency and security of the power delivery system by promoting the dispersal of power resources
Green Power	Helping to manage the intermittency of renewable and promoting the deployment and integration of energy-efficient and environmentally friendly technologies
Power System	Assisting in optimizing the power delivery system, including the provision of services
Service Differentiation	Providing different levels of service quality and value to customer segments at different price points

Different types of energy sources like variable frequency sources (wind), high frequency sources (microturbine) and direct energy conversion sources producing dc voltage (PV) can affect the operation of a microgrid differently due to their different

characteristics. Thus power management and fast, flexible power flow control strategies are requisite for islanded microgrid operation where no infinite source is available in the presence of different types small DG units [8]. The real and reactive power output of a DG can be independently controlled by changing the voltage angle (based on frequency) and the magnitude respectively [9-12]. Therefore, frequency and voltage droop controls are the most common methods used to share the real and reactive load power in a microgrid.

DGs in a microgrid can be classified as either inertial or non-inertial. A diesel generator and a doubly fed induction generator (DFIG) are inertial sources while other sources like solar PV, microturbine, fuel cell and batteries are non-inertial sources. In addition, there are inertial loads, like induction motors, and non-inertial passive loads. Usually each of the non-inertial sources is connected to the system through a three phase converter. Thus they can respond very quickly to changes in real and reactive power demands. However the synchronous generator response will be slower due to its rotating mass and internal combustion engine.

A microturbine is emerging as a very promising technology for short term distributed power production option, even though they are not necessarily driven by renewable fuels. It can be used by industry and major commercial user to reduce cost and also can be connected to critical loads like hospitals, data processing centers etc., to provide high quality emergency power. Since a microturbine generates high frequency ac signal, it must be converted to a 50 Hz signal through power electronic converters [13].

Furthermore, solar PVs and wind turbines (DFIG) need to operate in maximum power point tracking mode to extract the maximum available power from these sources. These are called non-dispatchable energy sources. Since they are already supplying the maximum available power, any deficit in power demand need to be supplied by the sources (microturbine, batteries, diesel generator) in which the output power can be controlled up to a maximum limit. These are called dispatchable sources. The dispatchable DGs need to control the frequency and voltage of the system, while supplying the balance amount of the load power as per their ratings in a droop control mode [14]. In an islanded microgrid (also called autonomous microgrid), the droop

control algorithms facilitate power sharing based only on local measurements without using any communication channel.

The main aims of a microgrid controller are [15]:

- Voltage and frequency control in both operating modes (grid connected and islanded mode)
- Proper load sharing between DGs
- Maintaining steady state and transient stability

1.1. DROOP CONTROL

The droop control is used for real and reactive power sharing amongst the DGs such that each DG supplies power in proportion to its rated value. There are several methods discussed in the literature [16-25]. Some of these are discussed below.

1.1.1. CONVENTIONAL FREQUENCY DROOP CONTROL

In a conventional frequency droop control method, each DG uses its real power output to set the frequency at its point of connection. The conventional frequency droop characteristic is given as

$$f = f_r + m \times (P_r - P) \tag{1.1}$$

where f and f_r are the instantaneous and rated frequency of the system respectively and P_r and P are the rated and measured real power respectively. The droop coefficient is denoted by m.

The reactive power is shared in proportion to voltage magnitude as

$$V = V_r + n \times (Q_r - Q) \tag{1.2}$$

where V and V_r are the instantaneous and rated voltage respectively. Q_r and Q are the rated and measured actual reactive power respectively. n is the voltage droop coefficient.

This method is more reliable because of no communication is required in the system. However, the droop coefficients should be selected appropriately due to their impact on the system stability [26]. The power sharing may be affected in low voltage distribution lines which are highly resistive [27]. Furthermore, the conventional

method has some drawbacks such as frequency and amplitude deviation and slow transient response.

1.1.2. ANGLE DROOP CONTROL

In angle droop control strategy, the active power is shared based on voltage angle as per [28]

$$\delta = \delta^* - m \times (P^* - P) \tag{1.3}$$

where δ^* is the rated voltage angle of each DG. The reactive power is shared in the same manner as given in (1.2). This method is suitable when all the DGs are converter interfaced. The advantage of this method is that proper load sharing can be achieved without significant steady-state frequency variation in the system [29]. Moreover, no communication is required amongst DGs. However the main drawback of this method is that accurate power sharing depends on the output inductance of the DGs.

1.1.3. INTEGRAL TO DROOP LINE

This method is the modified form of the conventional droop control strategy. When both inertial and non-inertial (NI) DGs are present in the microgrid, the steady state power sharing is not a problem. However during transients, the system might become unstable since non-inertial DGs, connected through converters, can have a significantly faster response than inertial DGs. To improve the dynamic power sharing in the presence of both inertial and non-inertial DGs integral droop line concept is introduced in [30]. In this method, time constant of the integrator is chosen according to the inertial DG dynamics and angle of DGs are calculated from the droop frequency. In this case the transient oscillation can be high, since angle is calculated from the droop frequency and measured frequency of the system.

1.1.4. DROOP CONTROL IN LOW VOLTAGE GRIDS

Conventional droop works well under the assumption that line impedance is mainly inductive and inverter output impedance is inductive. However, in low-voltage application, the line impedance can be predominantly resistive, where the reactive power depends on the phase shift (Q-δ) and active power depends on the voltage (P-V) [31-33]. Thus improved droop controllers are proposed to achieve accurate

proportional load sharing [34-35]. These strategies are robust against numerical error, disturbance, noises, feeder impedance and parameter drift.

1.2. INTEGRATION OF NON-DISPATCHABLE DG

The most common way to supply electricity to remote customers is with diesel generators [36]. However, power generation based on diesel fuel can be offset by wind energy. Wind resource is the most promising energy choice due to its enormous availability. The development of new technologies for renewable sources offers attractive economic and environmental merits for energy support [37]. In Canada, integration of wind energy in distribution network to meet energy requirement in rural and remote areas is growing rapidly [38]. In Ramea wind-diesel project, a wind generator is integrated with the diesel generators to supply an islanded system [38]. Various designing aspects are reported in [39] for diesel generators operating in conjunction with wind turbine and energy storage. A design methodology and analysis approach for unit sizing of an islanded wind-diesel system is developed in [40].

In [41], integration of doubly-fed induction generator (DFIG) based wind generator within microgrid is introduced. It focuses on variable droop control for DFIG to adjust the output power according to available wind power. The droop coefficients value changes according to available wind power. A case study of Rhodes Island power system is investigated in [42]. It introduces a frequency controller for permanent magnet synchronous generator (PMSG) and DFIG types of wind turbine to regulate frequency in an islanded microgrid. In [43], an isochronous controller is discussed for load sharing in inverter based distributed generation system. In this, the inverter operates at constant set reference frequency regardless of load. The main drawback of this method is that continuous measurement of load power is required.

The frequency regulation in an islanded microgrid using wind system is discussed in [44]. In this, the frequency of the microgrid is maintained constant irrespective of load variation through wind system. The controller regulates power from the wind system according to the load variation in the microgrid. Thus, the wind system is used only to maintain the microgrid frequency constant rather than harnessing the maximum available renewable power to support the load.

The integration of wind and solar power within DC microgrid is investigated in [45]. It discusses about an aggregated model of wind and solar to support the quantification of the operational real scheduling and reserve for day-ahead. An interconnection control strategy is introduced in [46] for grid connected PV and wind. In this case grid frequency is considered constant and sources are integrated at same frequency. However the frequency in an islanded microgrid, which operates in frequency droop control, can deviate within the droop limit according to load requirement.

1.3. RELIABILITY

An islanded microgrid only relies on the local resources to ensure the power balance between generation and load. Reliability of the local load in the microgrid can be improved by smoothly switching between grid connected and islanded mode [47]. The reliability in an islanded microgrid with renewable energy sources [48-49] and the reliability of microgrid in a grid connected mode or an islanded mode with intermittent DGs is evaluated in [50-51]. Islanded microgrid stability relies on the local frequency and voltage control strategies, controllable DGs, battery storage units and local load [52]. The deployment of the storage units may offer additional resources to an islanded microgrid operating under emergency conditions [53].

In islanded mode, Electrical Energy Storage (ESS) can facilitate the seamless transition of power to the customer in case of generation shortage. Various EESs are available for power system operations. Stationary EESs are referred as Distributed Storage Units (DSUs). These can be used either at the time of high emergency power demand or to smooth out intermittent power generation [54].

When customer load demand is high and the generating sources are operating at their maximum capacity, DSUs can be utilized to avoid the use of a more expensive option like spinning reserve. Furthermore, DSUs can provide a level of uninterrupted power to the customers [55]. It also permits distributed generator (DG) units to run at a constant and stable output despite load fluctuations. Thus, it enhances the overall performance of an autonomous microgrid [56].

There are numerous forms of DSUs, such as, fuel cells, battery energy storage units, solar fuel, capacitors, super capacitors, superconducting magnetic energy

storages, thermal energy storage system and compressed air energy storage system. Several types of batteries are available currently. For example, Nickel Metal Hydride (Ni-MH), Nickel-Cadmium (Ni-Cad) or Lithium-Ion batteries have high power density and can be used as DSUs [57].

In microgrid, DGs can be either dispatchable or non-dispatchable. To fulfill the load demand, selection of the size of dispatchable DGs should be in accordance to the peak load demand in islanded microgrids because the non-dispatchable DGs are dependent on weather conditions. However, the peak load can keep on increasing. The dispatchable DGs can share the power according to their rating in presence of non-dispatchable DGs under the assumption that peak load demand is less than the total rating of all the dispatchable DGs. To cater to an ever increasing load demand, resizing of existing DGs or installation of another DG may not be a favourable option. A better strategy is to have some battery energy storage systems (BESSs) to aid the autonomous microgrid operation [58]. These BESSs need not be operational all the time, but should come online quickly when peak load exceeds the total generation of the DGs [59]. In an islanded microgrid, how BESS performs energy balance during quick fluctuation in load demand is explained in [60]. However, main focus of this paper is on configuration of the modular power converter for BESS. In [61], optimized economic operation by load transfer is discussed for grid connected microgrid with BESS to reduce the microgrid operating cost. The centralized control is discussed for optimizing operation of microgrid which consists of various distributed generators, storage devices and controllable loads [62]. A coordinated control is introduced for the micro-resources with solar PV and battery storage to support the voltage and frequency in an islanded microgrid in [63].

1.4. INTERCONNECTION OF MICROGRIDS

An islanded microgrid can be established as an effective solution of the power supply in remote areas. The variety of microgrids is analyzed in [55]. There are remote areas where the cost of bringing power lines is prohibitive. An isolated (islanded) microgrid in these areas is a more attractive option. However, as mentioned before, storage units must be readily available for such microgrids to prevent system collapse. Despite the presence of storage, the load shedding may still be required in remote area

microgrids [64]. The different load shedding techniques are discussed in literature to maintain the system frequency within limit [2, 65].

When two microgrids are available in close proximity, they can be connected together. It is preferable to interconnect them through a back to back (BTB) converter such that each can nominally operate independent of the other. However during an emergency overloading in one microgrid (MG), the other can provide support with its surplus available power [66]. In [67], a hierarchical structural control strategy has been proposed which consist of primary, secondary and tertiary control with economically optimal operation. The advanced control and power management in multi microgrids with coordinated control of distribution system and centralized control of microgrids have been investigated in [68, 69]. A multi-microgrid system composed of several low voltage microgrids, interconnected through medium voltage feeders, is presented in [69]. In this system, a hierarchical control structure is developed in which the frequency and voltage of LV microgrids are controlled using a coordinated control scheme.

In [19], a microgrid is connected with a utility through a back to back converter to facilitate bidirectional power flow. It has been shown, how the microgrid can exchange a pre-specified amount of power with the utility while operating in a droop control. As mentioned in [70], the cost of power electronic components is decreasing between 1-5% every year. Also the power electronic converters volume and weights are reducing progressively. Also with the progress in Silicon-Carbide (SiC) technology, the size of passive filtering components will reduce in the near future, and so will the converter losses. In [71, 72], a two microgrid interconnection in grid connected and islanded mode is introduced where each microgrid operates at a different frequency. If the frequencies are same then these microgrids can be intertied by a breaker or a static switch using appropriate synchronisation technique. However, having different values of the microgrid frequencies are more flexible. Therefore, for intertying these microgrids insertion of back to back converter is required to isolate the microgrids [73]. During the connection of these two microgrids, an interlinking droop scheme is proposed, based on which the real and reactive power are autonomously controlled. However, the operation and control for two microgrids which operate in different control modes are not investigated in the literatures.

A hybrid grid consisting of AC and DC microgrids connected through bidirectional converters, is discussed in [74]. In this paper, coordination control algorithms are used to control the smooth power transfer between ac to dc system. Single phase microgrids interconnection using single phase back to back converter is investigated in [75, 76]. To improve the performance of the multi-microgrids, hierarchical coordination and multi-objective optimal power flow algorithms are discussed in [77-79].

1.5. SMART DISTRIBUTION GRID

Recently the power industry is going through a substantial transformation based on the incorporation of assorted technological innovations [80]. Electricity delivery network is currently modernized using latest digital/information technologies to allow pervasive control and monitoring [81]. It is expected that in future, the smart grid will emerge as a system of organically integrated smart microgrids with pervasive visibility, command and control functions distributed across all levels. The topology of the emerging grid will therefore resemble a hybrid solution [82].

Interconnection of the microgrids has attracted the attention of the researchers in last few years. The interconnection of a number of microgrids can make a distribution system more reliable and efficient. The concept of power exchange in between inter-utilities is introduced in [83]. It discusses about decentralized and coordinated operation of power grid. The power exchange in between inter-utilities is coordinated using heuristic criteria. An optimal power flow technique is used in [84] to calculate the amount of power available for exchange between interconnected utilities. In [85], the clustering concept of distribution units is introduced. It discusses about the multi-level hierarchical control strategy for DGs with cluster concept of the power system. In [86], a decentralized optimal control algorithm is discussed for coordinated multi-microgrids.

1.6. OBJECTIVES OF THE THESIS AND SPECIFIC CONTRIBUTION

Based on the literature review presented in previous sections, some research gaps are identified. These gaps mainly pertain to the operation of microgrids under a mix of generation, the system reliability and power quality. Based on these, the thesis objectives are set, which are presented in the next sub-section.

1.6.1. OBJECTIVE OF THE THESIS

- Stable operation of an islanded microgrid in the presence of inertial and non-inertial, dispatchable and non-dispatchable (plug and play) DGs.
- Development of control strategy for smooth transition of battery energy storage system (BESS) to prevent the overloading in a microgrid.
- Enhancing the power quality in a hybrid microgrid which contains harmonic loads using custom power devices.
- Interconnection scheme of two microgrids, operating in different droop regimes for mutual support during contingency.
- Interconnection of microgrids cluster through a common ac system.

1.6.2. SPECIFIC CONTRIBUTION OF THE THESIS

Based on the above objectives, the specific contributions of this thesis are

1. An improved control strategy is developed for a hybrid microgrid under study where any communication between converters is not required. The response rates of inertial DGs are slower than non-inertial DGs due to their inertia, which can cause large transients in the system. Therefore, a pseudo inertia concept is introduced for non-inertial DGs to match their response rate with inertial DGs.
2. In hybrid microgrid, DGs (dispatchable DGs) may operate in a plug and play fashion. A new algorithm is designed for synchronization of DGs to integrate them smoothly in a microgrid. In this algorithm, no explicit frequency measurement is required – it relies only on the measurement of instantaneous PCC bus voltage.
3. A modification of the frequency droop control is proposed to include an isochronous controller such that the microgrid frequency can be brought back to 50 Hz despite any change in load or generation. This has been utilized for both integration of wind generator and for power quality improvement using a distribution static compensator (DSTATCOM).
4. An autonomous microgrid must be equipped with some distributed storage units that can quickly come online when peak load exceeds the total generation of DGs. A new control strategy is developed for smooth transition of battery energy storage system (BESS) in which it only supplies

the excess amount of power to support the microgrid during contingency. When there are several BESSs distributed throughout a microgrid, they must supply power according to their present rating (SOC). An algorithm based on the modification of angle droop control is proposed for this purpose.

5. Two microgrids that are in close proximity can be interconnected through back to back converter for mutual support during any contingency. An overall power flow control algorithm is developed for the interconnection of two microgrids that are operating under different droop control regimes.
6. A form of smart distribution grid can be visualized as a cluster of microgrids that can be joined together by a common ac feeder, which has been termed as a power exchange highway (PEH) [82]. A double layered droop control algorithm is proposed for a cluster of microgrids such that it can prevent a collapse in any of the microgrids in the cluster due to the lack of available generation.

1.7. THESIS ORGANIZATION

The thesis is organized in eight chapters. The organizations of the rest of the chapters are given below.

In **Chapter 2,** stable operation of a hybrid microgrid, which can consist of inertial and non-inertial DGs, is discussed. The combination of these various sources makes the microgrid control a challenging task in an autonomous (islanded) mode. Since the time response of the non-inertial DG is faster than the inertial DG, it can create a large transient excursion in the system. Therefore, a pseudo inertia concept is introduced in this chapter to make non-inertial DG response rate similar to the inertial DG. Also a modification of the angle droop of [70] is proposed to make this insensitive to the output inductances of the DGs.

Some strategies for connection/disconnection of non-dispatchable DGs in an islanded microgrid, operating in a frequency droop control, are proposed in **Chapter 3**. The DGs must be connected to the microgrid at the same frequency of the microgrid, therefore a simple algorithm of synchronization based on symmetrical component theory is proposed. In this algorithm, only instantaneous bus voltage measurement is required and no frequency measurement is needed.

Alternatively, a microgrid can be forced to operate at 50 Hz even when it is operated under a frequency droop control. A modification of the frequency droop control proposed in this chapter that includes an isochronous controller. Both the synchronization and isochronous control algorithms are demonstrated for both wind and PV integration.

Chapter 4 proposes the control strategies for the BESS to prevent the overloading in an autonomous microgrid. Since non-dispatchable DGs may not be in the system all the time, the dispatchable DGs should cater to the peak load demand. However since the peak load keeps on growing, this also cannot always be assured. Therefore, an islanded microgrid must be equipped with storage units that can quickly come online during any contingency.

Three different BESS interconnection strategies are proposed in this chapter. In the first one, a BESS comes online when an overload is detected and supplies its maximum available power. In the second one, the BESSs start operating in the same frequency droop as the rest of the DGs in the microgrid. However, a BESS is expensive and its life time can be shortened by several charge/discharge cycles. Therefore such a unit must come online only when required and must supply only the amount of power that cannot be supplied by DGs in the autonomous microgrid. This is achieved through the modified angle droop control discussed in Chapter 2, which is the third strategy presented in this chapter.

In **Chapter 5**, two different strategies are proposed to operate a DSTATCOM at the same frequency of the microgrid to mitigate harmonics produced by a polluting load. If a microgrid contains a diesel generator, the harmonic current flow through the armature of the synchronous generator will distort the armature reaction and lead to electromagnetic torque pulsation. This will reduce the life time of the generator and may even cause generator failure. To prevent this a DSTATCOM is connected at the PCC of the load bus at which the harmonic load is connected.

Two DSTATCOM operating strategies are proposed in this chapter – one is recovering the microgrid frequency to 50 Hz through the isochronous controller proposed in Chapter 3. The other strategy uses a simple frequency estimation technique and generates the reference for DSTATCOM using this synthesized

frequency. The effect of frequency mismatch on the dc capacitor voltage of the DSTATCOM is also analyzed.

The interconnection of two microgrids that are in close proximity through a back to back converter is discussed in **Chapter 6**. An overall power flow control algorithm is developed for the interconnection of two microgrids that are operating under different droop control regimes. The interconnection of microgrids which operate in different droop control modes is a challenging task. A step by step algorithm is developed for overload power calculation, surplus power calculation, based on which the power flow control scheme for the interlinking converters is developed.

Chapter 7 proposes a new topology of the interconnection of a number of microgrids. The microgrids are interconnected through a common ac bus which is termed as power exchange highway (PEH). The microgrids are connected to the PEH through back to back converters which are termed as power exchange converters because their main purpose is to control the power flow between the PEH and the microgrid. A double layered droop control is proposed in which all the microgrids operate in the inner layer frequency droop control. The outer layer consists of a dynamic droop control that regulates the power flow through the PEH. The microgrids can support to other microgrid depending on their available surplus power. Therefore, the dynamic droop control gains are calculated from their respective available surplus power. The selection of the droop gains have an important role for this power flow control scheme.

The general conclusion and scope for the future works are given in **Chapter 8**. **Appendix A** discusses the converter structures and control methods and **Appendix B** discusses the frequency estimation technique used in this thesis.

CHAPTER 2

POWER SHARING CONTROL IN HYBRID MICROGRID

Dynamic responses of inertial and non-inertial DGs in a microgrid are different. The inertial DGs show a slower response, while non-inertial (NI) DGs can respond very quickly. This mismatch of response rate in different types of DGs creates transient oscillations in an autonomous microgrid where no strong source is present to control the system frequency and voltage. In this chapter, we shall analyze the behavior of an autonomous hybrid microgrid that contains both inertial and non-inertial DGs. In this thesis, the term hybrid microgrid will be used for those systems which have both inertial and non-inertial DGs. These DGs can also be either dispatchable or non-dispatchable.

A new control algorithm for a converter interfaced DG is proposed which facilitates smooth operation in hybrid microgrid. In order to achieve this, the converter response speed is matched to be of the same order as that of an inertial DG. To investigate the system response with the dynamics of the DG units, the sources and all power electronics converters are modelled in detail. Furthermore, effective control strategies for power sharing in a microgrid according to available DGs are also discussed.

2.1. SYSTEM STRUCTURE

For simplicity, the microgrid structure under consideration is comprised of two DGs, one of them is inertial DG (Diesel Generator) and other one is converter interfaced DG (Microturbine), as shown in Fig. 2.1. The DGs supply a balanced load and share it in proportion to their respective ratings. The converter interfaced DG_1 (MT) is operated in voltage control mode, which is connected to a permanent magnet synchronous generator (PMSG). The PMSG rotates at high speed 96,000 rpm and hence generates voltage at 1600 Hz. Therefore, the output of the PMSG is converted into dc and then converted into fixed frequency ac output through the voltage source converters [87]. The converter interfaced DG can also be a UPS. DG_2 is an inertial diesel generator, driven by an IC engine [88]. The real and reactive powers supplied

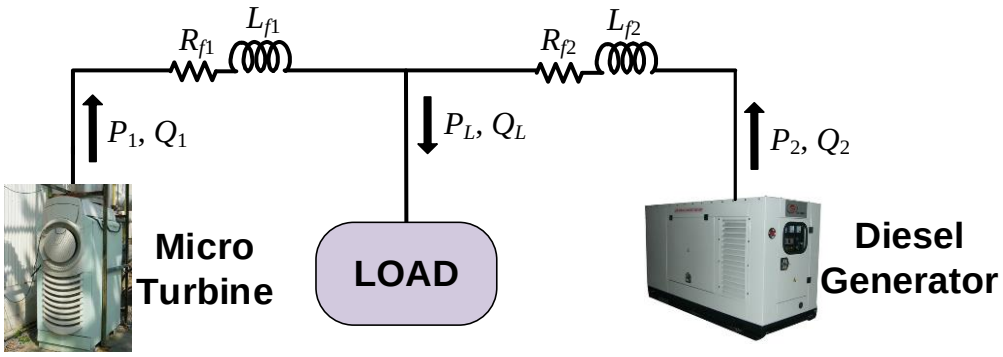

Fig. 2.1. Microgrid structure under consideration.

by DG$_i$ are denoted by P_i and Q_i respectively. The real and reactive power demands of load are denoted by P_L and Q_L. Detailed model of the DGs are discussed below.

2.2. DIESEL GENERATOR

The diesel generator set consists of a 4-stroke internal combustion (IC) engine coupled to a synchronous generator. The schematic diagram of the generator set is shown in Fig. 2.2. The IC engine is integrated with a governor for controlling the output speed of the engine shaft by adjusting the amount of fuel supplied to the engine. There is a dead time associated with the change of fuel supply to change in output torque of the IC engine due to its inertia. The governor is controlled by using a PID controller to maintain a reference set speed. The synchronous generator is incorporated with an excitation system, which is combination of an exciter and a automatic voltage regulator (AVR). The voltage regulator controls the field supply of the generator to maintain the required terminal voltage. The automatic voltage regulator contains a stabilizing feedback loop. The each component of the generator set is described below.

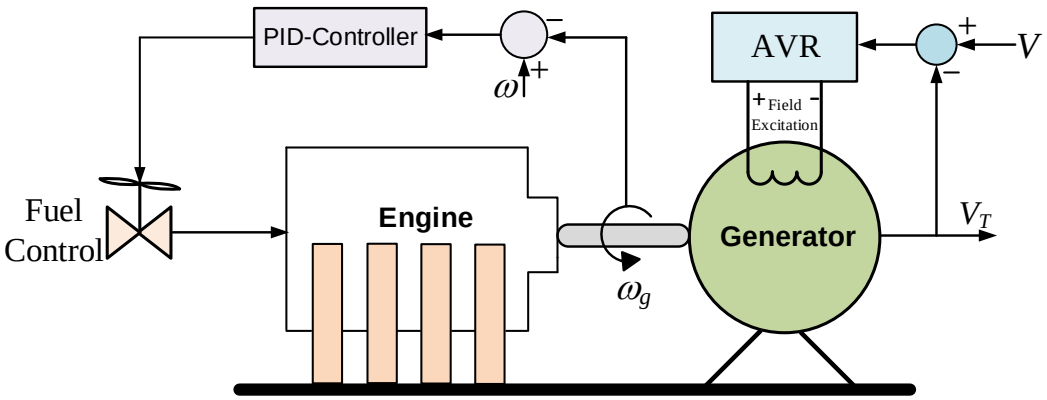

Fig. 2.2. Schematic diagram of diesel generator set.

2.2.1. SYNCHRONOUS GENERATOR

The synchronous generator (SG) converts mechanical energy supplied by the prime mover to electrical energy [89]. It is the most popular form of energy generator. The mechanical rotational speed (ω_g) of the generator is proportional to its electrical speed (ω_e) as

$$\omega_g = \frac{\omega_e}{n_p} \tag{2.1}$$

where, n_p is the number of pole pair in the SG.

The PSCAD model of the synchronous generator is used for the diesel generator modelling [90]. The model along with dynamic calculation [91], calculates the torque using dynamic equation as

$$\frac{d}{dt}\omega_m = \frac{1}{J_{rl}}(T_m - T_e - B\omega_m) \tag{2.2}$$

where, J_{rl}, B are the combined inertia and viscous friction of load and rotor respectively, T_e is the electromagnetic torque, T_m is the mechanical input torque for the generator. The dynamic parameters of 500 kVA rated generator is listed in

Table. 2.1. The parameters of SG are normalised as described in [91]. The rated power and the voltage of SG are considered as the base values for the calculation of per unit values.

2.2.2. EXCITER

The excitation system controls the output voltage of the generator [92]. Depending on the excitation power source, distinctive type of excitation system can be identified as follows [93]:

a) Type DC excitation systems: In this type of excitation system, DC generator with a commutator is utilized.
b) Type AC excitation systems: In this type of excitation system, alternator with either stationary or rotating rectifiers is utilized.

Type ST excitation systems: In this type of excitation system, power is supplied through transformer with rectifier.

Table. 2.1. Diesel generator set data.

System data	**Value**
Rated voltage	11 kV
Rated current	0.02624 kA
Rated frequency	50 Hz
Rated speed	1500 rpm
Reactance	Value (pu)
X_d: Unsaturated *d* axis synchronous reactance	0.116
X'_d: Unsaturated *d* axis transient synchronous reactance	7.4×10^{-3}
X''_d: Unsaturated *d* axis subtransient synchronous	2.94×10^{-3}
X_q: Unsaturated *q* axis synchronous reactance	6.37×10^{-3}
X''_q: Unsaturated *q* axis subtransient synchronous reactance	5.24×10^{-3}
X_2: Negative-sequence reactance	0.044
X_0: Zero-sequence reactance	2.45×10^{-3}
Time constants	**Value (ms)**
t''_{do}: *d* axis subtransient open circuit time constant	25
t''_{qo}: *q* axis subtransient open circuit time constant	4
t'_{d0}: *d* axis transient open circuit time constant	368
t_a: Armature time constant	25

For considered diesel generator set, the exciter system is chosen type AC. The transfer function model of Type AC2A is presented in Fig. 2.3., which is a high initial response field controlled alternator-rectifier excitation system. This type of excitation system is available in PSCAD library. The typical parameters of the system are given in Table. 2.2.

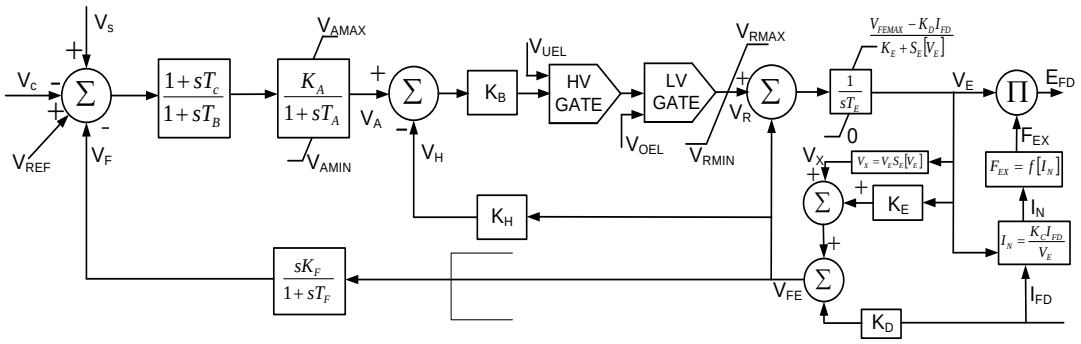

Fig. 2.3. Type AC2A- transfer function model [94].

Table. 2.2. Excitation system model parameters.

Parameters	**Values**
Voltage regulator gain K_A	400 (pu)
Voltage regulator time constants T_A, T_B, T_C	0.01, 0, 0 (s)
Second stage regulator gain K_B	25 (pu)
Exciter field current feedback gain K_H	1 (pu)
Max & Min regulator output limits V_{RMAX}, V_{RMIN}	105, -95 (pu)
Exciter time constant T_E	0.60 (s)
Exciter constant related to field K_E	1 (pu)
Demagnitizing factor K_D	0.35 (pu)
Excitation control system stabilizer gain K_F	0.03 (pu)
Rectifier loading factor proportional to commutation reactance K_C	0.28 (pu)
Rate feedback time constant T_F	1 (s)

2.2.3. GOVERNOR

The essential device which controls the speed or output power of the engine or the turbine is called a governor. The governor regulates the speed of the IC engine by changing the fuel rates. The governor is controlled by a PID controller to maintain a reference set speed. The PID controller is responsible for the control of the system frequency [94]. The considered PID controller for diesel generator set is presented in Fig. 2.4, where input is speed error (between the actual speed of the generator (ω_g) and the desired speed (ω)). The output of the controller is the fuel rate (F_L) of the IC engine. The parameters of the controller are listed in Table. 2.3. The Internal Combustion (IC) engine model is available in PSCAD library. It takes fuel rate and generator speed as the inputs and supplies mechanical torque as an output. The parameters of the IC engine are given in Table. 2.4.

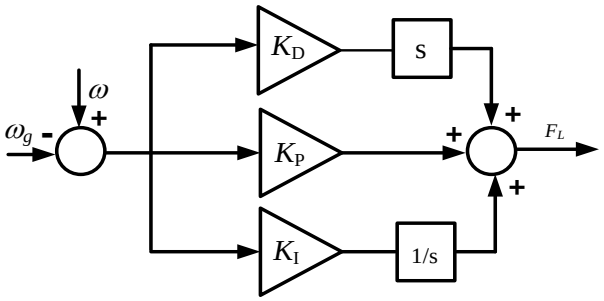

Fig. 2.4. PID speed controller.

Table. 2.3. PID controller parameters.

Parameters	**Values**
K_p	5000
K_I	1000
K_D	200

Table. 2.4. Internal Combustion Engine parameters.

Parameters	**Values**
Engine rating	500 kW
Machine rating	500 MVA
Engine rated speed	1500 rev/min
Number of engine cylinders	12
Number of engine cycles	4

2.3. MICROTURBINE (MT)

The schematic diagram of the MT system is shown in Fig. 2.5. It consists of a gas turbine that produces rotating mechanical power P_m through the fuel mass flow rate $\dot{m}_a$, which is then converted into an electrical power P_{eg} by a permanent magnet synchronous generator (PMSG) [95-99]. The thermodynamic model of the turbine [100] is shown in Fig. 2.6. The typical parameters are given in Table. 2.5. The mass flow rate, input of the turbine is regulated through a PI controller to maintain the desired speed of the generator. The MT usually has one pole pair and rotates at a very high speed. The speed is chosen as 96000 rpm. This means that the PMSG generates power at 1600 Hz. A rectifier-converter stage is used to convert this high frequency power into an electrical power at 50 Hz. VSC-1 controls the power flow from the PMSG and operates at the same frequency of the PMSG. VSC-2 holds the voltage across the dc link capacitor constant.

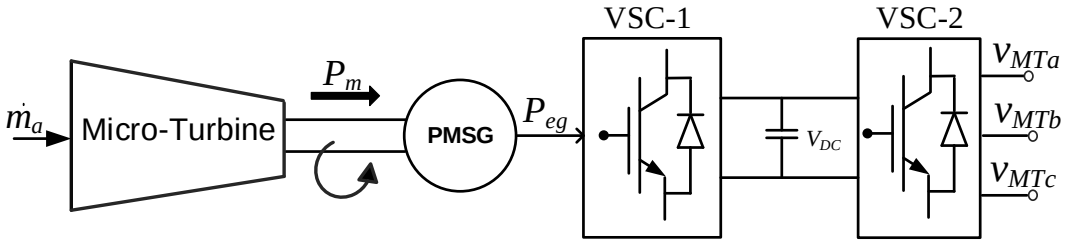

Fig. 2.5. Schematic diagram of microturbine.

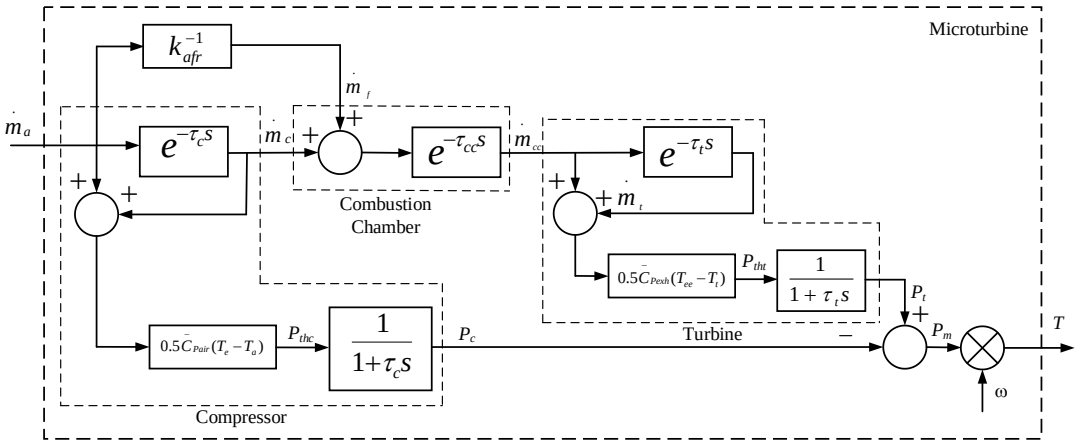

Fig. 2.6. Microturbine thermodynamic model [97].

Table. 2.5. Microturbine model parameters.

Parameters	**Values**
k_{afr} Intel air to fuel ratio	93.1
$\bar{C}_{Pair}$ Intel air average specific heat capacity	1157 [J/Kg °C]
$\bar{C}_{Pexh}$ Exhaust gas average specific heat capacity	1321 [J/Kg °C]
T_a Intel air ambient temperature	28.7 [°C]
T_c Compressor outlet temperature	180.9 [°C]
T_{cc} Combustion chamber outlet temperature	893.9 [°C]
T_t Turbine outlet temperature	634.9 [°C]
τ_c Compressor time constant	1.3 [ms]
τ_{cc} Combustion chamber time constant	1.4 [ms]
τ_t Turbine time constant	0.3 [ms]

2.4. VOLTAGE SOURCE CONVERTER (VSC)

In this thesis, two different types of VSCs are used, along with their switching control strategies. These are presented in Appendix A. Depending on the applications, a VSC can have either an LC filter or an LCL (T) filter, as shown in Fig. 2.7. The

filters are denoted by L_f, C_f and L, while the resistance R_f represents the converter and transformer (if any) losses. The switching control law takes the advantage of the voltages and/or currents across the filters.

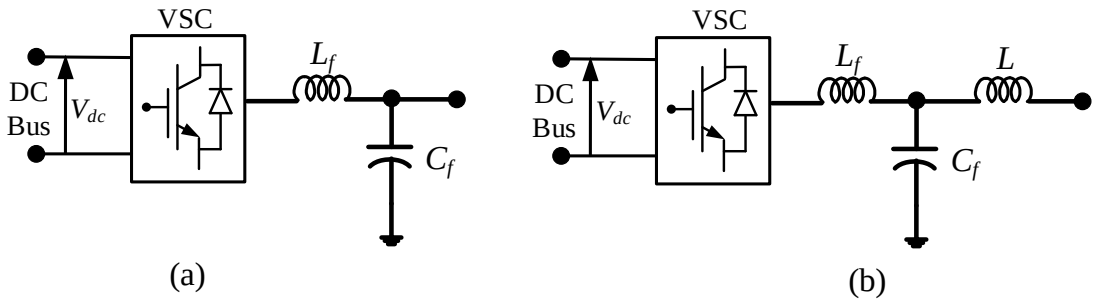

Fig. 2.7. VSC with different filter structures.

2.5. DROOP CONTROL

Proper control of a microgrid is prerequisite for stable and economically efficient operation, in both grid connected and islanded modes [18]. The same control strategy cannot be used in both modes. For grid connected operation, the system frequency and voltage of the microgrid are mainly controlled by the grid. However, in the absence of grid, DGs in the microgrid need to be controlled such that the frequency and voltage in the islanded microgrid are maintained within standard limits. Therefore, droop control is employed for this purpose. This type of control method avoids the need of any communication interface between DGs. The main purpose of ignoring the communication for primary control is to avoid the single point of failure and to increase the reliability of the microgrid [34, 101]. Various droop control methods have been discussed in [24] to control an autonomous microgrid.

Frequency and voltage droop are the most common way of controlling DGs to achieve frequency/voltage control and load power sharing in an islanded microgrid. The angle droop control strategy can also be applied for a microgrid which consists of only converter interfaced DGs [28]. In this chapter, it has been assumed that total power demand in the microgrid can be supplied by the DGs connected to it. This assumption will be relaxed from Chapter 4.

2.5.1. ANGLE DROOP

When a microgrid consists of only converter interfaced DGs, the angle droop control strategy can be applied to control the accurate power sharing amongst DGs.

Let us assume that there are only two DGs supplying a load as shown in Fig. 2.8. Comparing this figure with Fig. 2.7 (b), we have L_1 as the output inductor of the LCL filter. The voltage $V_g \angle \delta_g$ is synthesized across the filter capacitor C_f. In this case, the real and reactive power sharing amongst DGs can be controlled by changing the voltage magnitude and its angle as

$$\begin{aligned} \delta_{gi} &= \delta_{gi}^{*} + m_{ai} \times \left(P_i^{*} - P_i\right) \\ V_{gi} &= V_{gri} + n_{ai} \times \left(Q_i^{*} - Q_i\right) \end{aligned} \tag{2.3}$$

where V_{gr} and δ_g^* are the rated voltage magnitude and angle of each DG and P^*, Q^* are the rated value of real and reactive power respectively. V_g and δ_g are the actual measured value of voltage magnitude and its angle, when the DG supplies reactive power of Q and real power of P. The angle and voltage droop coefficients are m_a and n_a respectively.

The requirement for an angle droop is that all DGs must operate with respect to a single reference angle. If an autonomous microgrid contains only converter interfaced DGs, the reference angle can be set arbitrarily. This is because the actual power flow depends on the relative angle difference and not the actual values of the angles. Since there is no strong source in the system, the bus angle can be easily set by the DGs.

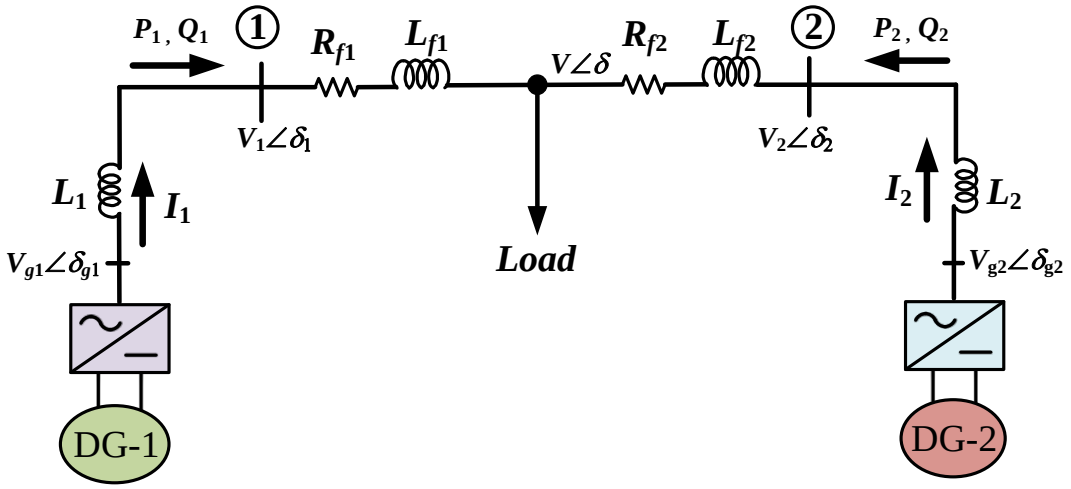

Fig. 2.8. Microgrid structure with converter interfaced DGs only.

In an angle droop control, it has been shown in [19] that the output inductance of the DGs plays a crucial role in power sharing, which is given by

$$\frac{P_1}{P_2} = \frac{X_2 + X_{L2} + m_{a2}}{X_1 + X_{L1} + m_{a1}} \tag{2.4}$$

where $X_1=\omega L_1/(V_{g1}V)$, $X_2 = \omega L_2 / (V_{g2}V)$, $X_{L1} = \omega L_{f1}/(V_{g1}V)$ and $X_{L2} = \omega L_{f2}/(V_{g2}V)$.

The droop coefficients are chosen in such a way that

$$m_{a1} >> X_1 >> X_{L1} \text{ and } m_{a2} >> X_2 >> X_{L2}$$

Therefore from (2.4)

$$\frac{P_1}{P_2} \approx \frac{m_{a2}}{m_{a1}} = \frac{P_1^*}{P_2^*} \tag{2.5}$$

The error in power sharing can be further reduced by taking the output inductance of the DGs inversely proportional to the power ratings of the DGs.

For example, Let us consider the system of Fig. 2.8, where the converter interfaced DGs are connected to a 200 kW load. DG-1 and DG-2 are rated with 200 kW and 100 kW respectively. The system data are given in Table. 2.6. These DGs operate in angle droop control to share the power according to their ratings. In Fig. 2.9, effects of the DGs output inductance on the power sharing is shown. In Fig. 2.9 (a), the output inductances are considered in the reciprocal ratio of the DGs rating, therefore, the power sharing is in the ratio of their ratings. However, in Fig. 2.9 (b), same output inductances are considered for both DGs and it can be seen that power sharing ratio is not equal to 2:1. Hence, it implies that for accurate power sharing amongst DGs, the output inductance of the DGs selection should be inversely proportional to their rating.

Table. 2.6. Parameters of DGs connected in the microgrid (Fig. 2.8).

System Quantities	**Values**
DG_1 Feeder impedance	R_{f1} = 3.025 Ω, L_{f1} = 57.8 mH
DG_2 Feeder impedance	R_{f2} = 3.025 Ω, L_{f2} = 57.8 mH
DG Rated Power	DG-1: 200 kW, DG-2: 100 kW
Output Inductor	$L_1 = L_2$ = 10 mH
Droop Coefficient (Angle–Voltage)	
m_{a1}	2.0 rad/MW
m_{a2}	1.0 rad/MW
n_{a1}	1.0 kV/MVAr
n_{a2}	0.5 kV/MVAr

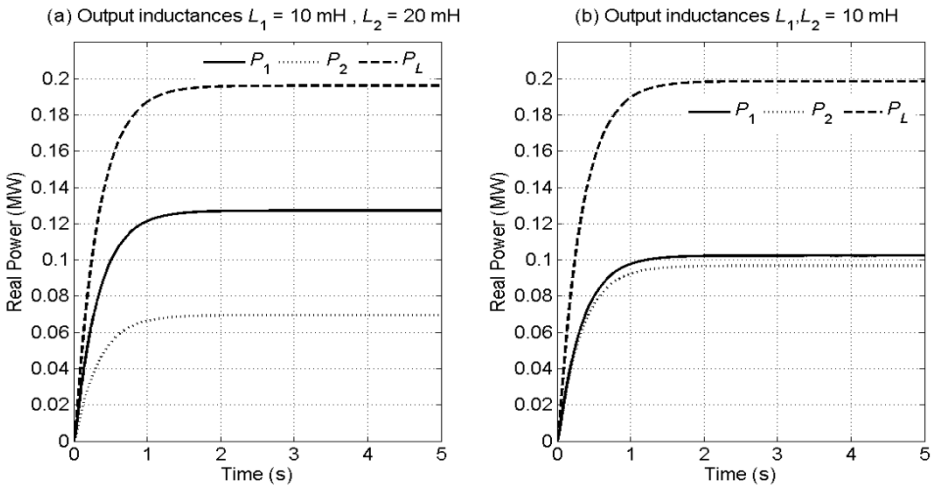

Fig. 2.9. The output inductance effect on power sharing using angle droop control.

Therefore, there are two drawbacks of this scheme. One is that the output inductance of each DG has to be higher than the line impedance. The other is that the inductance must be in reciprocal proportion to the power rating of the DG. In order to overcome these drawbacks, a modified droop control is discussed below.

2.5.2 MODIFIED ANGLE DROOP CONTROL

The main purpose of the modified droop control is to overcome the effect of the output inductance of the DGs on power sharing control. As it is mentioned before angle droop control depends on the output inductance of DGs. Therefore, in modified droop control the angle droop is given with respect to the bus voltages as

$$\delta_i = \delta_i^* + m_{ai} \times \left(P_i^* - P_i \right) \tag{2.6}$$

$$V_i = V_i^* + n_{ai} \times \left(Q_i^* - Q_i \right) \tag{2.7}$$

DC load flow is used as a non-iterative solution to calculate power flow in ac systems. In this, nonlinear ac system model is simplified to a linear form through the following assumptions:

- Line resistances are assumed to be negligible compared to line reactances.
- Bus voltage angle differences are assumed to be small.
- Magnitudes of bus voltages are set as equal to have a flat voltage profile.

Applying DC load flow with all these necessary assumptions [19] we get,

$$\begin{aligned}\delta_1 - \delta &= X_{L1}P_1 \\ \delta_2 - \delta &= X_{L2}P_2\end{aligned} \tag{2.8}$$

$$X_{L1} = \frac{\omega L_{f1}}{VV_1}, \quad X_{L2} = \frac{\omega L_{f2}}{VV_2} \tag{2.9}$$

Let us choose the following

$$m_{a1} \times P_1^* = m_{a2} \times P_2^* \tag{2.10}$$

$$\delta_1^* = \delta_2^* \tag{2.11}$$

Combining (2.6, 2.10 & 2.11), we get

$$\delta_1 - \delta_2 = -m_{a1}P_1 + m_{a2}P_2 \tag{2.12}$$

Also from (2.8) we get

$$\delta_1 - \delta_2 = X_{L1}P_1 - X_{L2}P_2 \tag{2.13}$$

Combining (2.12-2.13), we get

$$\frac{P_1}{P_2} = \frac{X_{L2} + m_{a2}}{X_{L1} + m_{a1}} \tag{2.14}$$

Since,

$$m_{a1} >> X_{L1} \text{ and } m_{a2} >> X_{L2}$$

$$\frac{P_1}{P_2} = \frac{m_{a2}}{m_{a1}} = \frac{P_1^*}{P_2^*} \tag{2.15}$$

Equation (2.15) implies that the droop gains should be in reciprocal to the DG power ratings. In that case, the powers will also be shared in reciprocal to the droop gains, i.e., in accordance with the DG ratings.

Once the angles are calculated from the angle droop and the voltage magnitude is calculated from the voltage droop, the voltage references for the DG output converters need to be calculated. For this, the real and reactive power flow from DG-1 to bus-1 will be considered. In per phase basis, these are given by

$$\frac{P_1}{3} = \frac{V_1 \times V_{g1} \sin\left(\delta_1 - \delta_{g1}\right)}{\omega L_1}$$
$$\frac{Q_1}{3} = \frac{V_1 \times V_{g1} \cos\left(\delta_1 - \delta_{g1}\right) - V_1^2}{\omega L_1} \quad (2.16)$$

From these two expressions, the angle of the DG-1 converter output voltage is calculated as

$$\delta_{g1} = \delta_1 - \tan^{-1}\left(\frac{\omega L_1 P_1}{\omega L_1 Q_1 + 3V_1^2}\right) \quad (2.17)$$

Once δ_{g1} is obtained, the voltage magnitude is calculated from (2.16) as

$$V_{g1} = \frac{P_1 \omega L_1}{3 \times V_1 \sin\left(\delta_1 - \delta_{g1}\right)} \quad (2.18)$$

In a similar way V_{g2} and δ_{g2} can also be calculated. Once, these quantities are calculated then instantaneous three phase reference voltage is obtained as

$$v_{DG1a} = \sqrt{2} V_{g1} \sin\left(\omega t + \delta_{g1}\right)$$
$$v_{DG1b} = \sqrt{2} V_{g1} \sin\left(\omega t + \delta_{g1} - 120°\right) \quad (2.19)$$
$$v_{DG1c} = \sqrt{2} V_{g1} \sin\left(\omega t + \delta_{g1} + 120°\right)$$

The use of (2.16 - 2.19) eliminates the need of precise determination of converter output inductances for power sharing. Equation (2.15) remains valid as long as the line impedance is much smaller than the angle droop gain, which is true when the microgrid spans a small geographical area.

Let us consider now these DGs are operating in modified angle droop to share power according to their ratings. The output inductances of the DGs are considered equal (i.e. L_1=L_2=10 mH). It can be seen in Fig. 2.10 that power sharing amongst DGs is in the ratio of 2:1. When the system is operating in the steady state, the load suddenly reduces to 150 kW. The power shared by the two DGs and the power consumed by the load are shown in Fig. 2.10. It can be seen that during the entire process, DG-1 supplies twice the amount of power supplied by DG-2.

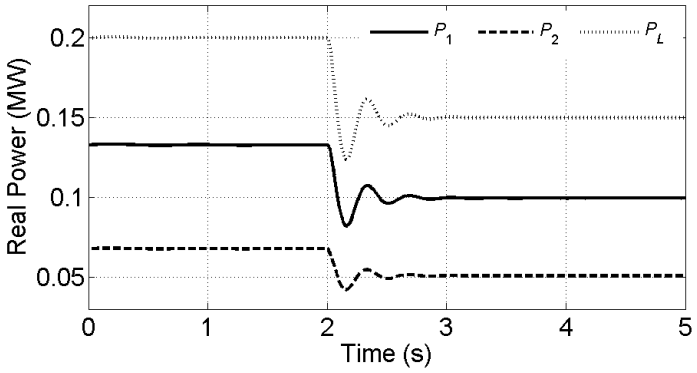

Fig. 2.10. Real power sharing in MG using modified angle droop control.

2.5.3. FREQUENCY DROOP

In a conventional frequency droop control method, each DG uses its real power output to set the frequency at its point of connection [92]. The conventional frequency droop characteristic, given in (2.20), is shown in Fig. 2.11.

$$\omega = \omega^* + m_f \times (0.5 \times P^* - P) \tag{2.20}$$

where ω and ω^* are the instantaneous and rated frequency of the system respectively and P^* and P are the rated and measured actual real power respectively. The droop coefficient is denoted by m_f. The frequency variation $\Delta\omega = \omega - \omega^*$ is zero when a DG supplies half of its rated power. The frequency is higher than 50 Hz when the load power is less than half rated power and is lower than 50 Hz when the load power higher than half rated power. Note that the droop gain m_f is chosen so as to maintain the frequency deviation (f_d) within ± 0.3 Hz from the base frequency of 50 Hz. In an islanded microgrid containing synchronous generators, it is desirable to limit the frequency variation to within ± 0.5 Hz [92, 102]. We have added a more stringent restriction of ± 0.3 Hz for these studies.

The value of the droop coefficient can be calculated from (2.20) using the frequency deviation limit of the system and power rating of the DG. The value of the droop coefficient is reciprocal of the rating of the DG. Therefore, each DG may have unique value of the droop coefficient (m_f) for its droop line. The proper selection of droop coefficients for each DG allows sharing the total load power requirement among the DGs proportionally to their rated power.

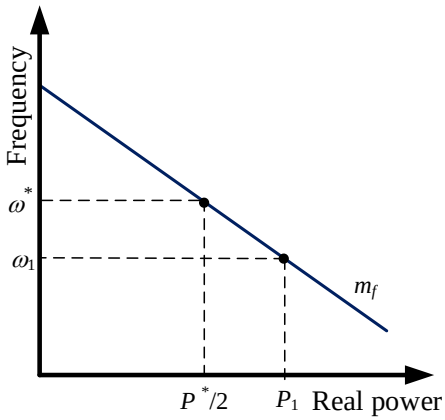

Fig. 2.11. Frequency droop characteristic.

Consider the frequency droop of (2.20). From this we get

$$0.5P^* - P = \frac{\omega - \omega^*}{m_f} \tag{2.21}$$

Assume that the minimum frequency is ω_m rad/s (which is equivalent to 49.7 Hz). At this frequency, the DG must supply the maximum rated power i.e., $P = P^*$. Then the value of m_f can be calculated from (2.21) as

$$m_f = 2\frac{\omega^* - \omega_m}{P^*} \tag{2.22}$$

The reactive power is shared in proportion to the voltage magnitude as

$$V = V^* + n_f \times (Q^* - Q) \tag{2.23}$$

where V and V^* are the instantaneous and rated voltage respectively and Q^* and Q are the rated and measured actual reactive power respectively. The droop coefficient is denoted by n_f. The conventional voltage droop characteristic is shown in Fig. 2.12. In LV networks, in general, the voltage variation is limited to between 0.94 per unit and 1.05 per unit. Therefore the voltage limits in the islanded microgrid is set as ± 5%.

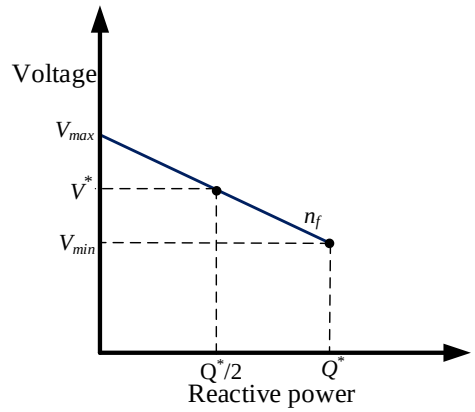

Fig. 2.12. Voltage droop characteristic.

For example, consider an autonomous 11 kV microgrid with two DGENs as shown in Fig. 2.13. The ratings of DGEN-1 and DGEN-2 respectively are 250 kW and 500 kW. The frequency deviation limit is considered as ± 0.3 Hz. The droop gains are calculated according to the ratings of DGs. The values of the droop coefficients and system parameters are given in Table. 2.7.

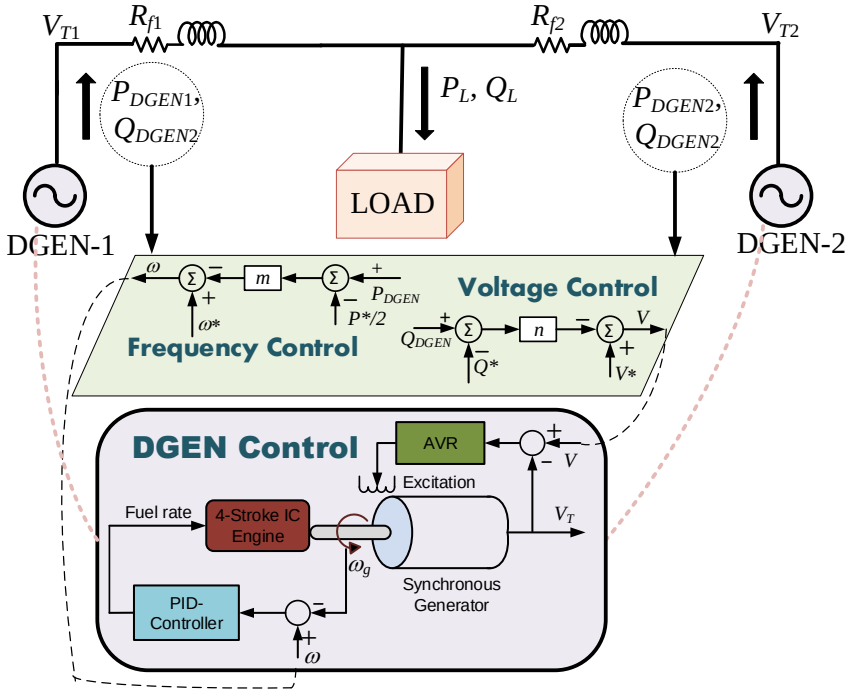

Fig. 2.13. Microgrid structure with two DGENs.

Table. 2.7. Parameters of the DGs connected in Microgrid (Fig. 2.12).

System Quantities	**Values**
DG_1 Feeder impedance	R_{f1} = 3.025 Ω, L_{f1} = 57.8 mH
DG_2 Feeder impedance	R_{f2} = 3.025 Ω, L_{f2} = 57.8 mH
DGs Rated Power	DGEN-1: 500 kW, DGEN-2: 250 kW
Droop Coefficient (Frequency–Voltage)	
m_{f1}	0.0075 rad/MWs
m_{f2}	0.015 rad/kWs
n_{f1}	0.02 kV/MVAr
n_{f2}	0.04 kV/MVAr

At the beginning, the load demand is 350 kW, which is below half of the total DGEN rating. Subsequently at 3 s, the load demand increases to 500kW. The load power shared by the DGENs according to their ratings are shown in Fig. 2.14, while the frequencies of the DGENs are shown in Fig. 2.15, which are above or below 50 Hz depending on the total load requirement.

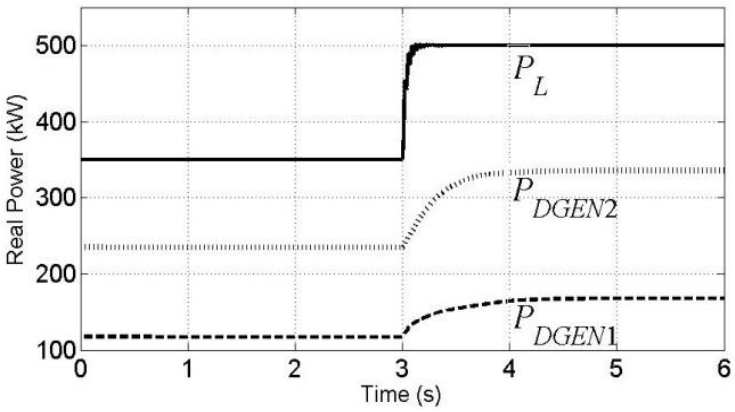

Fig. 2.14. Load power sharing by the DGENs.

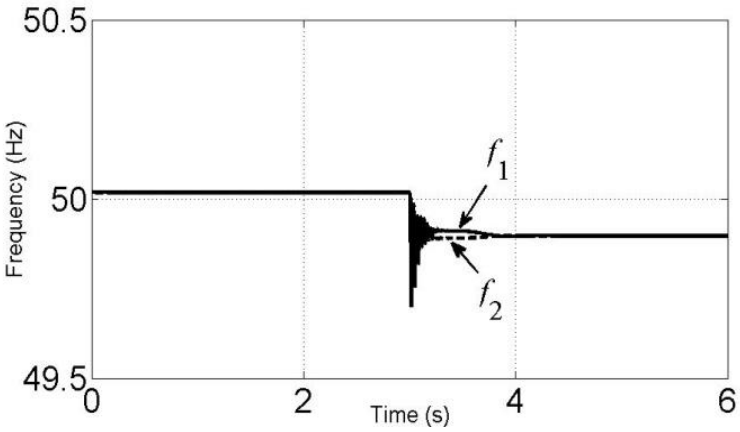

Fig. 2.15. DGEN frequencies before and after load change.

Usually in LV networks, *R*/*X* ratio is high. Both the droop control strategies presented before depend on decoupling of real and reactive power assuming that *R*/*X* is small. In such cases, the conventional droop method may not be suitable for active and reactive power sharing [103-104]. Furthermore, this method has some drawbacks, such as frequency and amplitude deviation, slow transient response [105]. The decoupling in retrofilled networks may be difficult. However for greenfield networks, cables can be easily chosen to satisfy this condition.

2.6. PSEUDO INERTIA CONCEPT

When a microgrid contains of both inertial and non-inertial DGs, there may be large power and frequency excursions during transients. Consider the Fig. 2.1 with a DGEN and a non-inertial DG. The system response for a cold start is shown in Fig. 2.16 and Fig. 2.17. From Fig. 2.16, it can be seen that high frequency oscillations lasts for about 0.5 s. Following this, the NI DG starts drawing power and the diesel generator balances this out by supplying a large amount of power for about 1.5 s. Also the system takes a long time to reach steady state, while the frequencies of the two DGs never coincide, as evident from Fig. 2.17. Note that the DGEN may never be able to supply the transient power resulting in a system collapse.

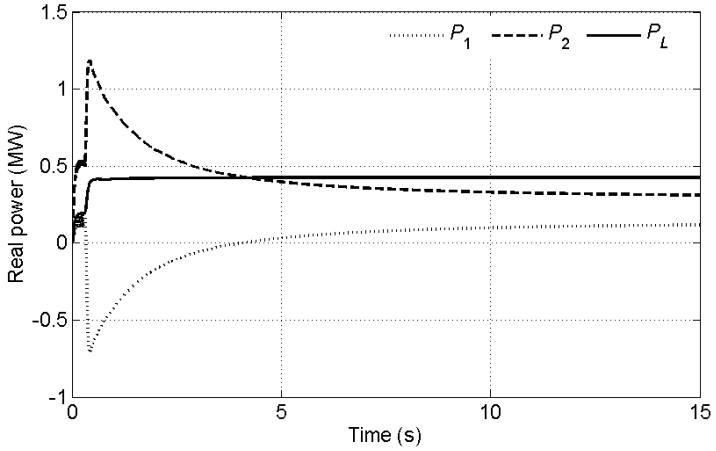

Fig. 2.16. Real power sharing in microgrid (operating in frequency droop).

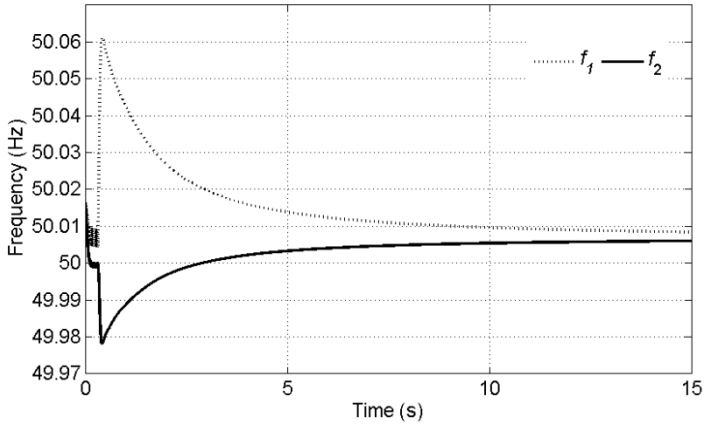

Fig. 2.17. Frequencies of DGs (operating in frequency droop).

The angle droop control is discussed for a hybrid microgrid containing inertial and non-inertial DGs [106]. To match the rates of change in power output of inertial and non-inertial DGs, a derivative term is added in power output of the NI- DG. This method has few limitations as: 1) To add derivative term, droop parameter must be chosen very carefully and 2) It can add noise to system. The governor of synchronous machine controls the output power of the engine using the PID controller. This controller takes as input of frequency error and output power error. This also contains a logical signal control which is decided according to the state of the generator. Therefore, the response of the generator is sluggish.

In [107], the dynamic responses of DGs are discussed in hybrid microgrid containing inertial and non-inertial DGs. In this paper, non-inertial DGs are synchronised with a microgrid which consist of inertial DG using angle droop control. The inertial DG operates in a frequency droop control. The angle for non-inertial DG

is calculated from the droop frequencies. However, when both sources are connected from cold start is not considered. In this case, transient oscillations can be high, since the angle is calculated based on the droop frequency and the measured frequency at the point of connection. To overcome these issues the pseudo inertia concept is developed.

This involves a new converter reference voltage generation technique as shown in Fig. 2.18. This includes a speed governor and a swing equation.

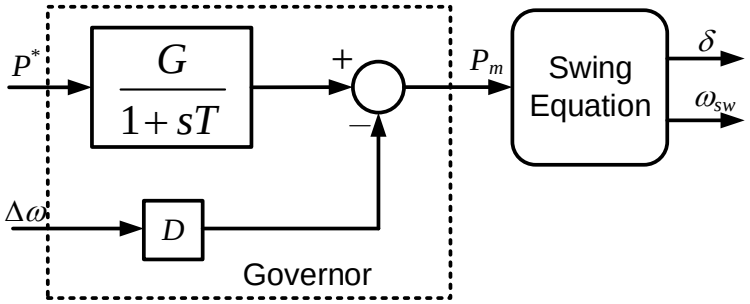

Fig. 2.18. Block diagram of governor and swing equation.

2.6.1. GOVERNOR

The governor generates a mechanical power output that will be used in the swing equation. The reference power (capacity of the DG) is passed through transfer function block, as shown Fig. 2.18. The error in speed is then added to the output of this block [102]. The mechanical power is then given by

$$P_m = \frac{G}{1+sT} P^* - D\Delta\omega \tag{2.24}$$

where ω is obtained from droop (2.20) and

$$D = \frac{1}{m_f}, \quad \Delta\omega = \omega - \omega^*$$

2.6.2. SWING EQUATION

Once the mechanical power is obtained from (2.24), it is used in a swing equation, in which the inertia and damping parameters are chosen carefully. The swing equation [92] is solved by

$$\frac{d\delta}{dt} = \omega^* \Delta\omega_{sw} \tag{2.25}$$

$$\frac{d\Delta\omega_{sw}}{dt} = \frac{1}{2H}(-K_D)\Delta\omega_{sw} + \frac{1}{2H}(P_m - P_e) \tag{2.26}$$

$$\omega_{DG} = \omega + \Delta\omega_{sw} \tag{2.27}$$

In the above equation, the electrical power P_e is measured at the DG terminal. K_D and H are the damping ratio and the inertia constant respectively. The parameters are given in Table. 2.9.

2.6.3. REFERENCE VOLTAGES

Once the frequency droop equation (2.20) is solved, the frequency error is used to determine the required mechanical power P_m. This is then used in the swing equation to determine δ and ω_{DG}. Also, the magnitude of the required voltage is generated from the reactive power droop equation in (2.23). Once these quantities are available, the instantaneous reference voltages for the three phases are obtained as

$$\begin{aligned} v_a^* &= \sqrt{2}V\sin(\omega_{DG}t + \delta) \\ v_b^* &= \sqrt{2}V\sin(\omega_{DG}t + \delta - 120^\circ) \\ v_c^* &= \sqrt{2}V\sin(\omega_{DG}t + \delta + 120^\circ) \end{aligned} \tag{2.28}$$

These reference voltages are then tracked by the VSC as discussed in Appendix A.

2.7. SIMULATION STUDIES

Let us consider the system shown in Fig. 2.1. The DGEN has a rating of 500 kW and the MT has a rating of 250 kW. They should therefore share power in a ratio of 2:1. Furthermore, the frequency should not deviate more than ± 0.3 Hz. From (2.14), we find that the DGs should operate at 50 Hz when they are supplying half of their rated power. Also both DGs should operate at the same frequency. For the DGEN, the droop coefficient can be calculated from (2.16) as

$$\begin{aligned} &\omega - \omega^* = -0.3 \times 2 \times \pi \text{ rad/s} = -m_{f2} \times 250 \text{ kW} \\ &\Rightarrow m_{f2} = 0.0075 \text{ rad/kW - s} \end{aligned}$$

In the same way, the droop gain for the MT (m_{f1}) will be twice of m_{f2}, i.e., 0.0150 rad/kW - s.

Table. 2.8. Parameters of the DGs connected in Microgrid (Fig. 2.1).

System Quantities	Values
DG_1 Feeder Impedance	R_{f1} = 3.025 Ω, L_{f1} = 57.8 mH
DG_2 Feeder Impedance	R_{f2} = 3.025 Ω, L_{f2} = 57.8 mH
DGs Rated Power	MT: 250 kW, DGEN: 500 kW
PQ Load	600 kW, 500 kVAR (before 10 s) 300kW, 500 kVAR (after 10 s)
Droop Coefficient (Frequency–Voltage)	
m_{f1}	0.015 rad/MWs
m_{f2}	0.0075 rad/kWs
n_{f1}	0.02 kV/MVAr
n_{f2}	0.04 kV/MVAr

Let us assume that the two DGs are required to supply 600 kW. The system is cold started at t = 0 s and load is changed to 300 kW at t = 10 s. The load power and the power generated by the two DGs are shown in Fig. 2.19. The ratio P_1:P_2 remains 1:2 during entire period except during transients. It can be seen that MT also has slow response, so has the diesel generator. This response depends on the selection of the swing and governor parameters. During the load change, there is no large transient in the power supplied by the DGs.

The frequencies of the two DGs are shown in Fig. 2.20. It can be seen that, due to the proper choice of droop gains, they merge following transients. Since DGEN rating is twice than of MT, it must supply 400 kW before 10 s and 200 kW after 10 s. Also note that the frequency becomes below synchronous (BS) before 10 s and above synchronous (AS) after 10 s. We can verify these frequencies from (2.14) as

$$f_{BS} = 50 + \frac{0.0075 \times (0.5 \times 500 - 400)}{2\pi} = 49.82\ Hz$$

$$f_{AS} = 50 + \frac{0.0075 \times (0.5 \times 500 - 200)}{2\pi} = 50.06\ Hz$$

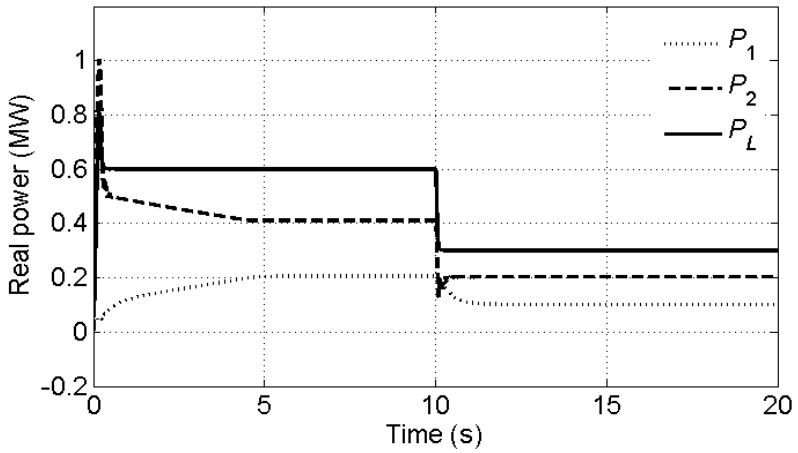

Fig. 2.19. Real power sharing in between MT and DGEN.

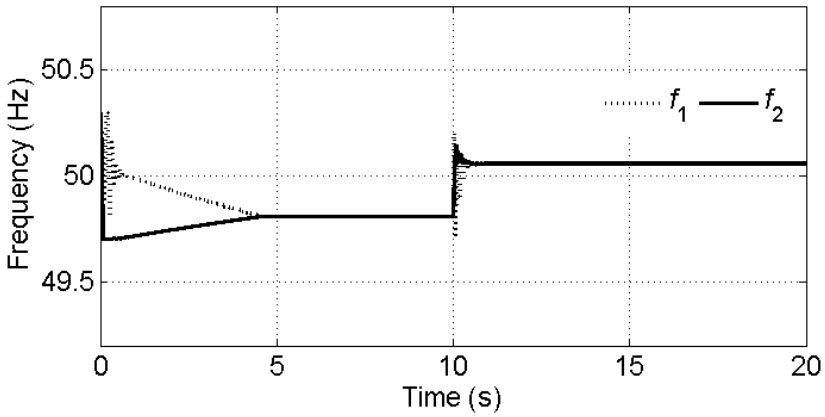

Fig. 2.20. Frequencies of MT and DGEN.

Table. 2.9. Swing equation and governor parameters.

System data	**Value**
Damping constant (K_D)	5 MWs/rad
Inertia constant (H)	2 MJ/MVA
Gain (G)	1
Time constant (T)	0.001 s

2.8. CONCLUSION

This chapter discusses the operation of DGs in a hybrid microgrid. A modification to angle droop has been proposed, which makes the power sharing independent of the output inductance. However the angle droop does not work satisfactorily in the presence of inertial DGs. In such cases (i.e., in hybrid microgrids), frequency droop is a better choice. In the frequency droop control, a new control algorithm for a converter interfaced DG is proposed which facilitates smooth operation

in the presence of inertial and non-inertial DGs. The response speed of a converter is reduced by introducing a governor action and a swing equation. In this way, the converter can be tailored to respond in harmony with inertial rotary generators.

CHAPTER 3

INTEGRATION OF NON-DISPATCHABLE DGS WITHIN A MICROGRID

A hybrid microgrid can have both dispatchable/non dispatchable and inertial/non-inertial DGs. When these varieties of sources are connected to an autonomous microgrid (MG), operating in frequency droop control all of them must operate at the same frequency. Under such a scenario, the connection and disconnection of the non-dispatchable DG becomes crucial, since these types of DGs usually have a plug-and-play nature. For example, a PV can only be connected to the microgrid in the morning and get disconnected in the evening and in the cloudy conditions.

For the connection of a DG with a microgrid, one of the following two options can be chosen

1) Synchronization
2) Isochronous operation

In the former method, the incoming DG is synchronized with the bus voltage to which it is getting connected. A simple method is proposed for this purpose. Alternatively, the microgrid can be forced to operate at 50 Hz such that other converter interfaced DGs can integrate at this frequency. An isochronous controller is proposed for this purpose. The discussions of this chapter are mainly focused on wind energy integration to a MG.

3.1. INTEGRATION OF NON-DISPATCHABLE DGS IN A MICROGRID

The wind energy conversion system (WECS) connected with a microgrid is shown in Fig. 3.1. Similarly, the PV connected with a microgrid is shown in Fig. 3.2. In Fig. 3.1, a permanent magnet synchronous generator (PMSG) based variable speed WECS is considered, which converts wind energy to a low frequency (≈10 Hz) ac power. Therefore it needs to be connected to the microgrid through a back to back (BTB) converter system. The BTB converter consists of two conventional voltage source converters (VSC-1 and VSC-2) connected through a common dc link capacitor.

VSC-1 is used to control the power flow from the wind turbine, while VSC-2 is used to hold the dc link capacitor voltage (V_{dc}) constant. Since the microgrid frequency varies within the droop limits according to the load demand, VSC-2 should operate at the same frequency of the microgrid. In Fig. 3.1, the microgrid structure is considered same as shown in Chapter 2, Fig. 2.13. Similarly in Fig. 3.2, the voltage source converter, interfacing the PV array to the microgrid, should operate at the same frequency of the microgrid. As mentioned before, two methods are proposed through which seamless interconnection is achieved.

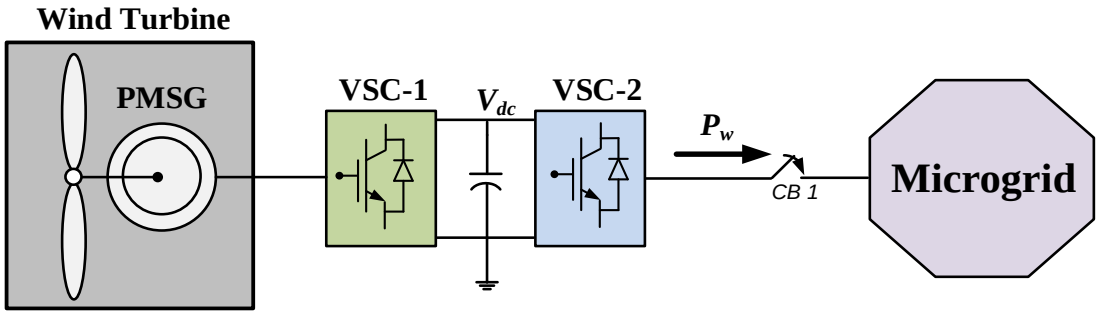

Fig. 3.1. Microgrid structure with WECS.

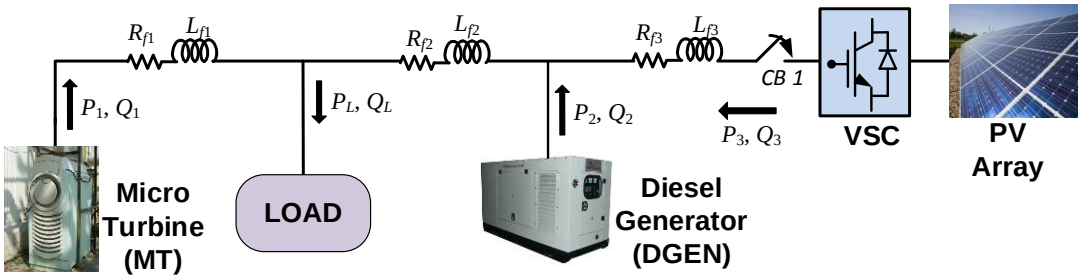

Fig. 3.2. Microgrid structure with PV.

3.2. WIND ENERGY CONVERSION SYSTEM

3.2.1. WIND TURBINE WITH PMSG MODEL

The wind power that is captured by the blade and converted into mechanical power can be calculated by [108]

$$P_M = \frac{1}{2}\rho A v_\omega^3 C_p \tag{3.1}$$

where ρ is the air density (kg m^{-3}), A is the cross-sectional area (m^2) through which wind passes, v_ω is the wind speed (m s^{-1}) and C_p is the power coefficient of the blade. The power coefficient C_p is calculated from [109]

$$C_p = 0.5176\,(\frac{116}{\lambda_i} - 0.4\beta - 5)\,e^{\frac{-21}{\lambda_i}} + 0.0068\lambda \tag{3.2}$$

where β is the pitch angle (degrees), λ is the tip speed ratio (the blade tip moving speed divided by the wind speed), and λ_i is given by

$$\frac{1}{\lambda_i} = \frac{1}{\lambda + 0.08\beta} - \frac{0.035}{\beta^3 + 1} \tag{3.3}$$

The wind turbine operates at the generator control mode when the wind speed is below the rated wind speed, and works under the pitch control mode when the wind speed exceeds the rated value [110].

3.2.2. PMSG OPERATION WITH VARIED WIND SPEEDS

In this study, a variable wind speed has been created using following equations:

$$v_w = \begin{cases} v_m & t < t_1 \\ v_m + k\cdot(t - t_1) & t_1 < t < t_2 \\ v_m + k\cdot(t_2 - t_1) & t > t_2 \end{cases} \tag{3.4}$$

$$v_{ES} = k\cdot(t_2 - t_1) \tag{3.5}$$

where v_w is the wind speed available to the turbine, v_m is the mean wind speed, k is the ramp change in the wind speed, t_1 and t_2 are the starting and ending time respectively of the wind speed ramping duration, v_{ES} is the external wind speed of the wind source.

3.2.3. CONTROL OF BTB CONVERTERS WITH PMSG

The schematic diagram of the PMSG with BTB voltage source converters is shown in Fig. 3.3. The kinetic energy of the wind is converted into mechanical energy by the wind turbine and then transmitted to the generator. VSC-1 controls the active power through MPPT, while VSC-2 maintains the DC voltage constant [111].

To extract the maximum power from the wind energy, turbine blades should change their speed as the wind speed changes. Reference [112] gives out three methods to realize the MPPT control. Based on the PMSG model, to control the generator power, a method similar to Optimal Torque Control (OTC) is applied here, which is named Optimal Power Control (OPC). The principle of the OTC is that the wind

turbine mechanical torque T and the turbine speed ω have the following relationship at MPPT

$$T \propto \omega^2 \tag{3.6}$$

Assuming that the generator power is denoted by P_g, in OPC we get

$$P_g \propto \omega^3 \tag{3.7}$$

It should be noted that the values of the turbine speed and the generator speed are equal, considering that the PMSG model is a direct drive.

To control MPPT wind power flow to the microgrid, VSC-1 generates voltage across the filter capacitor (C_{fw}) with an angle deviation from the PMSG output voltage. This power angle is calculated by a PI controller as

$$\delta_1 = K_{P1}(P_g - P) + K_{I1}\int (P_g - P)\, dt \tag{3.8}$$

where P_g is the wind power calculated from (3.7) and P is the actual power from the PMSG.

VSC-2 holds the voltage across the dc link capacitor constant. This is achieved by controlling angle (δ_2) across the capacitor (C_{fg}) and this angle is computed by another PI controller as

$$\delta_2 = K_{P2}(V_{dcref} - V_{dc}) + K_{I2}\int (V_{dcref} - V_{dc})\, dt \tag{3.9}$$

where V_{dcref} is the reference dc capacitor voltage and V_{dc} is the actual dc capacitor voltage. K_{P2} and K_{I1} are the proportional and integral gain of the controller respectively.

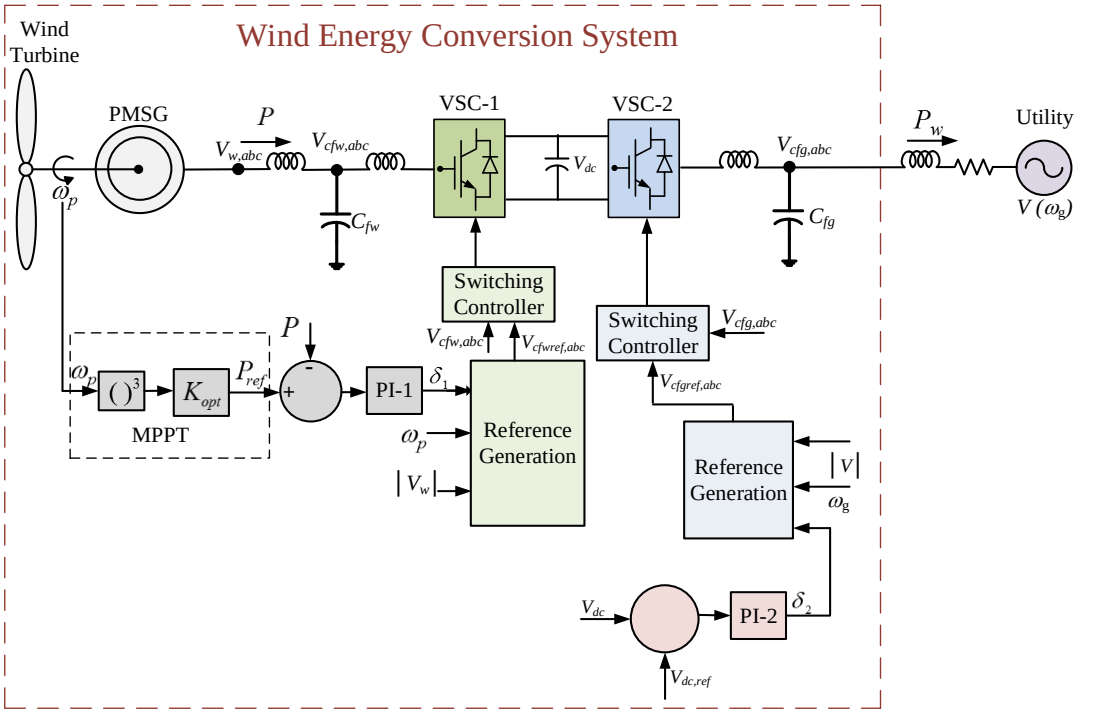

Fig. 3.3. Schematic diagram of wind energy conversion system

To illustrate the operation of OPC based MPPT control, consider the WECS that is connected to an infinite bus (Fig. 3.3). The parameters of wind turbine and PMSG used are listed in Table 3.1. The wind speed pattern is assumed as

$$t_1 = 3s, t_2 = 4s, k = 1, V_m = 10\ m/s$$

Fig. 3.4 (a) shows the wind speed variation pattern. At the beginning the wind speed is 10 m/s, which then ramps up to 11 m/s between 3 and 4 s. The power output of the WECS follows the same pattern of the wind speed, as shown in Fig. 3.4 (b). It has been assumed that the utility operates at a fixed known frequency and VSC-2 operates at this frequency. However when the WECS gets connected to an MG, the frequency can be variable depending on the load and generation. For example, assume that a microgrid is supplying its load at a frequency f_1. When the WECS gets connected, the MG frequency which become higher than f_1. Therefore, VSC-2 first must synchronize with the MG frequency and remain synchronized for any frequency change in MG.

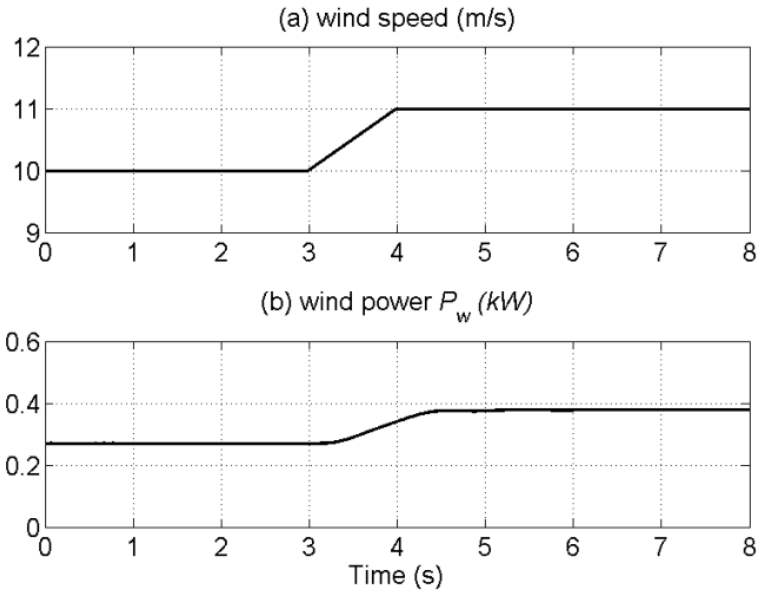

Fig. 3.4. Variable wind speed and power.

Table 3.1. Wind turbine and PMSG parameters.

Parameters	**Values**
Rotor radius	58 cm
Air density	1.225 kg/m^3
Rated wind speed	12 m/s
Rated apparent power	0.5 MVA
Rated line-to-line voltage	11 kV
Rated frequency	10 Hz
Number of pole pairs	49

3.3. TECHNIQUES FOR INTEGRATION OF WECS WITH MICROGRID

As mentioned before two methods are proposed for integration of WECS with a microgrid. These are discussed below.

3.3.1. FREQUENCY DROOP CONTROL WITH ISOCHRONOUS OPERATION

In this method, the frequency of the microgrid is held constant at 50 Hz through isochronous operation of frequency droop control. Therefore, VSC-2 can be connected to the microgrid at the constant frequency of 50 Hz. In the islanded microgrid, the DGs operate in frequency droop control given by

$$\omega = \omega^* + m_f \times (0.5 \times P^* - P) \tag{3.10}$$

Equation (3.10) signifies that when the system frequency is rated (50 Hz), the DG should supply half of its rated power. The frequency will be below (above) 50 Hz when the DG supplies more (less) than half of its rated power. The droop gain is calculated based on a frequency limit (f_d) of ± 0.3 Hz. In isochronous mode, the frequency of the microgrid must remain constant at 50 Hz. Therefore, if the droop control and the isochronous mode are combined, the system operates at the set reference frequency while sharing load power according to DG ratings.

To achieve this, the droop line is shifted according to the load variation while preserving its slope. For constant droop coefficient, each DG has its own droop line according to its rating. The droop line shifts in such a way that it retains the same slope and can supply load power demand at set reference frequency.

The droop lines of Fig. 3.5 for one of the DGs are considered. Ordinarily, the DG operates in line-1. This implies that when it supplies P_1 the frequency should be ω_1. However it is required that the DG operates at 50 Hz (ω^*). Therefore the frequency must be compensated by the amount $\Delta\omega = \omega^* - \omega_1$. We also need to maintain the power sharing, which depends on the slope of the droop lines. Therefore the quantity $\Delta\omega$ must be kept zero against any frequency variation due to load change. To achieve this, a PID controller is used. This is shown in Fig. 3.6. The output of the PID controller is added to the output of the droop controller, to produce ω_1', which is the input to a DG governor/controller. Note that in steady state, $\omega_1' = \omega^*$. This means that the droop line has been shifted to line-2 to give power output of P_1 at ω^*.

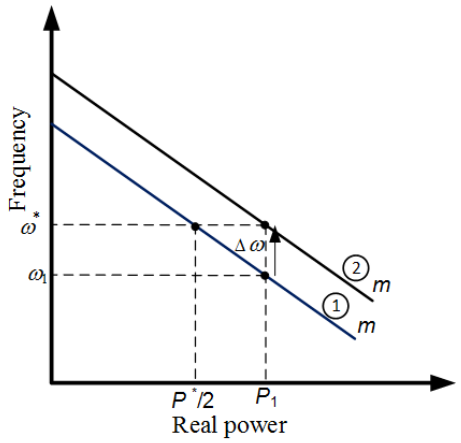

Fig. 3.5. Frequency droop control with isochronous mode.

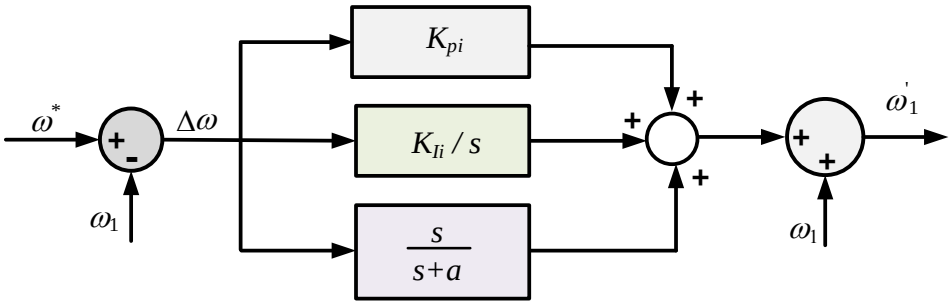

Fig. 3.6. Isochronous controller.

3.3.2. SYNCHRONIZATION WITH MICROGRID

In this method, the microgrid operates in conventional frequency droop control and its frequency varies within the frequency band according to load power demand. Therefore, to connect the WECS with the microgrid, VSC-2 must be synchronized with the microgrid to operate at same frequency. To achieve this, a simple algorithm is used for synchronization, which is discussed below.

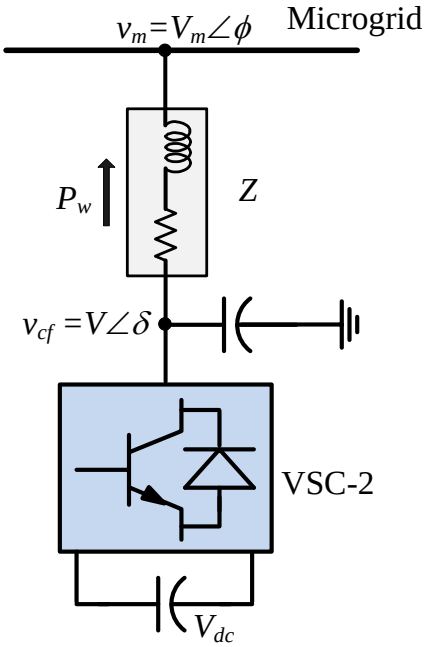

Fig. 3.7. VSC-2 connection with microgrid.

Let the frequency of the microgrid be set at ω. The instantaneous voltages (v_m) at the point of connection of VSC-2 are given as

$$\begin{aligned} v_{ma} &= V_m \times \sqrt{2} \sin(\omega t + \phi) \\ v_{mb} &= V_m \times \sqrt{2} \sin(\omega t - 120° + \phi) \\ v_{mc} &= V_m \times \sqrt{2} \sin(\omega t + 120° + \phi) \end{aligned} \tag{3.11}$$

Using symmetrical component theory [113], the positive sequence component of the instantaneous voltage of (3.11) will be

$$\begin{bmatrix} \mathbf{v_{m0}} \\ \mathbf{v_{m1}} \\ \mathbf{v_{m2}} \end{bmatrix} = \frac{1}{3}\begin{bmatrix} 1 & 1 & 1 \\ 1 & a & a^2 \\ 1 & a^2 & a \end{bmatrix}\begin{bmatrix} v_{ma} \\ v_{mb} \\ v_{mc} \end{bmatrix} \tag{3.12}$$

$$\begin{aligned} \mathbf{v_{m1}} &= \left(v_{ma} + v_{mb}a + v_{mc}a^2\right)/3 \\ &= \frac{V_m}{\sqrt{2}}\left[\sin(\omega t + \phi) - j\cos(\omega t + \phi)\right] \end{aligned} \tag{3.13}$$

$$\mathbf{v_{m1}} = \frac{V_m}{\sqrt{2}}(\alpha + j\beta) \tag{3.14}$$

where $a = e^{j120^\circ}$ and

$$\alpha = \sin(\omega t + \phi),\ \beta = -\cos(\omega t + \phi) \tag{3.15}$$

The positive sequence of the reference voltage (v_{cf}) across the filter capacitor of VSC-2 is

$$\begin{aligned} \mathbf{v_{cf1}} &= \frac{\sqrt{2}\times V}{3}\left[\sin(\omega t + \phi + \delta_2) + a\sin(\omega t + \phi + \delta_2 - 120^\circ)\right. \\ &\qquad \left. + a^2\sin(\omega t + \phi + \delta_2 + 120^\circ)\right] \\ &= \frac{V}{\sqrt{2}}\left[\sin(\omega t + \phi + \delta_2) - j\cos(\omega t + \phi + \delta_2)\right] \end{aligned}$$

where $\delta = \phi + \delta_2$

$$\begin{aligned} \mathbf{v_{cf1}} &= \frac{V}{\sqrt{2}}\left[\sin(\omega t + \phi)\cos\delta_2 + \cos(\omega t + \phi)\sin\delta_2\right. \\ &\qquad \left. - j\cos(\omega t + \phi)\cos\delta_2 + j\sin(\omega t + \phi)\sin\delta_2\right] \\ &= \frac{V}{\sqrt{2}}\left[(\alpha + j\beta)\cos\delta_2 - (\beta - j\alpha)\sin\delta_2\right] \end{aligned} \tag{3.16}$$

Note that from the instantaneous measurement of three phase bus voltage, α and β can be calculated. Let the magnitude of the voltage across the VSC-2 filter capacitor (v_{cf}) be $V \approx V_m$. Also its angle (δ) is obtained by the phase shifting of v_m angle (ϕ) by δ_2. It is obtained from (3.9).

From (3.15) and (3.16), $\mathbf{v_{cf1}}$ can be calculated. The instantaneous negative sequence ($\mathbf{v_{cf2}}$) is the complex conjugate of the positive sequence. Also, since the

system is assumed to be balanced, the instantaneous zero sequence ($\mathbf{v_{cf0}}$) will be zero. Therefore, using inverse symmetrical component transform, the instantaneous reference voltages across the capacitor are obtained. Thus VSC-2 can track this reference output voltage across the capacitor (v_{cf}) without any explicit frequency measurement.

3.3.3 SIMULATION STUDIES

Three different case studies of WECS and microgrid integration are considered. These are

(a) Nominal operation of the islanded microgrid.
(b) WECS integration with the microgrid using isochronous operation of frequency droop.
(c) WECS integration with the microgrid using frequency synchronization

The system (Fig. 3.1) parameters are listed in Table 3.2.

Table 3.2. System parameters considered in Fig. 3.1.

System Quantities	**Values**
DG_1 Feeder impedance	R_{f1} = 3.025 Ω, L_{f1} = 57.8 mH
DG_2 Feeder impedance	R_{f2} = 3.025 Ω, L_{f2} = 57.8 mH
DGs Rated Power	DGEN-1: 500 kW, DGEN-2: 250 kW
Droop Coefficient (Frequency–Voltage)	
m_1	0.0075 rad/MWs
m_2	0.015 rad/kWs
n_1	0.02 kV/MVAr
n_2	0.04 kV/MVAr

CASE (A): The microgrid has two DGENs with ratings of 500kW and 250kW respectively and its local load. The droop coefficients for each DG are calculated based on their ratings. The local load is assumed to be 625 kW. As shown in Fig. 3.8 (a), DGENs share the power in the ratio of 2:1 according to their ratings. The microgrid frequency is 49.8 Hz with the conventional droop control method as shown in Fig. 3.8 (b). The isochronous controller is applied at 2 s and it can be seen from Fig. 3.8 (b) that the frequency converges to 50 Hz within 3 s. However the powers remain

unaltered. The parameters of the PID controller are listed in Table 3.3. Subsequently, the load power is calculated at 11 s. The results are shown in Fig. 3.9. It can be seen from Fig. 3.9 (a) that the power supplied by the DGs also changes maintaining the same ratio. However the system frequency does not diverge from 50 Hz, as can be seen from Fig. 3.9 (b), due to the action of isochronous controller.

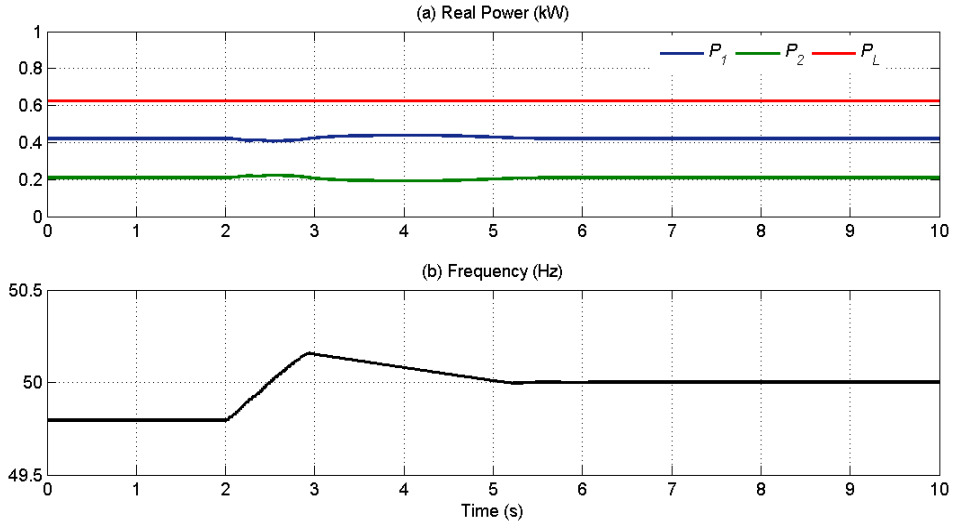

Fig. 3.8. Real power sharing and frequency of microgrid with conventional droop and with isochronous controller.

Table 3.3. Parameters of the PID controller.

System data	**Value**
Proportional gain (K_{Pi})	0.1
Integral gain (K_{Ii})	10
Constant coefficient (a)	200

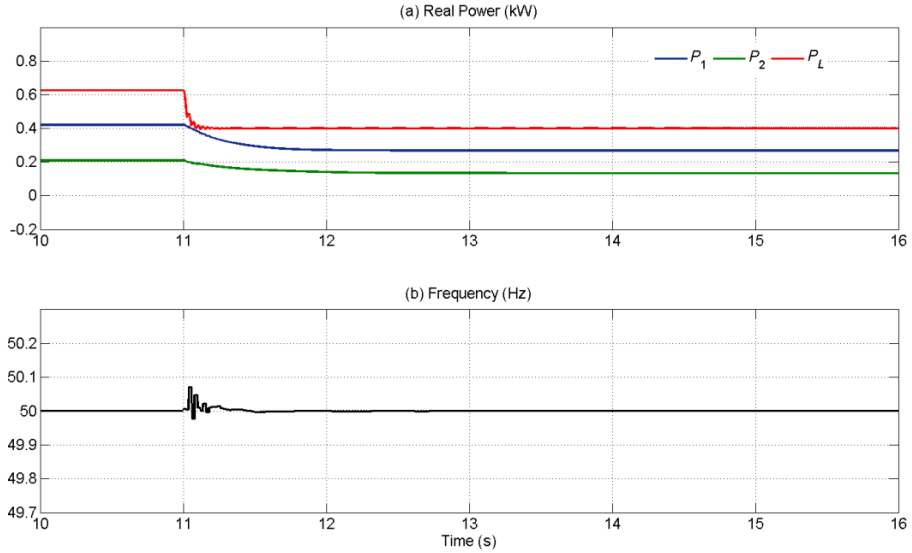

Fig. 3.9. Real power sharing and frequency with load variation in Case (A).

CASE (B): The microgrid operates in frequency droop control with isochronous mode. Therefore, the microgrid operates at the constant reference frequency of 50 Hz and hence VSC- 2 can operate at 50 Hz. The results are discussed below.

CASE (B.1): MICROGRID WITH CONSTANT SPEED WECS

For this case, it has been assumed that when the WECS system is connected to the microgrid at 2 s, the sources are operating in the steady state. The WECS supplies its total power to the microgrid. The real power flow in the microgrid is shown in Fig. 3.10 (a). It can be seen from this figure that the power supplied by the DGs reduces proportionally, maintaining the sharing ratio. The frequency of the microgrid is shown in Fig. 3.10 (b). It can be seen that the system frequency is retained at the set reference value of 50 Hz even after the integration of the WECS. The dc link capacitor voltage is shown in Fig. 3.11. It is held constant at 2.5 kV by VSC-2 barring some transients when the WECS connects to the microgrid.

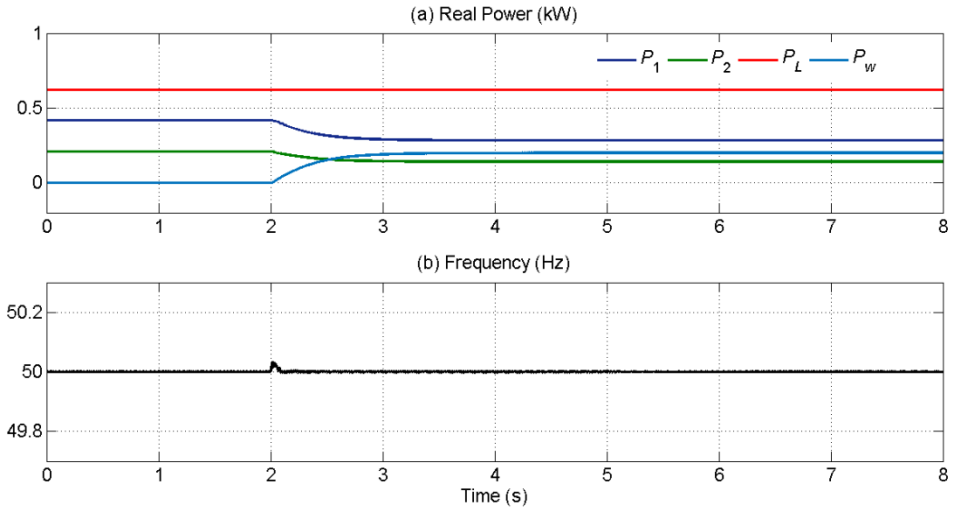

Fig. 3.10. Real power flow in microgrid with WECS and microgrid frequency in Case (B.1).

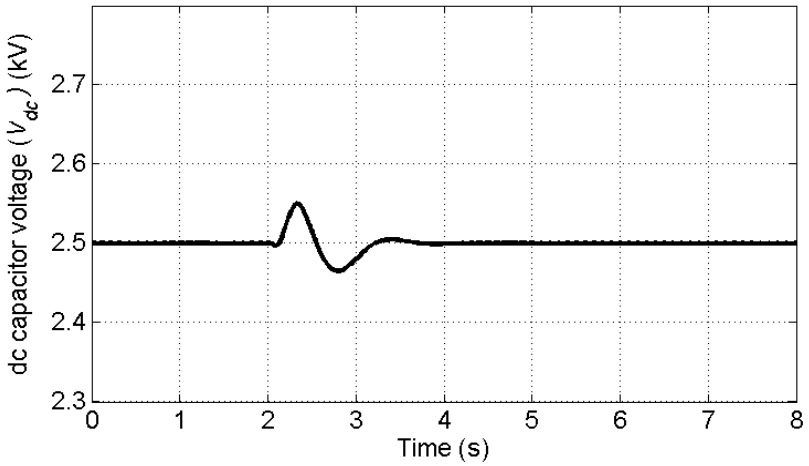

Fig. 3.11. DC capacitor voltage in Case (B.1).

CASE (B.2): MICROGRID WITH VARIABLE SPEED WECS

In this case, the wind speed of the WECS is considered variable. As shown in Fig. 3.12, initially the wind speed is constant at 10 m/s. Then at 10 s, it starts ramping up to 12 m/s till 12 s. The output power of WECS also follows the pattern of the wind speed as shown in Fig. 3.13 (a). Once the wind speed increases the output power of WECS also increases and therefore the power supplied by the DGENs reduces. The system frequency however is maintained at the set reference value of 50 Hz as shown in Fig. 3.13 (b).

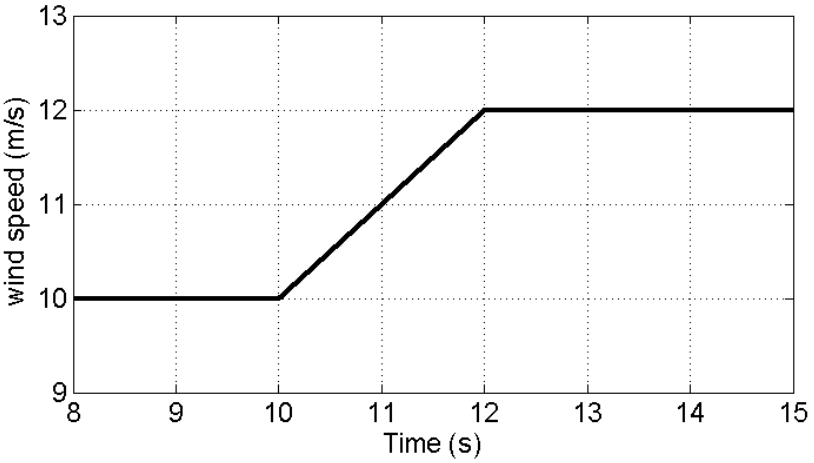

Fig. 3.12. Wind speed in Case (B.2).

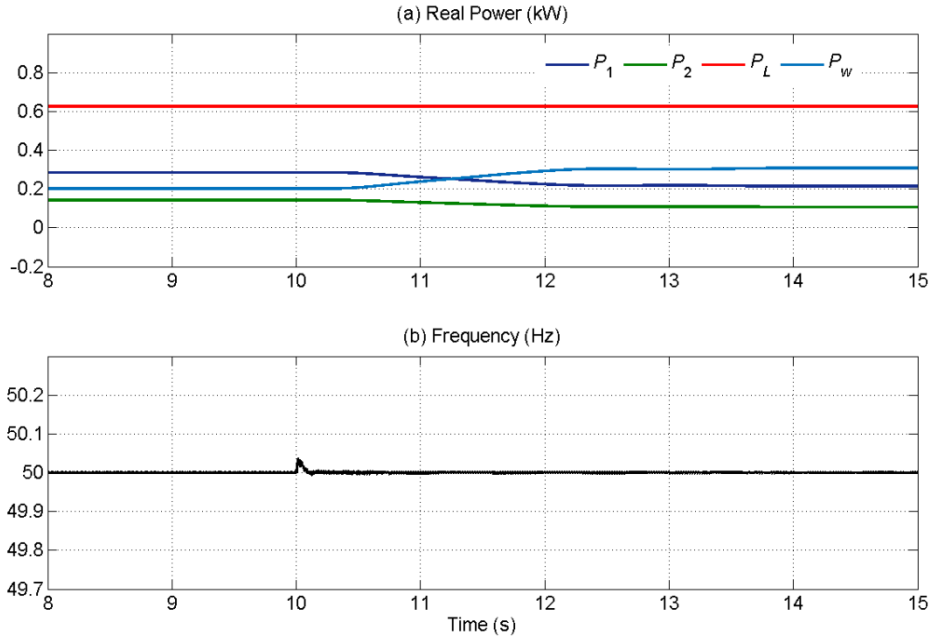

Fig. 3.13. Power flow in microgrid with WECS and microgrid frequency in Case (B.2).

CASE (B.3): TRIPPING OF WECS

Usually wind turbines start to operate when the wind speed exceeds 4-5 m/s, and are shut off at speed over 25 to 30 m/s [108]. If wind speed is less than the cut in speed or higher than the cut off speed then WECS will be disconnected from the microgrid. In this case, the wind speed is reduced from 10 m/s to the cut in speed of 4 m/s as shown in Fig. 3.14. Therefore, the power P_W from WECS becomes zero after 11 s. It can be seen in Fig. 3.15 (a) that now load power is supplied only from the DGENs. Furthermore, the system frequency is retained constant at the set reference value of 50 Hz as shown in Fig. 3.15 (b).

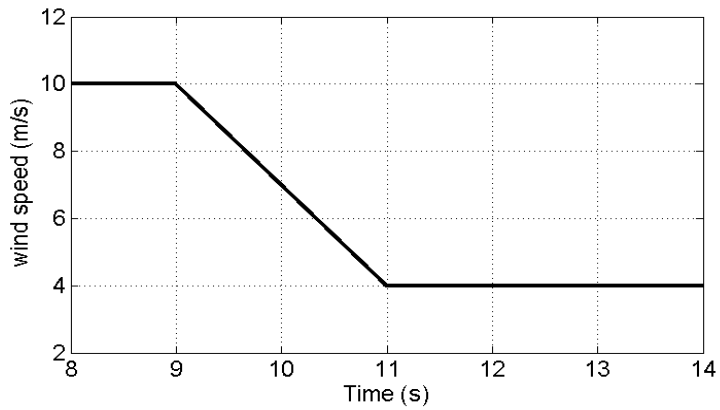

Fig. 3.14. Wind speed in Case (B.3).

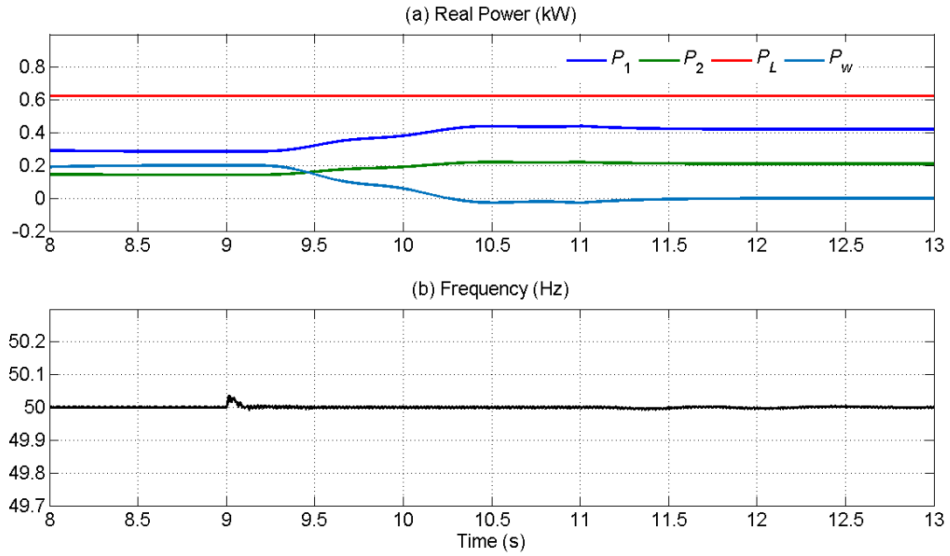

Fig. 3.15. Power flow in microgrid with WECS and frequency in Case (B.3).

CASE (C): The microgrid operates in conventional frequency droop control and the frequency of the microgrid varies within the frequency band according to load variations. Therefore, for connecting the WECS with the microgrid, the synchronization algorithm is used. The simulation results are discussed below

CASE (C.1): MICROGRID WITH CONSTANT SPEED WECS

It is assumed that when WECS connects to the microgrid at 2 s, the wind speed is constant at 10 m/s. From Fig. 3.16 (a), it can be seen that the power supplied from the DGENs reduces and the system frequency also increases due to power reduction. This is shown in Fig. 3.16 (b). The dc capacitor voltage is held constant by VSC-2 during the connection of WECS with microgrid as shown in Fig. 3.17.

It can be seen in Fig. 3.18 (a) that once the load is increased to 625 kW at 10 s, the power of DGENs increases in the same proportion and the power of WECS (P_w) remains constant. The frequency of the microgrid also reduces as shown in Fig. 3.18 (b).

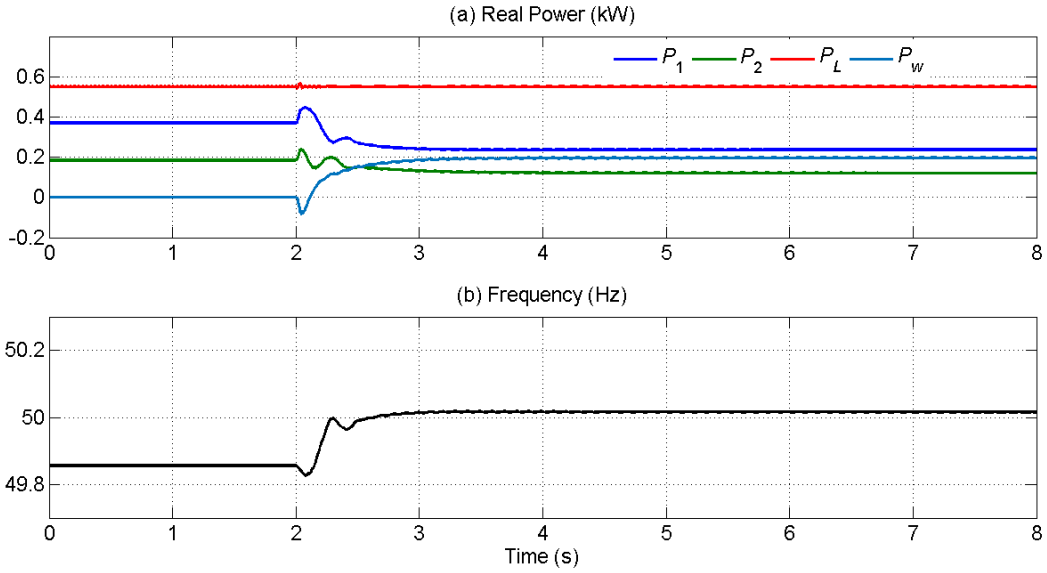

Fig. 3.16. Real power sharing and frequency of the microgrid in Case (C.1).

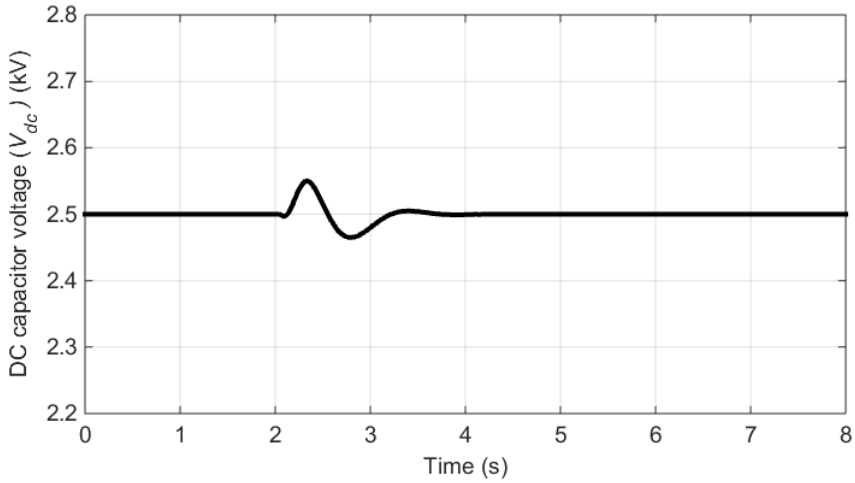

Fig. 3.17. DC capacitor voltage (V_{dc}) in Case (C.1).

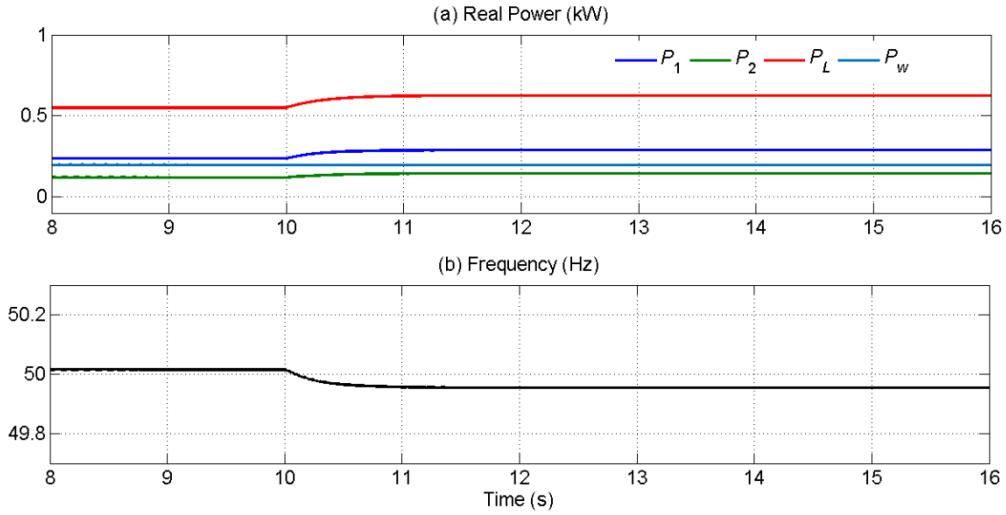

Fig. 3.18. Real power sharing and frequency of the microgrid with local load variation in Case (C.1).

CASE (C.2): MICROGRID WITH VARIABLE SPEED WECS

In this case, it is assumed that the wind speed ramps up from 10 m/s to 11 m/s. The power flow from the WECS follows the wind speed pattern and the DGENs power reduce according to the available WECS power and load requirement. This is shown in Fig. 3.19 (a). The variation in microgrid frequency is shown in Fig. 3.19 (b).

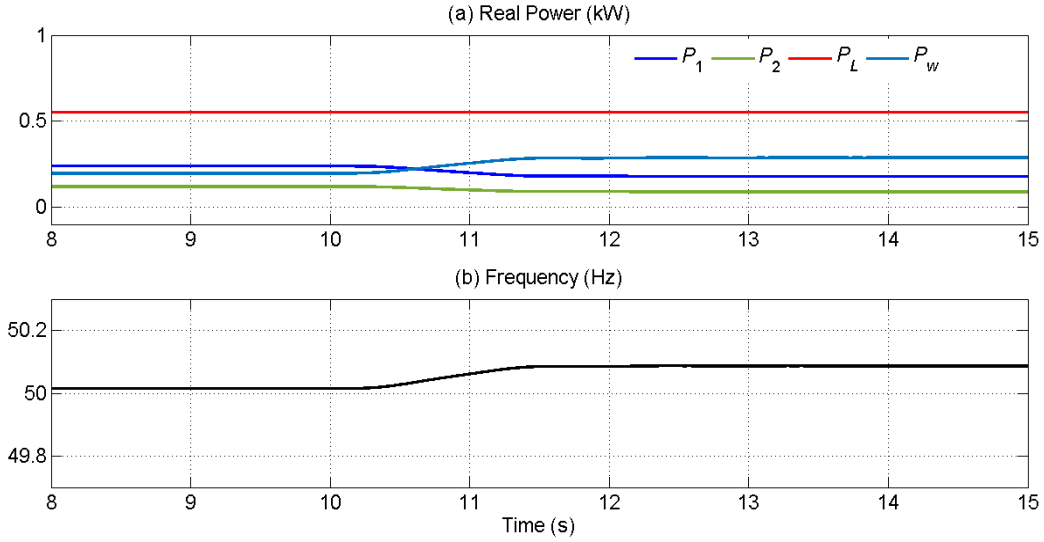

Fig. 3.19. Real power sharing and frequency of microgrid in Case (C.2).

3.4. INTEGRATION OF PV

In this section, the integration of a PV array to a microgrid is discussed. It is assumed that the PV array operates in MPPT control to supply maximum available power. Therefore, the VSC interfacing the PV array to microgrid must supply this amount of power to the microgrid [114]. Hence, VSC must be synchronized with the microgrid. To achieve this, synchronization algorithm explained in Section-3.3.2 is used.

Note that the load angle (δ_2) used for synchronization (3.16) is obtained from the maximum power available from the PV array, i.e.,

$$\delta_2 = K_P\left(P_{MPPT} - P\right) + K_I \int \left(P_{MPPT} - P\right) dt \tag{3.17}$$

where P_{MPPT} is the MPPT available power and P is the actual power from the VSC.

3.4.1. SIMULATION STUDIES

For integration of the PV, two different case studies are considered. The system (Fig. 3.2) parameters are given in Table 3.4.

CASE (A) LOAD SHARING IN THE PRESENCE OF PLUG AND PLAY PV:

The microgrid shown in Fig. 3.2, contains microturbine (MT) and diesel generator (DGEN) with the rating of 250 kW and 500 kW respectively. Together, they are supplying 500 kW load power, when the PV is connected at 5 s using synchronization method. It is assumed that the PV injects 150 kW power at upf. It is disconnected at 15 s. The results are shown in Fig. 3.20 and Fig. 3.21. It can be seen from Fig. 3.20 that the power sharing is in the ratio 1:2 even when the PV is connected. Also both power and frequency return to their initial states (before PV connection) once the PV is disconnected, as can be seen from these figures. This proves that the power sharing control scheme works effectively in the presence of plug and play DG. Also no frequency oscillation occurs since the VSC can effectively track PCC voltage for PV connection using synchronization method.

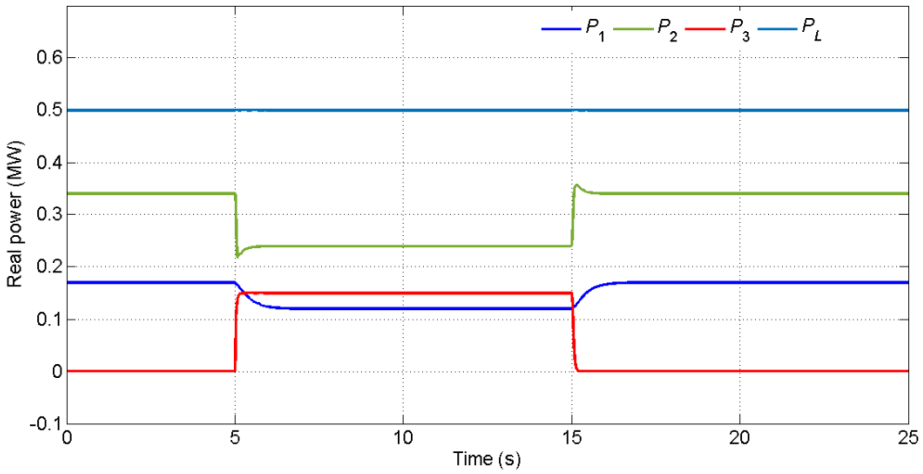

Fig. 3.20. Power sharing in presence of plug and play PV.

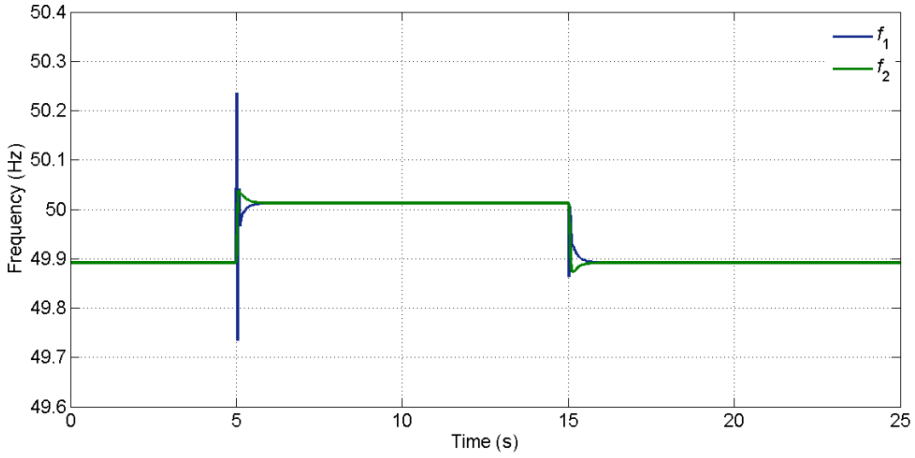

Fig. 3.21. Frequency variations in the presence of plug and play PV.

Table 3.4. System parameters considered in Fig. 3.2.

System Quantities	Values
DG_1 Feeder impedance	R_{f1} = 3.025 Ω, L_{f1} = 57.8 mH
DG_2 Feeder impedance	R_{f2} = 3.025 Ω, L_{f2} = 57.8 mH
DG_3 Feeder impedance	R_{f3} = 3.025 Ω, L_{f3} = 57.8 mH
DG Rated Power	PV: 150 kVA at unity power factor MT: 250 kW; DGEN: 500 kW

CASE (B) LOAD SHARING IN THE PRESENCE OF PLUG AND PLAY PV WITH LOAD VARIATION:

In this case also the MT and the DGEN supply 500 kW power initially when the PV, supplying 150 kW power, is connected at 5 s. Subsequently, the load power drops to 150 kW at 10 s. The load, PV, MT and DGEN powers are shown in Fig. 3.22. It can be seen from this figure that, since the PV generates the same amount of power as the load, the MT and DGEN generate almost negligible power. They only supply the line losses. Their frequencies are shown in Fig. 3.23, where they reach the no-load frequency of 50.3 Hz after load reduction. Also notice that the MT has a slightly faster response than the DGEN. These two responses however can be made exactly the same by tuning the inertia and damping parameters of the MT swing equation as discussed in Chapter 2.

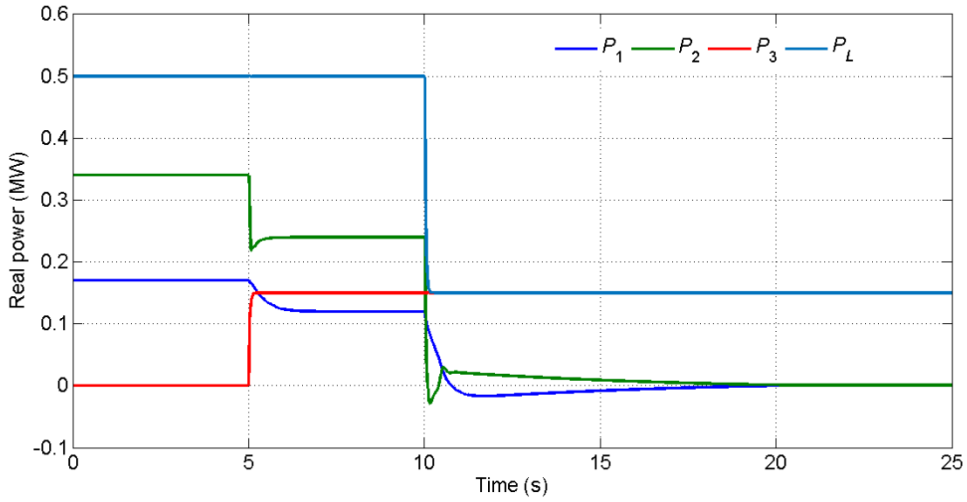

Fig. 3.22. Real Power sharing in case (B).

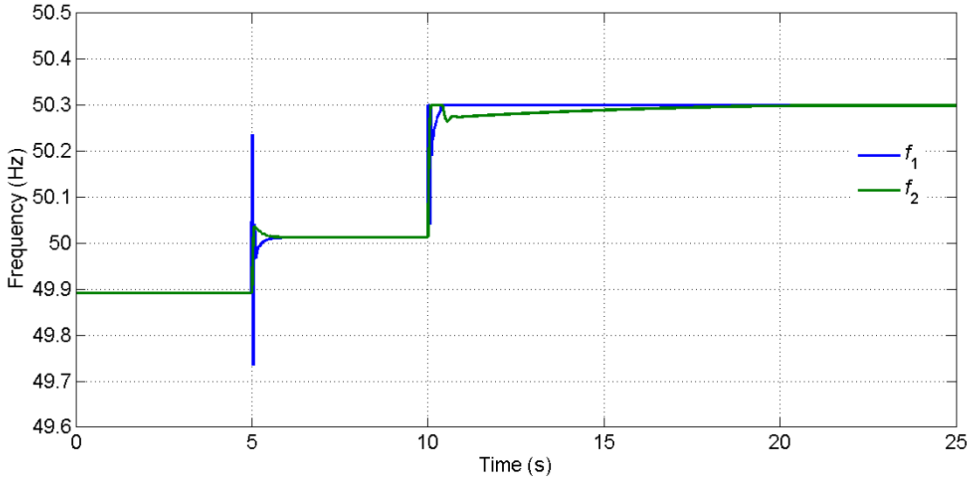

Fig. 3.23. Frequency variations in case (B).

3.5. CONCLUSION:

In this chapter, two different methods of integration of non-dispatchable DGs with a microgrid are proposed. The microgrid operates in frequency droop control. In the first method, an isochronous controller is used in which the droop line is shifted such that each DG supplies its required power at 50 Hz. The other approach is to synchronize the non-dispatchable DGs at the microgrid frequency. A simple synchronization method is proposed in which only measurements of the instantaneous PCC voltages are needed. Both these two proposed methods are validated through computer simulation using PSCAD/EMTDC. It has been shown that both of them work satisfactorily during load change and non-dispatchable DGs connection or disconnection with the microgrid. The operation is seamless where no large transient is visible.

CHAPTER 4

TECHNIQUES FOR BESS CONNECTION TO PREVENT OVERLOADING IN AN ISLANDED MICROGRID

For an autonomous microgrid, if total load demand plus losses exceed the combined available power of all DGs then overloading can occur. Thus, to maintain reliability, battery energy storage systems (BESSs) are viable options [115]. It has been shown in Chapter 3 that dispatchable DGs in an autonomous hybrid microgrid can share power in the ratio of their rating, even in the presence of plug and play of non-dispatchable DGs, under the assumption that the peak load demand is less than the total rating of the all dispatchable DGs. Since the non-dispatchable DGs are not operational all the time, the DGs size selection should be made in such a way that dispatchable DGs are able to meet the total peak power demand. This however is a difficult proposition since the peak load keeps on increasing. Resizing of existing DGs is not an option. Therefore every autonomous microgrid must be equipped with some storage devices that can quickly come online when peak load exceeds the total generation of DGs. However, the load shedding may be required in an autonomous microgrid, if there is not sufficient number of storage power available [64]. This scenario is however not considered in this thesis.

In this chapter, three control strategies are proposed for smooth transition of BESSs to prevent the overloading of distributed generators (DGs) in an autonomous microgrid.

4.1. SYSTEM STRUCTURE

Fig. 4.1 shows the structure of the autonomous microgrid under consideration, which contains DGs, loads and BESSs. The BESS normally floats at the microgrid bus neither consuming nor supplying power. It can then come online quickly without any substantial transient during any contingency. Since the main purpose is to provide power support during overloading in an autonomous microgrid through BESS, only two dispatchable sources are considered in the microgrid. The DGs supply a balanced load and share it in proportion to their respective ratings.

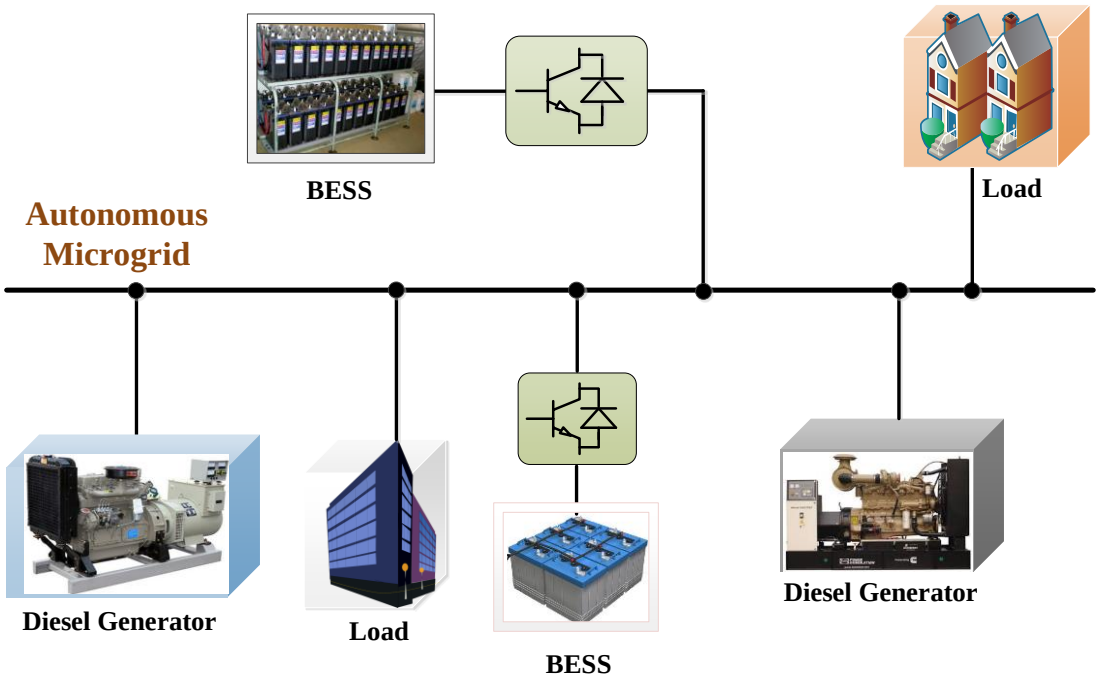

Fig. 4.1. System Structure.

4.2. Effect of DGs Overloading in an Autonomous Microgrid

DGs in the microgrid are controlled through a frequency droop, given by

$$\omega = \omega_r + m_f \times \left(0.5P^* - P\right) \tag{4.1}$$

Dispatchable DGs (inertial and non–inertial type) in an autonomous hybrid microgrid can share the power according to their rating using frequency droop control as already discussed in Chapter 2. However, if the load requirement is higher than the total rating of the DGs, there can be some catastrophic failure.

For example, let us consider the system of Fig. 4.2, where the DGEN-1 has a rating of 250 kW and the DGEN-2 has a rating of 500 kW. The droop parameters of the DGs are chosen such that the frequency excursion (f_d) is limited to ± 0.3 Hz from the nominal value of 50 Hz [92]. This means that when DGs supply zero power, the frequency will be 50.3 Hz and the frequency will become 49.7 Hz when DGs supply 750 kW.

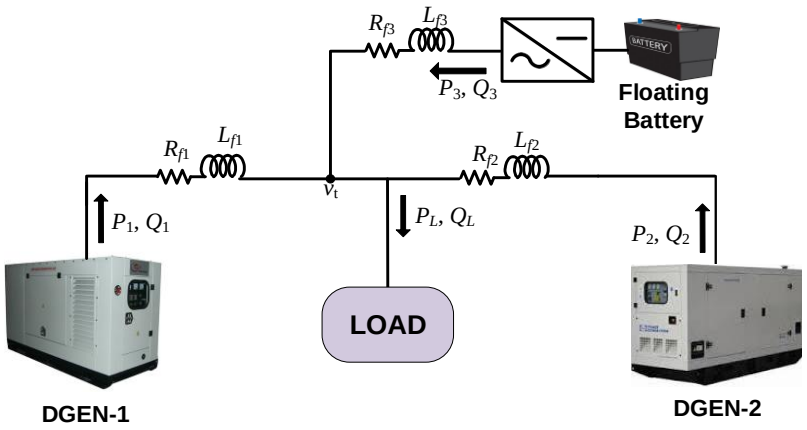

Fig. 4.2. The schematic diagram of the microgrid.

First let us assume that the total load demand is 700 kW and both DGs are supplying power according to their rating (i.e. 2:1). At 5 s, the load is increased by 150 kW, which is beyond the total rating of the DGs. It can be seen in Fig. 4.3 that due to their inertias, the DGENs start releasing their stored kinetic energy to support the load demand. However, the DGENs speeds, shown in Fig. 4.4, keep on dropping till 16.8 s, after which a catastrophic failure occurs. This causes voltage (shown in Fig. 4.5) to collapse and forces the powers to become zero (Fig. 4.3). It is to be noted that this behavior is shown for demonstration purpose. In practice however, the under frequency relays will trip the DGs much before the collapse can occur.

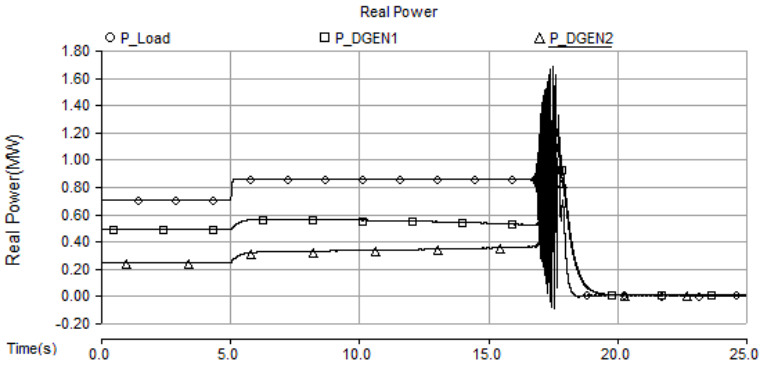

Fig. 4.3. Real power sharing between DGEN-1 and DGEN-2.

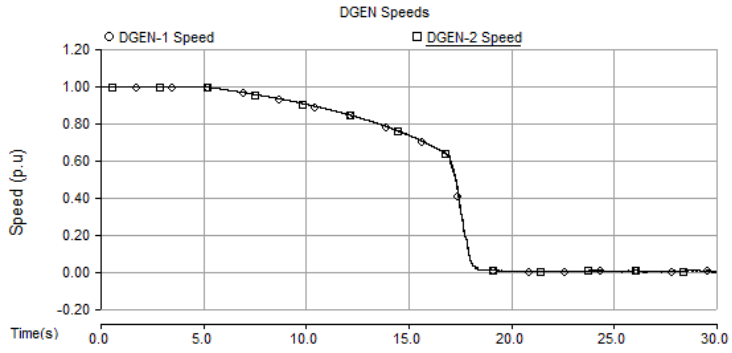

Fig. 4.4. Speed of DGENs during overloading.

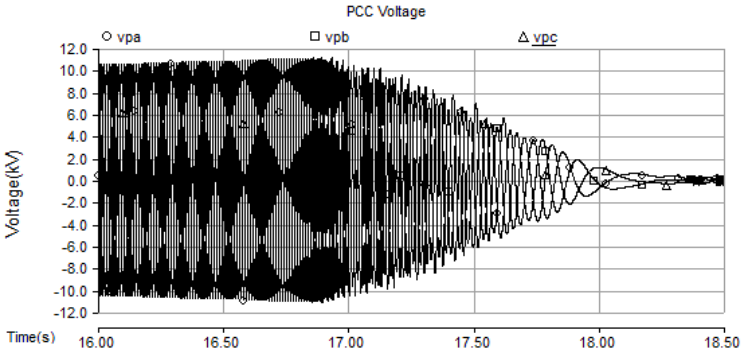

Fig. 4.5. PCC voltage during overload.

In an autonomous microgrid, system frequency differs from 50 Hz depending on the load. However, the frequency should not deviate more than frequency band (± f_d). With this band of frequency, proper droop gain of DGs can be chosen as discussed in Chapter 2. When the DGs are supplying their maximum available power, the frequency of the system hits to its lower limit (f_m). Since the maximum allowable frequency deviation (f_d) is chosen as 0.3 Hz, f_m = 50- f_d = 49.7 Hz. When the loads increase such that the microgrid frequency falls below f_m, storage devices must be switched on. In this chapter, only BESS as the storage option has been considered. Three different BESS operational strategies are proposed. These are

- BESS supplies a fixed amount of power.
- BESS supplies power under droop control.
- BESS supplies only that amount of power which cannot be supplied by the DGs.

4.3. BESS Operation to Supply Fixed Amount of Power

In this scheme, the BESS supplies its rated power and rest of the load demand is supplied by the DGs in the ratio of their ratings. This implies that, the droop frequency of the system will rise above the threshold value. As the battery turns on, it injects power at the same frequency of the system. Thus, battery should synchronize with respect to v_t (terminal voltage as shown in Fig. 4.2). For this purpose, the synchronisation algorithm is used as discussed in Chapter 3, Section 3.3.2.

When the load demand reduces, battery should be disconnected from the system. The turn off signal can also be generated from the frequency. The threshold

value of the frequency depends on the rating of the battery. Let us define, the balance between the DG rated power and BESS rated power as

$$P_{dg} = P_1^* + P_2^* - P_b^* \tag{4.2}$$

where P_1^*, P_2^* and P_b^* are rated real power of DG-1, DG-2 and BESS respectively. When the load demand plus losses are less than of P_{dg}, the battery can be turned off. This can be detected from the frequency of the system with a threshold calculated from Chapter 2.

4.3.1. SIMULATION STUDIES

Let us consider the microgrid structure which is shown in Fig. 4.2, DGEN-1 has a rating of 250 kW, while DGEN-2 is rated at 500 kW and BESS has a rating of 100 kW. The parameters of the microgrid are listed in Table. 4.1. Initially, the total load demand is 400 kW and both DGs are supplying power according to their rating in frequency droop control as shown in Fig. 4.6. At t = 5 s, the load is increased to 800 kW that exceeds the total power rating of the DGs. It can be seen from Fig. 4.7 that frequency of DGEN-1 hits to lower limit of the frequency band, which triggers the battery turn-on signal, as shown in Fig. 4.8. Thereafter, the battery starts supplying its rated power as can be seen in Fig. 4.6. The terminal voltage of the system is sinusoidal at BESS transition time, as shown in Fig. 4.9 and this shows a smooth seamless operation when the battery starts supplying power.

Table. 4.1. The parameters of the microgrid (Fig. 4.2).

System Quantities	**Values**
DG1 Feeder impedance	R_{f1} = 3.025 Ω, L_{f1} = 57.8 mH
DG_2 Feeder impedance	R_{f2} = 3.025 Ω, L_{f2} = 57.8 mH
DG_3 Feeder impedance	R_{f3} = 3.025 Ω, L_{f3} = 57.8 mH
DG Rated Power	DGEN-1: 250 kW, DGEN-2: 500 kW BESS: 100 kW
Droop Coefficient (Frequency–Voltage)	
m_1	0.015 rad/MWs
m_2	0.0075 rad/kWs
n_1	0.04 kV/MVAr
n_2	0.02 kV/MVAr

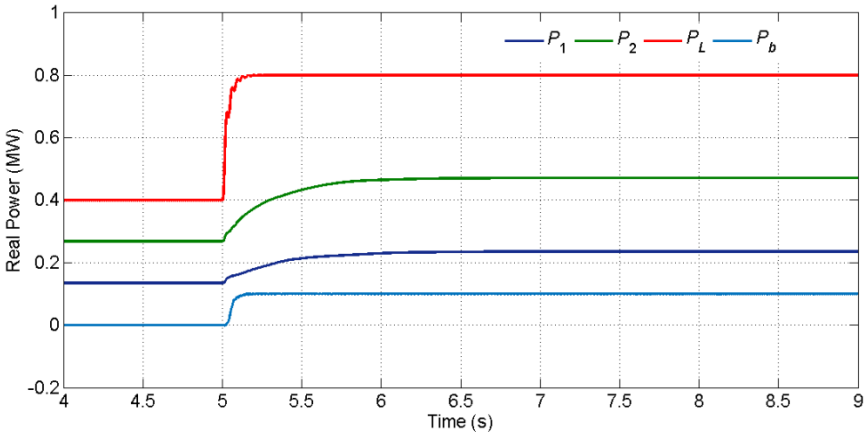

Fig. 4.6. Real power output of the DGs and load demand as battery connects (Fig. 4.2).

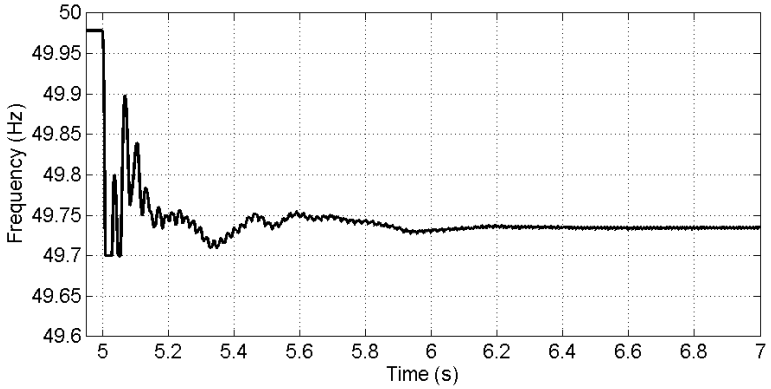

Fig. 4.7. Frequency variation of DG in autonomous microgrid (Fig. 4.2).

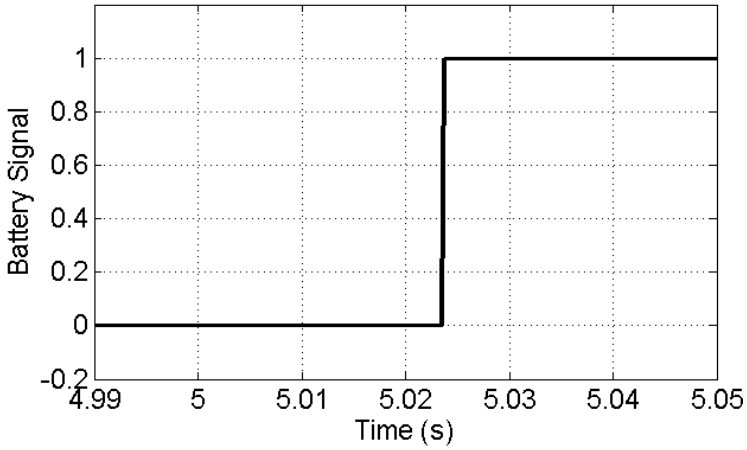

Fig. 4.8. Battery turn–on/off control signal (Fig. 4.2).

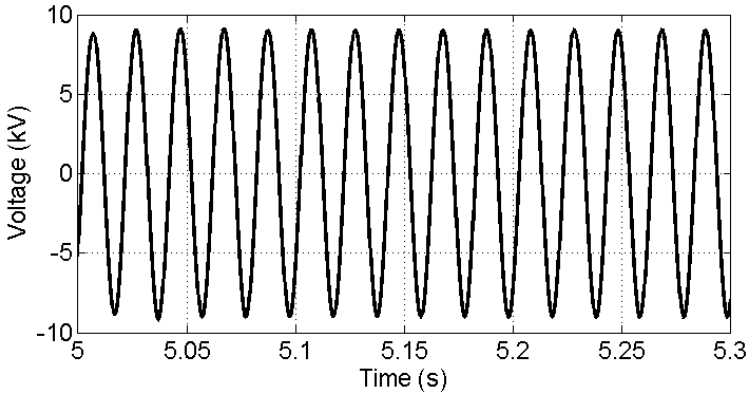

Fig. 4.9. BESS terminal voltage (Fig. 4.2).

At t = 10 s, the load demand reduces to 500 kW and it can be supplied by the DGs. The term P_{dg} then computed as from (4.2)

$$P_{dg} = 750 - 100 = 650\,\text{kW}$$

Since the rating of DGEN-2 is twice that of DGEN-1, the former must 2/3rd amount of the total power demand (P_{dg}), i.e., 2×650/3 = 433.33 kW. From this, the threshold value of the frequency to disconnect the BESS from the system can be calculated. Note that when DGEN-2 supplies 433.33 kW, the system frequency is

$$f_S = 50 + \frac{0.0075 \times (0.5 \times 500 - 433.33)}{2\pi} = 49.78\,Hz$$

Therefore, the system frequency falls below f_s, the load demand has reduced below total rating of the DGs. This is the trigger signal that the battery unit must be switched off. This is shown in Fig. 4.10. The power and frequency plots are shown in Fig. 4.11 and Fig. 4.12, respectively. From these figures, it can be seen that power supplied by battery is zero and other DGs supply load demand in frequency droop according to their rating. From Fig. 4.13, it can be seen that the terminal voltage of the system remains sinusoidal at the time of battery disconnection.

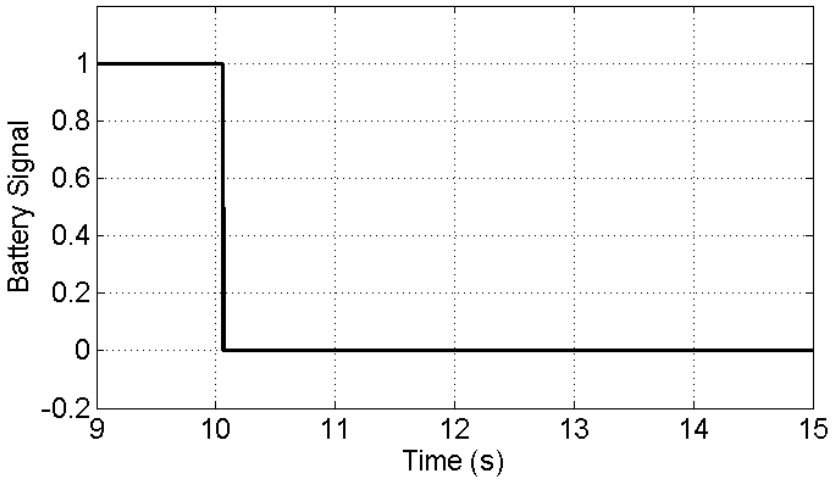

Fig. 4.10. Battery turn–on/off control signal.

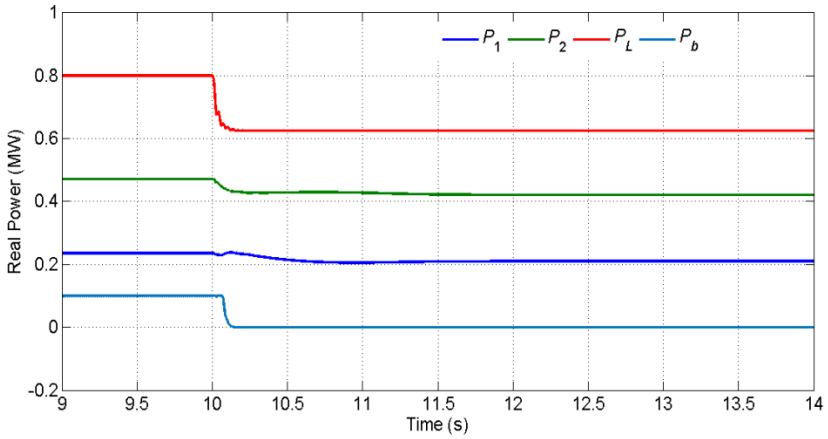

Fig. 4.11. Real power output of DGs and load demand as battery disconnects.

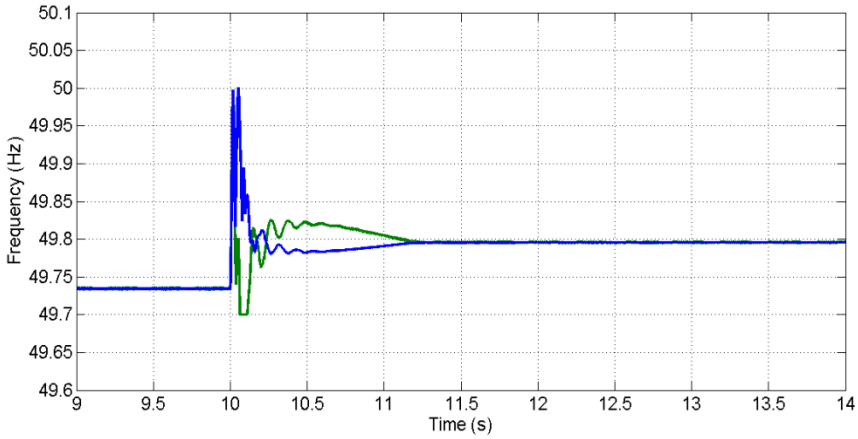

Fig. 4.12. Frequency variation of the DGs in autonomous microgrid.

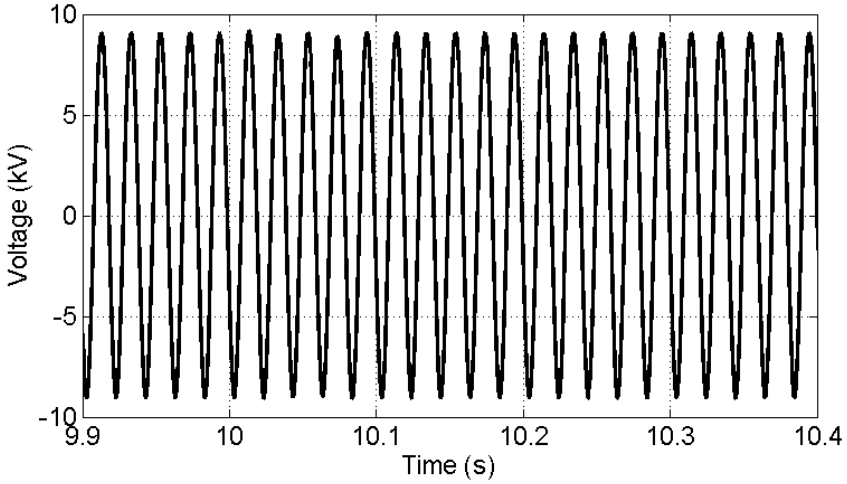

Fig. 4.13. BSU terminal voltage.

4.4. BESSs Operation in Frequency Droop control

In this schema, BESSs are connected in the microgrid during an overload to operate in the same frequency droop control as the dispatchable DGs operate. The schematic diagram of the microgrid is shown in Fig. 4.14 . The main purpose is to introduce the principle of BESS's power sharing during overload, therefore for simplicity two BESSs are considered. The droop coefficients for BESSs can be calculated in a same manner as for dispatchable DGs, as discussed in Chapter 2.

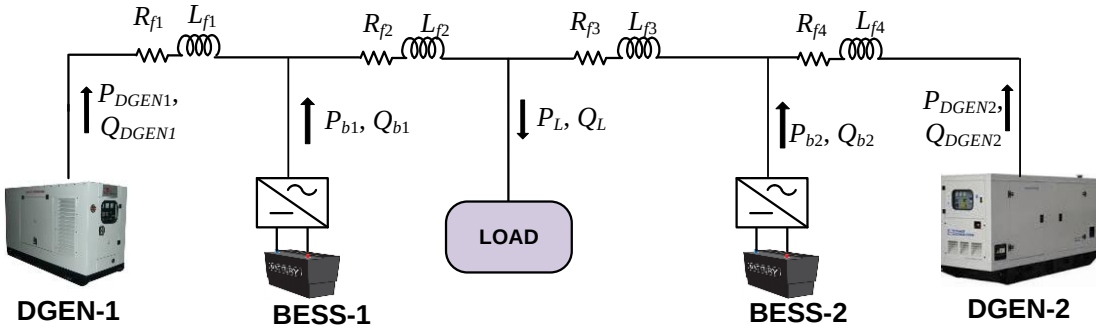

Fig. 4.14. Schematic diagram of the microgrid.

4.4.1. BESS Control

BESSs are the converter interfaced sources. The time response of BESS is faster than the DGENs. Therefore, pseudo inertia concept is used to slow down its response. This has been discussed in detail in Chapter 2, Section 2.6. The reference voltages of BESSs are calculated from (2.28), where frequency and angle are estimated from the swing equation and voltage magnitude is calculated from the voltage droop

control. The VSC structure and control used to track this reference voltage is discussed in Appendix A.

4.4.2. BESS TURN ON

In a microgrid, the load can be dispersed. Therefore if overload were to be detected by power consumption only, an aggregator and communication will be required. These may not be readily available. To avoid this, an algorithm is designed in which frequency is the triggering signal for overload protection. As mentioned before, the microgrid frequency excursion limit is ± f_d. Also it has been mentioned in (4.1) that if system frequency is f_m then DGENs operate at their rated power to supply local load plus losses. Also it can be seen from Fig. 4.3 that the DGs can supply an overload for over 16 s, according to available inertial source in a microgrid. This provides sufficient time for the BESSs to come online. The turn-on concept here is the same as that used in Section 4.3.

Once BESSs are turned-on, they operate in same frequency droop to supply power according to their current rated power rather than supplying fixed amount of power as in the previous case. This however will cause a shift in the frequency upwards as the DGs will reduce their power generation.

4.4.3. BESS TURN OFF

When the load demand reduces, BESSs should either be charged or come off from the grid. The turn off signal for BESSs can also be detected from the system frequency. The threshold value of frequency for turn-off signal depends on the power sharing ratio of the sources. In the microgrid (Fig. 4.14), the maximum rated power of DGEN-1, DGEN-2, BESS-1 and BESS-2 respectively are 500 kW, 250 kW, 50 kW and 100 kW. Therefore the power sharing ratio of BESS-1: BESS-2: DGEN-2: DGEN-1 is 1:2:5:10. Let us now assume that the load demand has dropped to or below 750 kW when the over loading condition is over. The BESSs still keep on supplying power as they share power in droop. Obviously, the BESSs should cut off when the load reduces to 750 kW or less. During this time, DGEN-1 supplies (10/18) × 750 kW. Therefore the frequency of DGEN-1 for this level of power supply is

$$f_{th} = 50 + \frac{0.0075 \times (0.5 \times 500 - 416.66)}{2\pi} = 49.80\ Hz \tag{4.3}$$

If the load demand is less than 750 kW, or system frequency will be less than f_{th}. In this case, BESSs are not required in system to supply load demand. Therefore, f_{th} is considered to be the threshold value of frequency to turn off the BESS. Also note that once the BESSs are switched off, the system frequency may fall below f_{th}.

4.4.4. BATTERY CHARGING STRATEGY

BESSs can be charged from DGs during the off peak times for their use during peak load event. We know that when the frequency is 50 Hz, DGs supply half of their rated power. Therefore, when the system frequency is 50 Hz or more, the microgrid load demand is half or less than half of its total capacity. This can be defined as off-peak time. Therefore, the BESSs can be charged when the frequency is 50 Hz or above.

4.4.5. SIMULATION STUDIES

In this section, three case studies are presented for the system of Fig. 4.14.

CASE (A): BSU CONNECTION

Let us consider the microgrid structure shown in Fig. 4.14. The parameters of the microgrid are listed in Table. 4.2. It is assumed that the microgrid is operating stably at beginning and supplying 550 kW load power. DGENs share load power according to their rating (i.e. 2:1). The load demand increases at 1.0 s to 800 kW, which is higher than the total rating of DGENs and therefore BESS are turned-on. The swing parameters of the BESSs are listed in Table 4.3. The real powers are shown in Fig. 4.15. The frequencies are shown in Fig. 4.16. It can be seen that the frequencies of all the units merge in the steady state. Since the load demand is now less than the total capacity of the DGENs and BESS, the frequency is higher than the lower threshold of 49.7 Hz. The PCC (load bus) voltages are maintained sinusoidal as shown in Fig. 4.17.

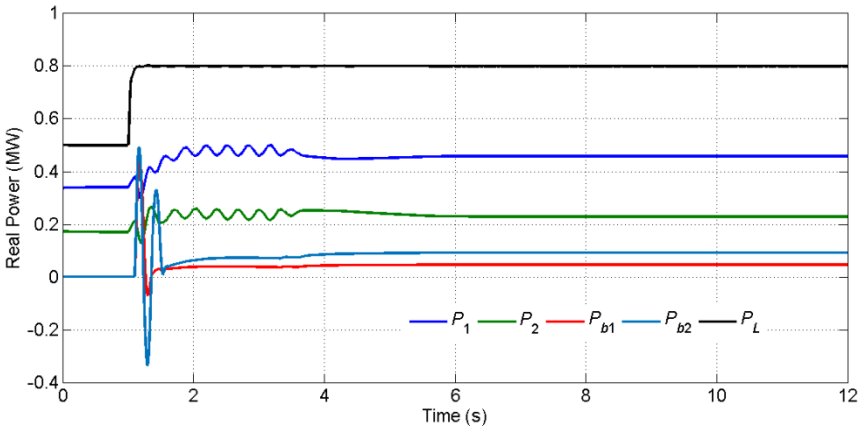

Fig. 4.15. Real power sharing in microgrid with BESSs.

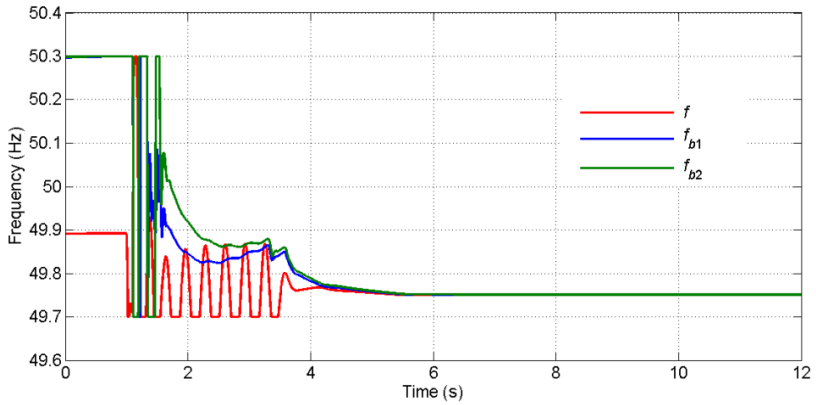

Fig. 4.16. Frequencies of BESSs and DGEN.

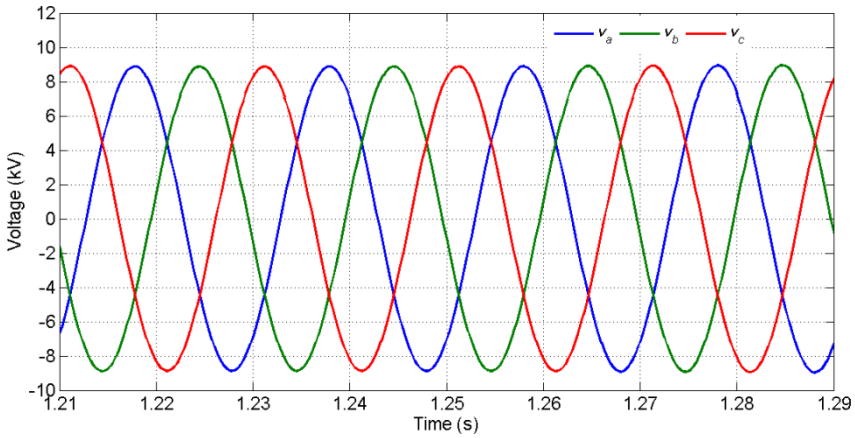

Fig. 4.17. PCC voltage.

CASE (B): BESS DISCONNECTION

In this case, the load reduces by 100 kW. This is shown in Fig. 4.18. Even though DGENs together can supply the load demand, BESSs still remain connected, as can be seen from this figure. The frequencies of the DGEN-1 and the two BESSs are shown in Fig. 4.19. The system frequency reaches 49.82 Hz ($\approx f_{th}$) at around 13.8 s, at which point, BESSs are turned off.

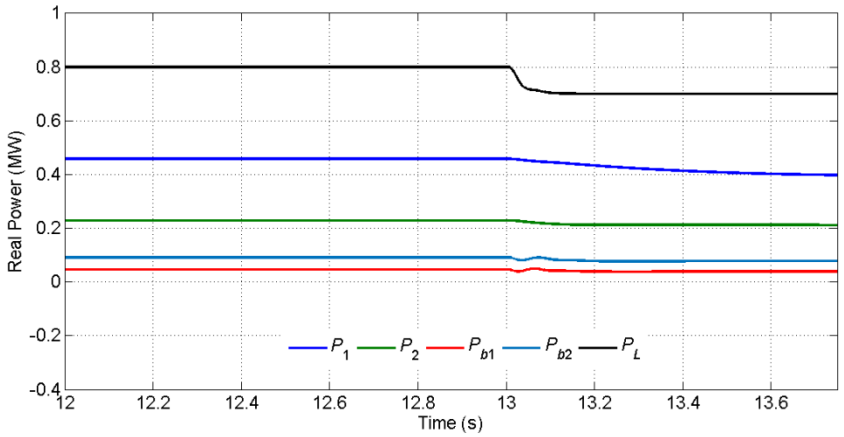

Fig. 4.18. Real power sharing in microgrid with BSUs.

The real powers when BESSs turn off are shown in Fig. 4.20. It can be seen when they turn off, the powers supplied by the DGENs increase. The frequencies of the DGEN-1 and the two BESSs are shown in Fig. 4.21. It can be seen that the BESS frequencies hit the upper limit as they are not supplying any power. The PCC voltages at the point of BESS disconnection are shown in Fig. 4.22. Since they do not undergo any large transient or sag/swell, it can be surmised that the BESSs disconnection is seamless.

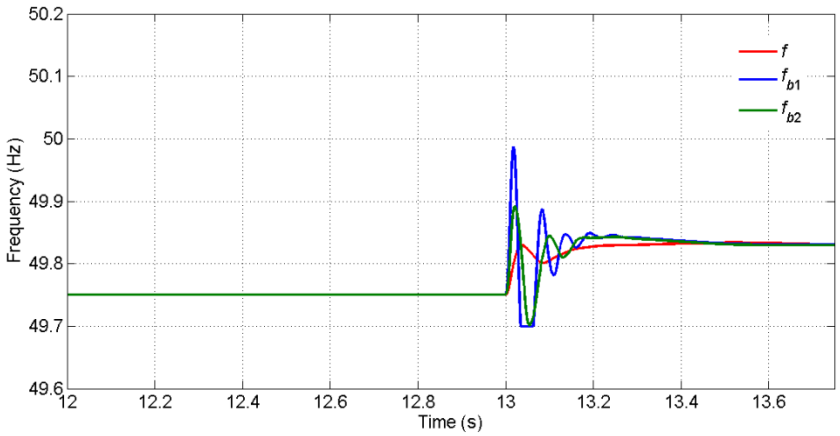

Fig. 4.19. Frequencies of BSUs and DGEN.

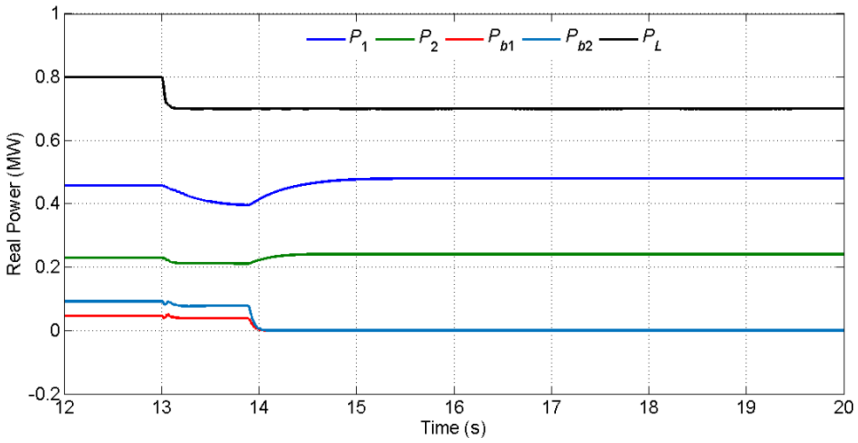

Fig. 4.20. Real power flow when BSUs are disconnected.

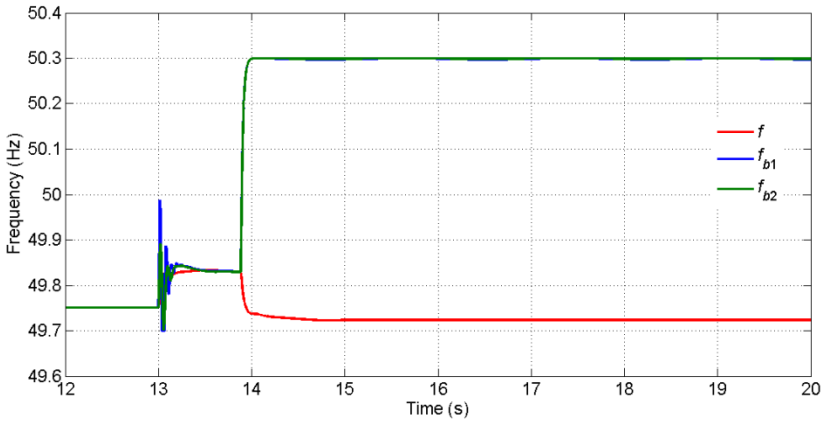

Fig. 4.21. Frequencies of BSUs and DGEN.

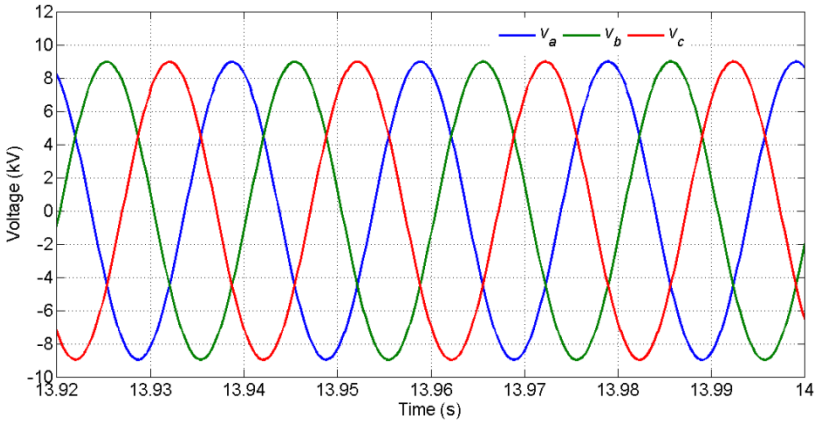

Fig. 4.22. PCC voltage.

CASE (C): BESS CHARGING

A case is considered when microgrid load is off peak. In Fig. 4.23, it is shown that load demand is 250 kW, where both DGENs are supplying power less of their half of rated and the system frequency is greater than 50 Hz. It is shown in Fig. 4.24. Therefore, at 5 s, BESSs are connected to the microgrid for charging. It can be seen

from Fig. 4.23 that both BESS powers are negative, indicating BESSs are drawing power. This causes the system frequency to reduce as can be seen in Fig. 4.24.

Table. 4.2. The parameters of the microgrid (Fig. 4.14).

System Quantities	**Values**
DG_1 Feeder impedance	R_{f1} = 3.025 Ω, L_{f1} = 57.8 mH
DG_2 Feeder impedance	R_{f2} = 3.025 Ω, L_{f2} = 57.8 mH
DG_3 Feeder impedance	R_{f3} = 3.025 Ω, L_{f3} = 57.8 mH
DG Rated Power	DGEN-1: 500 kW DGEN-2: 250 kW
BESSs Rating	BESS-1: 50 kW BESS-2: 100 kW
Droop Coefficient (Frequency–Voltage)	
m_1	0.0075 rad/MWs
m_2	0.015 rad/kWs
m_{b1}	0.075 rad/MWs
m_{b2}	0.15 rad/kWs
n_1	0.02 kV/MVAr
n_2	0.04 kV/MVAr

Table. 4.3. Swing equation parameters for BESSs.

System data	**Value**
Damping constant (K_{D1})	5 MWs/rad
Inertia constant (H_1)	2 MJ/MVA
Damping constant (K_{D2})	2.5 MWs/rad
Inertia constant (H_2)	1 MJ/MVA

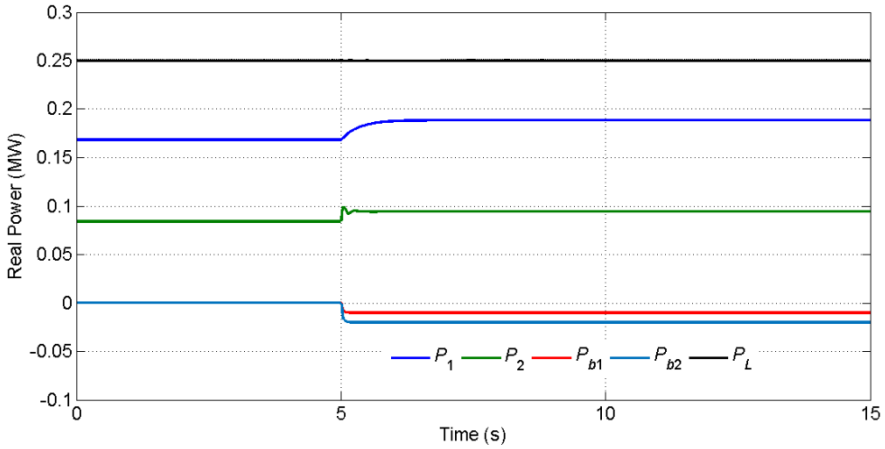

Fig. 4.23. Off peak load power and BSUs charging.

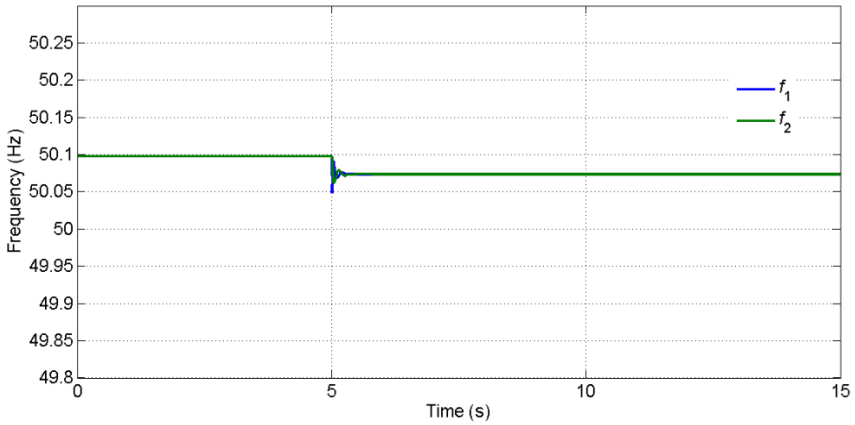

Fig. 4.24. Frequencies of DGEN-1 and DGEN-2.

4.5. BESS OPERATION TO SUPPLY ONLY OVERLOAD POWER

Usually a BESS is expensive and its life time can be shortened by several charge/discharge cycles. Therefore such a unit must come online only when required and must supply only the amount of power that cannot be supplied by DGs in an autonomous microgrid. Normally, the microgrid operates in frequency droop control. To prevent any overloading, if the BESS is also controlled in the same frequency droop control as DGs, it will share the load power with the existing DGs according to its rating, thereby failing to supply only the required excess power. Therefore, DGs will not be utilized to their maximum capacity and BESS will discharge faster. Therefore it might be completely discharged if the overload persists longer. Also note that when more than one BESS is used for overload prevention, they should be optimally utilized such that each of unit shares power in accordance to its current state of charge (SOC). To achieve this objective, BESS operates in angle droop control to fill the gap in between power generation and load, when the generation of the two DGENs is at its maximum. The microgrid structure is shown in Fig. 4.25.

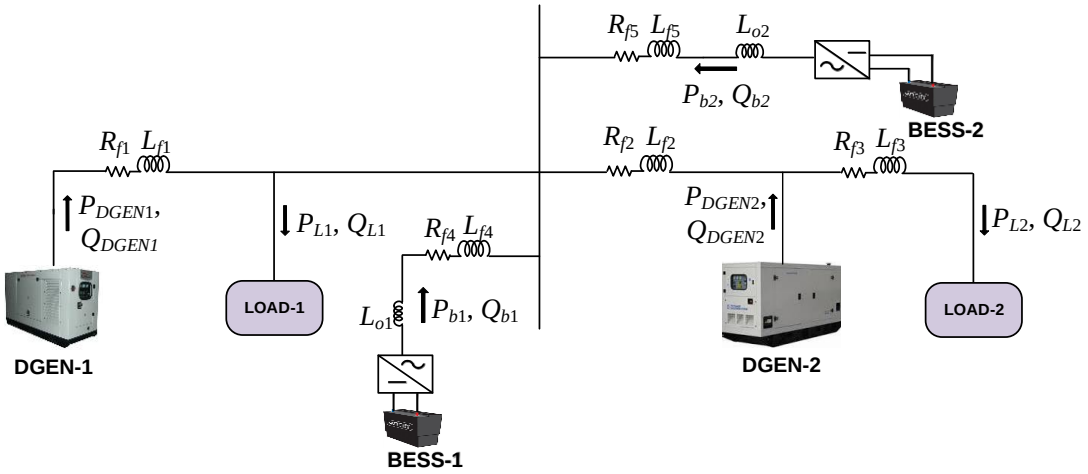

Fig. 4.25. Microgrid Structure.

4.5.1. DYNAMIC BRIDGING THROUGH BESS

As mentioned before, BESSs are used to reduce the gap between load and generated power. Therefore the BESS acts as a bridge to meet the load requirement and hence this type of BESSs utilisation is termed as dynamic bridging. Through this process, the BESSs can prevent both system collapse and load shedding, thereby enhancing the overall system performance.

Therefore the overload detection plays a vital role in this process. This detection is carried out in the following manner.

1) A lower threshold of f_{th} is chosen, to be is slightly higher than f_m. When the droop frequency hits this threshold, both frequency droop controllers operate at minimum frequency f_m and a trigger signal (t_{ON}) is generated. This trigger signal is used to command the BESSs to start supplying power.
2) The BESSs generate the power that is required to meet the shortfall under an angle droop control. The generation of the reference angle for this operation is discussed in the next section.

Once the BESSs start supplying power, they continue to do so till the overload is removed. The BESSs can be switched off when the power through them reverses. Consider the situation when a BESS is supplying the excess power demand and the load demand reduces below the maximum generation limit. Both the DGENs still supply a fixed amount of power with a fixed frequency of f_m. Therefore the excess generation will flow towards the BESS. From the angle droop discussed in Chapter 2, it can be seen that the BESS voltage angles will reduce and the BESSs will start

receiving power. When the power through BESSs reverses, the frequency droop automatically reverts back within specified limits. When this occurs, the BESSs are switched off. The flowchart of Fig. 4.26 explains this operation. Note that the BESSs can be charged when the system frequency is greater than 50 Hz, since the load demand is less than the half of the total capacity of the system during this time. The charging process of BESS is not discussed.

4.5.2. PROPOSED DYNAMIC BRIDGING CONTROL STRATEGY

When the load power exceeds the maximum limit of the two DGs, the excess load power is supplied through dynamic bridging BESS units. It has been shown in Chapter 2, Section 2.2.1, how two BESS units operate in an autonomous mode assuming a constant system frequency of 50 Hz, in which the reference angle is irrelevant and can be chosen arbitrarily. However, when they are connected for overloading prevention, they cannot operate at 50 Hz. Also, each BESS needs to be synchronized with the bus to which it is connected and its reference angle has to be determined depending on the prevailing system conditions as discussed below.

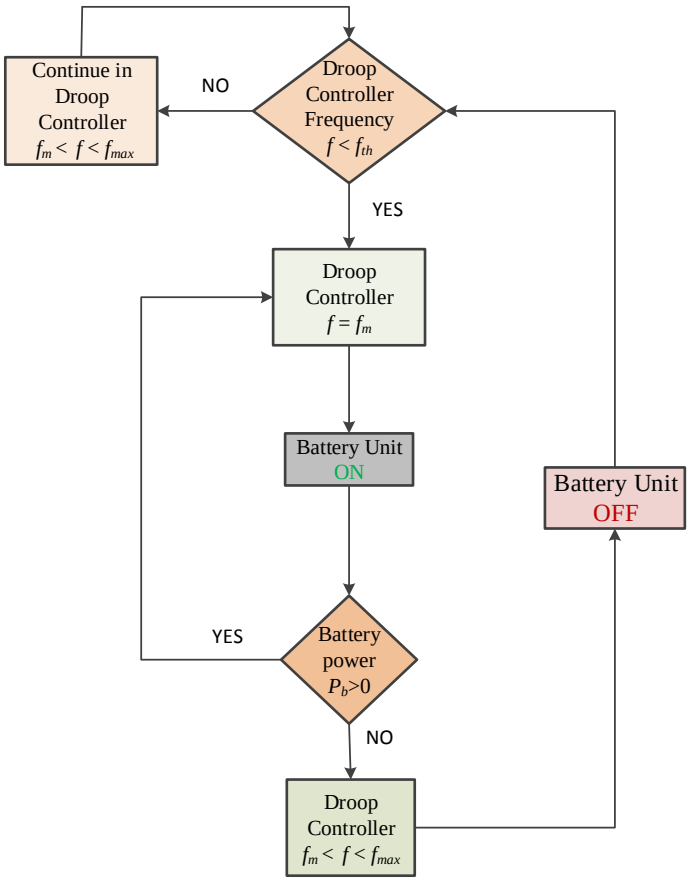

Fig. 4.26. Flowchart showing BESS connection and disconnection.

4.5.2.1. GENERATION OF REFERENCE ANGLE

When an overloading occurs, the system frequency keeps on dropping. Therefore the BESS should be synchronised with the system so as to inject power at the same frequency. Also, the reference angle of the BESS output voltage cannot be chosen arbitrary when it is connected in parallel with a strong source (like DGEN). One approach for this reference angle calculation is discussed below. One way of determining the reference angle is from a strong source in the system.

The DGEN is the strong source in the microgrid system of Fig. 4.25. The reference angle for BESSs is calculated with maintaining the power flow from the DGEN constant at its rated power. To achieve this, a PID controller is employed, which takes the error e between the rated DGEN power (P^*_{DGEN}) and the actual output power (P_{DGEN}). The output of the PID controller is the reference angle δ_b^*, given by

$$\delta_b^* = \left(K_P + \frac{K_I}{s} + K_D\, s \right) e \tag{4.4}$$

where

$$e = P^*_{DGEN} - P_{DGEN}$$

This reference angle (δ_b^*) is used in angle droop to calculate angle (δ_b) of BESS as

$$\delta_b = \delta_b^* + m_b \times \left(P_b^* - P_b \right) \tag{4.5}$$

where P_b^* and P_b are the rated and measured actual real power of BESS respectively. The droop coefficient is denoted by m_b.

4.5.2.2. DYNAMIC INTEGRATION

It has been mentioned in the previous sub-section that in order to avoid any large transient due to BESS connection, it needs to be synchronized at the system frequency with phase angle difference of (δ_b) to supply only the excess amount of power. To achieve this, a simple algorithm based on instantaneous symmetrical component theory is used as discussed in Chapter 3, Section 3.3.2.

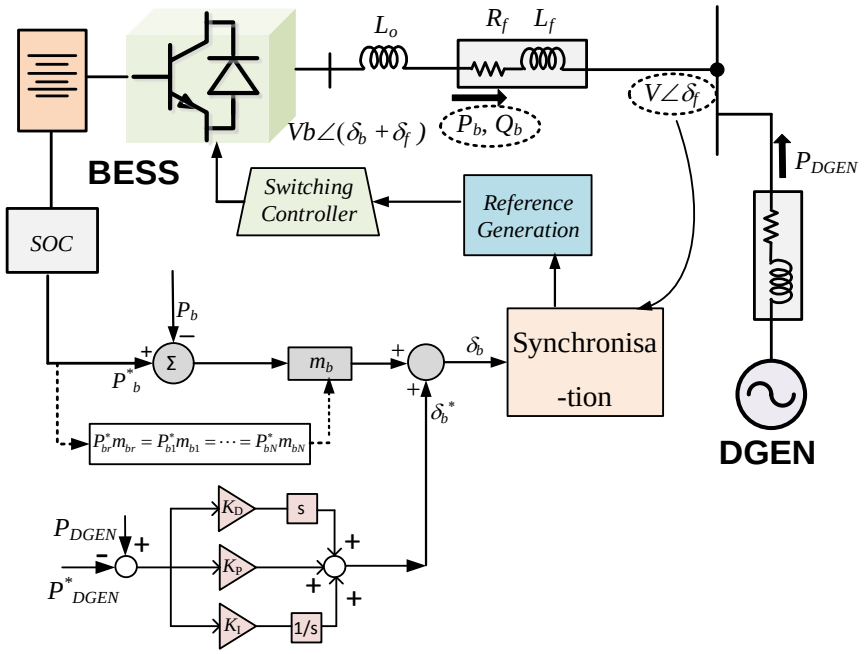

Fig. 4.27. Schematic diagram of a BESS connected to the microgrid.

Consider the system shown in Fig. 4.27 in which $V\angle\delta_f$ is the bus voltage to which a BESS is connected. The system frequency is unknown. The BESS injects at voltage $V_b\angle(\delta_f+\delta_b)$, where V_b is pre-specified voltage magnitude and δ_b is the angle obtained from angle droop (4.8). The positive sequence of BESS output voltage is obtained using δ_b from (3.16). Once positive sequence is calculated, negative sequence is also calculated by taking complex conjugate of it. The system is balanced, therefore zero sequence component is zero. Hence, using inverse symmetrical component transform, the three-phase instantaneous reference voltages required from BESS can be computed without explicit frequency measurements.

4.5.3. SIMULATION STUDIES

In this section, three case studies are presented for the system of Fig. 4.25.

CASE (A): BESS CONNECTION

Two different loads, Load -1 and Load-2 are considered. At the beginning Load-1draws a power of 400 kW, while the *R-L* Load-2 draws 120 kW. The total load demand is less than the maximum available power from DGENs. Therefore, BESS converter switches are blocked and both DGENs supply power according to their rating in frequency droop control. At 1 s, Load-1 is increased to 680 kW such that total load demand becomes 800 kW, which exceeds the total rating of DGENs. As a

consequence, the droop frequency reaches the lower threshold of 49.7 Hz, as evident from Fig. 4.28. It generates the trigger signal B_{Trig} ON as shown in Fig. 4.29. Thereafter, BESSs start supplying the excess power requirement of the system under angle droop control while sharing power according to their rating. This is shown in Fig. 4.30, where DGENs supply their maximum rated power.

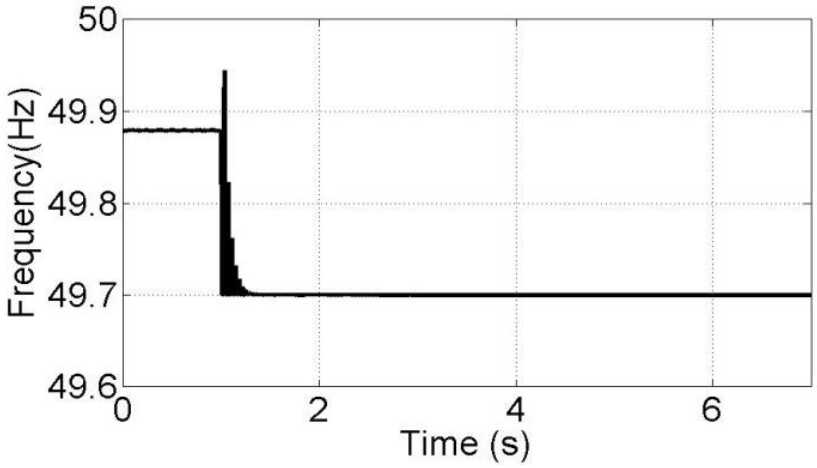

Fig. 4.28. Frequency variation during overload.

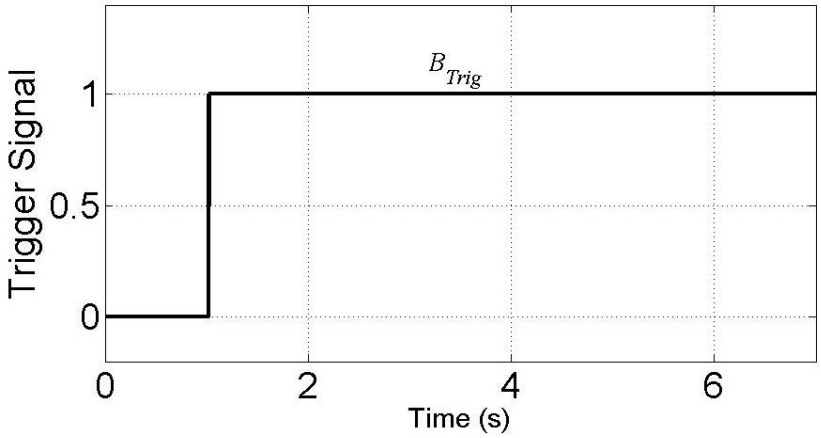

Fig. 4.29. Triggering signals for BESS and droop controller.

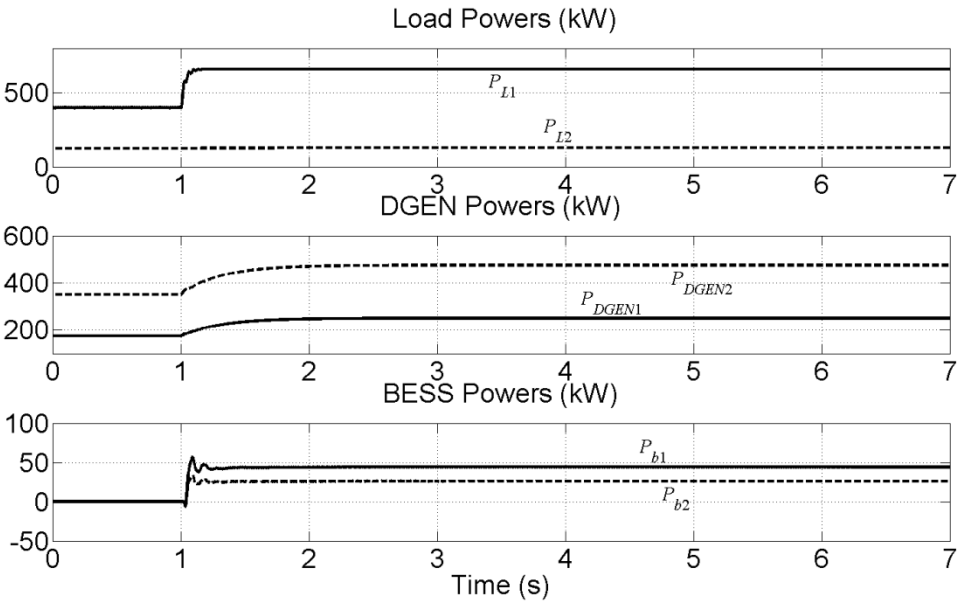

Fig. 4.30. Power flow in microgrid during overload with dynamic bridging.

CASE (B): LOAD VARIATION WHEN BESSS ARE CONNECTED

At 8 s, the load demand is further increased to 820 kW. It can be seen from Fig. 4.31 that both DGENs still supply their maximum rated power and this increased amount of power is supplied by BESSs. However, the system frequency does not vary from 49.7 Hz, as is evident from Fig. 4.32.

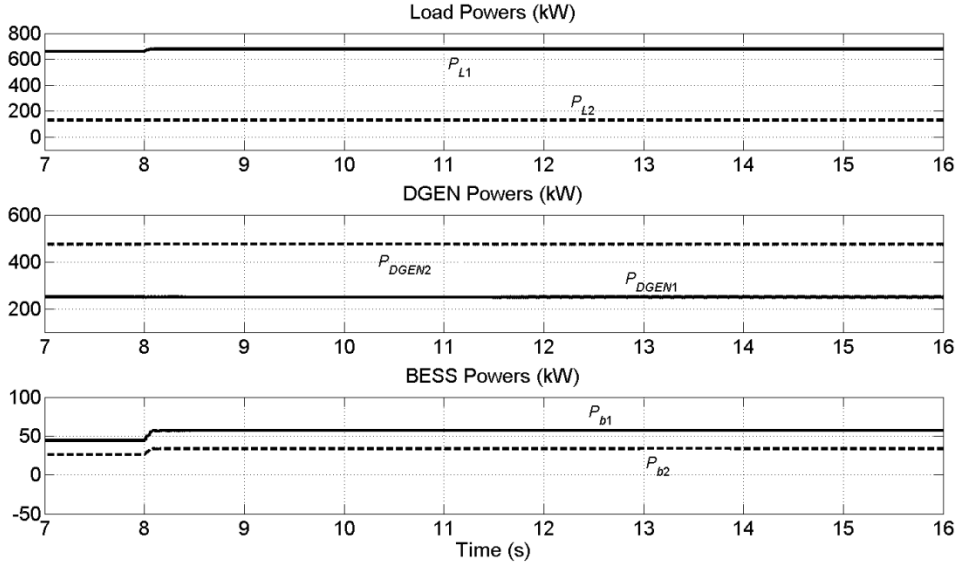

Fig. 4.31. Power flow in microgrid during further increase in overload.

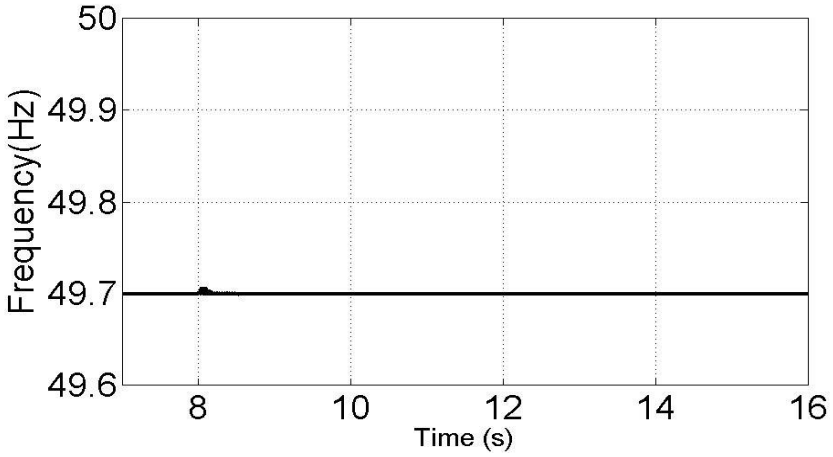

Fig. 4.32. System frequency during overload change.

CASE (C): BESS DISCONNECTION

At 16 s, the consumption of Load-1 is brought back to its nominal level of 400 kW. However both DGENs still supply their maximum rated power. Therefore the excess power that loads do not require will start flowing towards the batteries. The speciality of angle droop (4.8) is that it can work irrespective of the direction of the power flow. As a result, BESSs will start consuming power according to their ratings. The negative power flow to any or both BESSs is used to deactivate B_{Trig}, which will switch BESS units off. The load, DGEN and BESS powers are shown in Fig. 4.33. It can be seen that the BESS power becomes zero indicating that only DGENs are supplying the load demand. The frequency recovers to its nominal value as shown in Fig. 4.34.

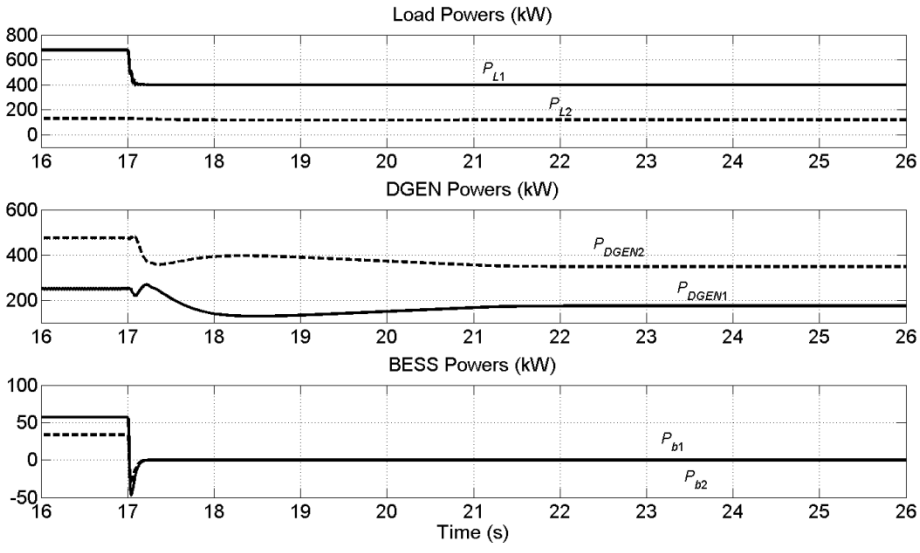

Fig. 4.33. Power flow in microgrid when overloading is removed.

Table. 4.4. The system parameters of microgrid (Fig. 4.25).

System Quantities	**Values**
Feeder impedance	R_{f1} = 3.025 Ω, L_{f1} = 57.8 mH R_{f2} = 3.025 Ω, L_{f2} = 57.8 mH R_{f3} = 3.025 Ω, L_{f3} = 57.8 mH R_{f4} = 3.025 Ω, L_{f4} = 57.8 mH R_{f5} = 3.025 Ω, L_{f5} = 57.8 mH
DGENs rated power	DGEN-1: 250 kW, DGEN-2: 500 kW
BESS rated power	Battery-1: 100 kW, Battery-2: 50 kW
Load-2	R_{La}=1000 Ω, L_{La}= 100 mH R_{Lb}=1000 Ω, L_{Lb} = 100 mH R_{Lc}=1000 Ω, L_{Lc} = 100 mH
Droop Coefficient (Frequency–Voltage)	
m_{f1}	0.015 rad/MWs
m_{f2}	0.0075 rad/kWs
n_{f1}	0.04 kV/MVAr
n_{f2}	0.02 kV/MVAr
Droop Coefficient (Angle Droop)	
m_{b1}	0.4 rad/MWs
m_{b2}	0.8 rad/MWs

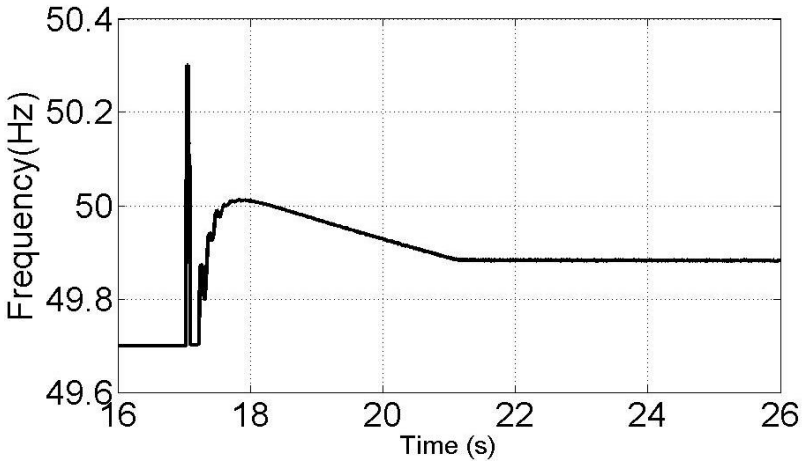

Fig. 4.34. System frequency when overloading is removed.

4.6. CONCLUSION

To prevent overloading during an autonomous operation, energy storage devices are brought online quickly. Three different methods of overload prevention are discussed in this chapter. These algorithms facilitate smooth transition of BESS in microgrid and power sharing algorithm also works perfectly either when BESS is

connected or disconnected. In the first method, BESS supplies its rated power and rest amount of load power is supplied by the available DGs in the microgrid. BESSs are smoothly synchronized with the microgrid using the algorithm discussed in Sub-section 3.3.2. In this only the measurements of the instantaneous three-phase voltages at the point of connection are required, irrespective of the microgrid frequency. In this way, large system transients are avoided at a time when the system is already stressed. This first method has limitation of providing only fixed amount of power for overload prevention and in this method, DGs are also not operated at their maximum capacity.

In the second method, various BESSs can be considered. For simplicity, only two BESSs are considered here. These BESSs share load power with available DGs in the microgrid rather than only supplying rated power. In this case, BESSs share the load power according to their ratings, also note that BESSs even share power with DGs. Therefore, DGs are not used at their maximum rate.

In third method, BESS operates in such a way that it supplies only the excess amount of power to prevent the overloading. Also note that when more than one BESS is used for overload prevention, they should be optimally utilized such that each of unit shares power in accordance to its current state of charge. To achieve this, BESSs operates in angle droop control. Ordinarily, the switches of BESS units are blocked and are unblocked depends upon receiving signal that an overloading in the system has occurred. They are switched off when the power flowing through them reverses polarity. Also note that if the BESS capacities are sufficient and if the overloading does not persist for a long time, no load shedding will be required.

CHAPTER 5

IMPROVING POWER QUALITY IN AN ISLANDED MICROGRID

Many industrial and domestic loads use switch mode power supplies, which generate harmonics. Propagation of harmonics in power system has been studied for a long time. Usually harmonics generated by a load can impact other loads connected to the same system. However in case of islanded microgrid, such loads can affect the performance of the synchronous generators. These deleterious effects of distorting loads can be corrected using a distribution static compensator (DSTATCOM).

A microgrid, which contains a group of parallel inverters with linear and non-linear loads, techniques for power sharing with non-linear loads have been discussed in [116-117]. These techniques enable the equal sharing of linear and non-linear loads. If a microgrid consists of inertial generators (e.g. diesel generators) that supply non-linear loads, harmonic current will flow through the armatures of the generators [118]. This will distort the armature reaction, leading to voltage distortion affecting output power. It will also lead to electromagnetic torque pulsation, generating heat and reducing the life of the generators [119, 120]. Therefore, to improve the power quality, capacity, reliability and redundancy, various custom power devices are being used [121]. A DSTATCOM can be used to eliminate load harmonics, as well as, for voltage regulation [122].

If an islanded microgrid operates in a frequency droop control to share the power according to available DGs, the frequency of the microgrid can vary within a specified limit. To mitigate the harmonics in an islanded microgrid, the DSTATCOM must operate at the same frequency of the microgrid. Therefore, in this chapter two different strategies are proposed as: 1) Synthesis the DSTATCOM voltage at the actual system frequency and 2) Maintain the frequency of microgrid at set reference value of 50 Hz through isochronous controller.

5.1. SYSTEM STRUCTURE AND CONTROL

The schematic diagram of the microgrid is shown in Fig. 5.1. It contains a diesel generator (DGEN) and a converter interfaced distributed energy resource

(DER). The diesel generator set consists of a 4-stroke internal combustion (IC) engine coupled to a synchronous generator. The IC engine speed is controlled through the fuel input rate by a speed governor. A PID controller is used in the governor to maintain output speed. The automatic voltage regulator (AVR) controls the field supply of the generator to maintain the required terminal voltage. The DER uses a voltage source converter (VSC) which is a three phase, three leg converter with 6 switches. Each switch is an insulated gate bipolar transistor (IGBT) with proper snubber circuit and anti-parallel diode. An LCL (T) filter is used with VSC to couple with the microgrid. The detailed operation and control of VSC is discussed in Appendix A and detailed model of DGEN is discussed in Chapter-2. The feeder with resistance of R_{fi} and inductance L_{fi}, $i = 1, 2$ are considered in Fig. 5.1. The load consists of a linear passive R_L-L_L component and a nonlinear component (uncontrolled rectifier). The microgrid operates in frequency droop control as discussed in Chapter-2, Section 2.2.3. Note that in the frequency droop, half the rated power is used such that the frequency can vary ± 0.5 Hz from the fundamental frequency of 50 Hz. The droop coefficients are chosen accordingly to restrict the frequency variation to within these specified limits.

The DSTATCOM is connected at the point of common coupling (PCC) of the load with the feeder. The DSTATCOM used in this research is a transformer-less three-phase three-leg DSTATCOM which consists of six switches. Each switch in VSC is an insulated gate bipolar transistor (IGBT) along with a snubber circuit and an anti-parallel diode. It is supplied from a dc storage capacitor (C_{dc}). Also an LC filter (L_f-C_f) is connected at the output of the VSC to suppress high frequency switching harmonics.

The main aim is to regulate the PCC voltage against any variation in the load. The load can be unbalanced and non-linear. Let the desired three-phase PCC voltage be given by

$$\begin{aligned} v_{Ta}^{*} &= |V_T|\sin(\omega t + \delta) \\ v_{Tb}^{*} &= |V_T|\sin(\omega t + \delta - 120^\circ) \\ v_{Tc}^{*} &= |V_T|\sin(\omega t + \delta + 120^\circ) \end{aligned} \tag{5.1}$$

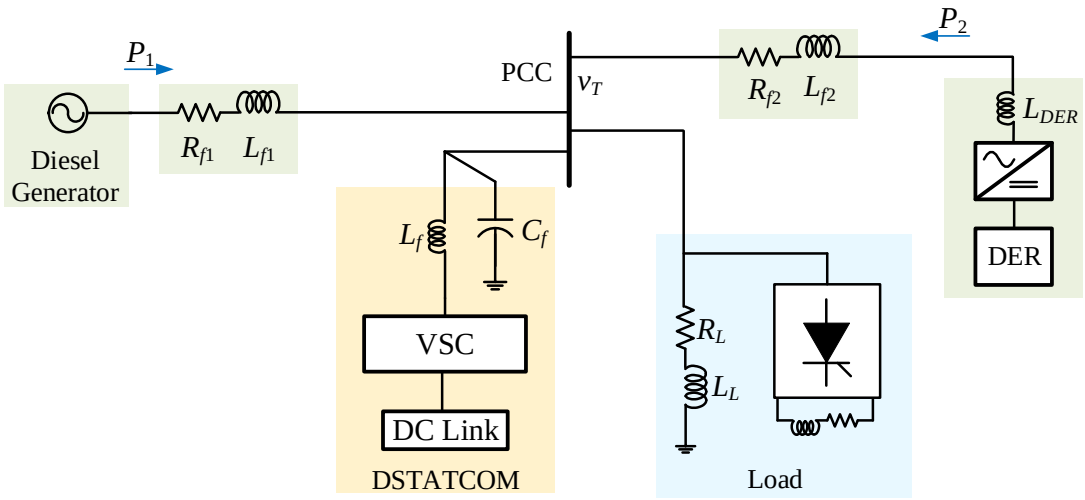

Fig. 5.1. The microgrid structure under consideration.

where $|V_T|$ is a pre-specified voltage magnitude and δ is an angle that maintains the power flow from the source to the load. When it is supplied through a dc capacitor, the angle δ should be such that the required amount of power flows from the source to the load and the DSTATCOM does not consume or generate any power. However, practically the DSTATCOM needs some amount of power from the source to compensate for its switching and internal losses. Therefore if the capacitor voltage can be held constant, then the required amount of power can flow from the source to PCC. Based on this logic, a PI controller is designed to regulate the dc voltage and its output sets the angle, given by

$$\delta = K_P\left(V_{dcref} - V_{dc}\right) + K_I \int \left(V_{dcref} - V_{dc}\right) dt \tag{5.2}$$

The DSTATCOM needs to synthesize these three-phase voltages (5.1) at its output. A linear quadratic regulator (LQR) based state feedback controller is used for switching control of the DSTATCOM. The converter structure and feedback control are discussed in Appendix A.

5.2. DSTATCOM Operation with Frequency Mismatch

The microgrid frequency can vary ± 0.5 Hz from the fundamental frequency of 50 Hz, while DSTATCOM injects a voltage at 50 Hz [92]. This frequency mismatch effect on microgrid performance is analysed for two different cases. Phase-a of the DSTATCOM voltage is given by

$$v_{Ta} = |V_T| \sin\left(\omega_0 t + \delta\right) \tag{5.3}$$

where ω_0 is the synchronous frequency (100π rad/s)

5.2.1. DC LINK OF VSC IS A DC SOURCE

In this case, the DSTATCOM operates at 50 Hz frequency and δ is chosen as zero. This implies that there is no regulated power flow between the MG and the DC bus. Since the DSTATCOM operates from strong source and holds its output voltage at a frequency of 50 Hz, it supplies/absorbs power from the MG such that its frequency becomes 50 Hz. The DSTATCOM supplies/consumes power such that other DGs available in microgrid only supply the half of their rated power to merge the system frequency to 50 Hz. It can be seen in Fig. 5.2 that the load power is 510 kW, which is higher than half of the total capacity (700 kW) of microgrid and DG-1 (rated at 500 kW), DG-2 (rated at 200 kW) supply 250 kW, 100 kW (P_1, P_2) respectively. The rest amount of the load demand is supplied by the DSTATCOM. The frequency of the microgrid, shown in Fig. 5.3, is constant at 50 Hz.

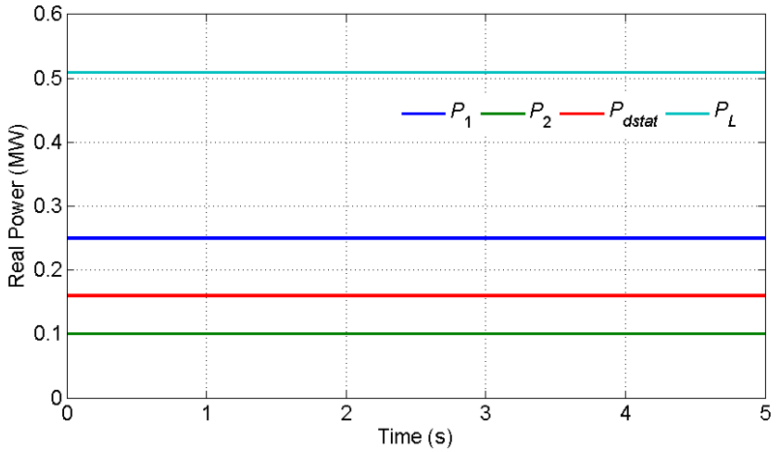

Fig. 5.2. Real power in the microgrid.

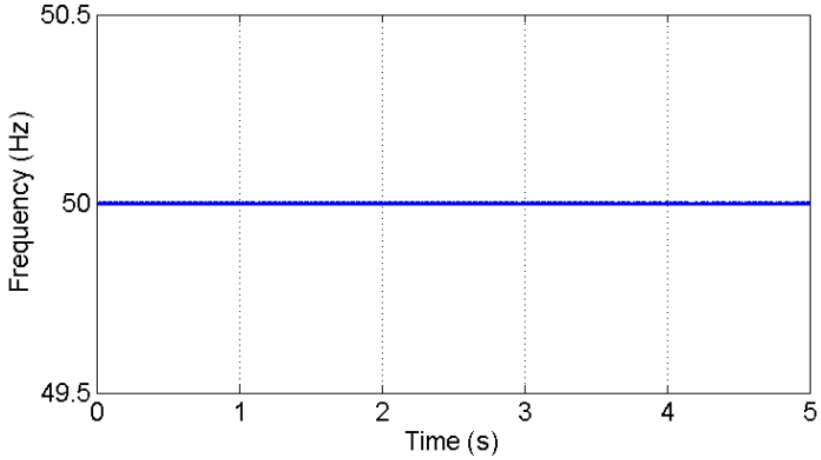

Fig. 5.3. Microgrid Frequency when load is 510 kW.

When a load variation occurs in the microgrid, power supplied by DSTATCOM is changed to retain the system frequency constant at 50 Hz. It can be seen in Fig. 5.4 that load power changes from 320 kW to 350 kW at 4 s and DSTATCOM power is also changed from negative value to zero to maintain the power supply from the other DGs constant. Therefore, the system frequency is retained constant at 50 Hz, as can be seen in Fig. 5.5.

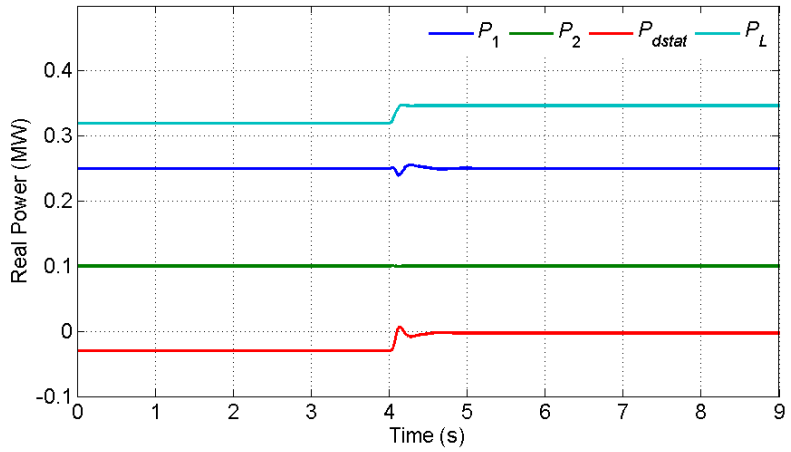

Fig. 5.4. Real power variation in the microgrid.

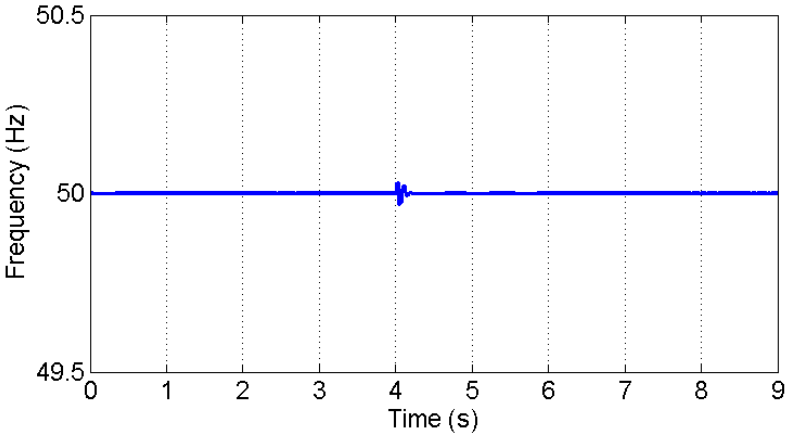

Fig. 5.5. Microgrid Frequency with load variation.

The above example shows that DSTATCOM with a dc source forces other DGs available in the microgrid to operate at 50 Hz. Therefore, DGs always supply their half rated power corresponding to load variation. It implies the DGs do not function efficiently when such a DSTATCOM is allowed to operate in this fashion.

5.2.2. DC LINK SOURCE OF VSC IS A DC CAPACITOR

In this case, DSTATCOM will not operate at 50 Hz but will latch on to the system frequency due to available DGs in the microgrid can be considered as strong

sources. Under this scenario, the angle δ calculated from the PI controller in (5.2) is not stationary. It will fall monotonically when the system frequency is sub-synchronous and will rise when the system frequency is super-synchronous.

Since the DSTATCOM latches on to the system frequency, the voltage that get injected is

$$v_{Ta} = |V_T| \sin(\omega_0 t + \Delta\omega t + \delta_1) \tag{5.4}$$

where δ_1 is a fixed offset angle that regulates the power flow [19].

Assuming the system frequency to be ω, from the above equation we get

$$\omega = \omega_0 + \Delta\omega \tag{5.5}$$

Therefore $\Delta\omega$ is negative when the frequency is less than 50 Hz and is positive when the frequency is above 50 Hz. Comparing (5.3) with (5.4), we get

$$\delta = \Delta\omega t + \delta_1 \tag{5.6}$$

This implies that the angle drops (rises) by 0.2π = 0.6283 rads each second for 0.1 Hz variation from the nominal frequency. The outputs of the angle controller for two different values of system frequency (49.76 Hz and 50.06 Hz) are shown in Fig. 5.6 (a) and Fig. 5.6 (b) respectively. It can be seen that the angle monotonically falls when the system frequency is sub-synchronous and rises when it is super-synchronous.

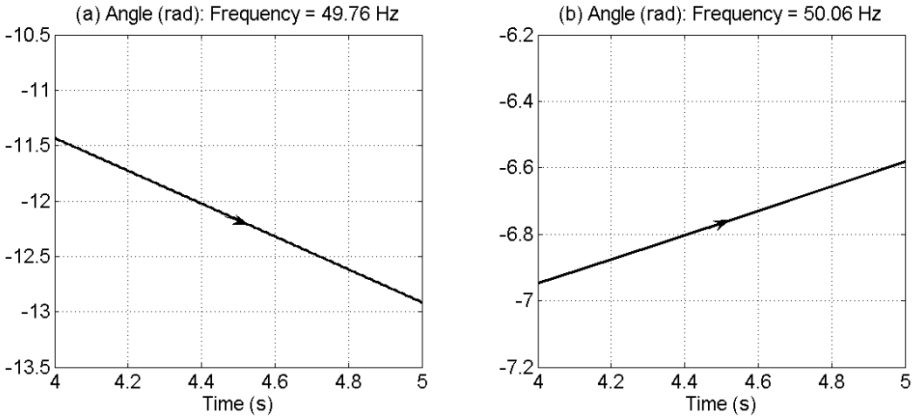

Fig. 5.6. The angle controller response when DSTATCOM injects voltages at 50 Hz.

The dc capacitor voltage also varies in sympathy with the variation in δ. Differentiating both sides of (5.2), we get

$$\frac{d\delta}{dt} = -1.0 \times \left(V_{dcref} - V_{dc}\right) \quad kV \tag{5.7}$$

Since $d\delta/dt$ is the frequency error, we can write

$$V_{dc} = V_{dcref} + \Delta\omega \quad kV \tag{5.8}$$

Therefore the dc capacitor voltage drops from nominal voltage 16 kV to 14.5 kV when the nominal frequency is 49.76 Hz ($\Delta\omega$ = - 1.5 rad/s), and rise to 16.38 kV from the nominal voltage 16 kV when the frequency is 50.06 Hz ($\Delta\omega$ = 0.38 rad/s). It is shown in Fig. 5.7.

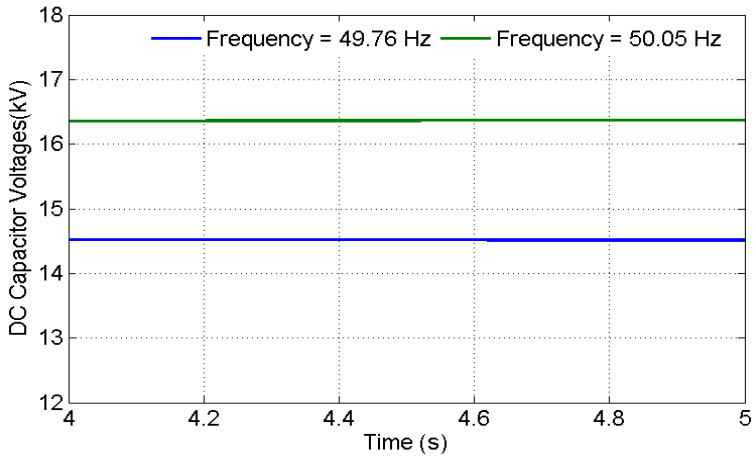

Fig. 5.7. The dc capacitor voltages when the DSTATCOM synthesis voltage at 50 Hz.

The above example shows that the DSTATCOM latches on the frequency of the source voltage, albeit at the cost of phase angle and dc capacitor voltage. Neither of these situations is acceptable. If the frequency deviation is restricted between ± 0.5 Hz, from (5.9) it can be estimated that the capacitor voltage can drop as much as 12.85 kV or rise to 19.14 kV. As the dc capacitor voltage drops, the VSC tracking performance degrades, eventually resulting in system voltage collapse.

Also, though all sources in the microgrid operate at the same frequency, there is no frequency mismatch in the system. This angle runs off due to the integrator in the loop. As a consequence, it might reach the integrator limits and saturate, which will

cause a system collapse. To alleviate this problem, the DSTATCOM must inject a voltage at the system frequency.

5.3. STRATEGIES OF DSTATCOM OPERATION IN MICROGRID

5.3.1. SYNTHESIS THE DSTATCOM VOLTAGE AT THE ESTIMATED FREQUENCY

From the discussion presented above, it is obvious that the DSTATCOM must inject a voltage at the actual system frequency. Therefore, frequency calculated from a simple frequency estimation technique is now utilized for the formation of the reference voltages. This frequency estimation technique based on the symmetrical component theory is discussed in Appendix B. Instead of (5.1), the reference voltages are now given by

$$\begin{aligned} v_{Pa}^{*} &= |V_P|\sin(\hat{\omega}t + \delta) \\ v_{Pb}^{*} &= |V_P|\sin(\hat{\omega}t + \delta - 120°) \\ v_{Pc}^{*} &= |V_P|\sin(\hat{\omega}t + \delta + 120°) \end{aligned} \tag{5.9}$$

where $\hat{\omega} = 2\pi\hat{f}$ and $\hat{f}$ is the estimated frequency, while the dc link control remains the same as given in (5.2).

To evaluate the performance of a DSTATCOM at actual system frequency using frequency estimation technique, simulation studies are described below.

5.3.1.1. SIMULATION STUDIES

For simulation studies, the DGEN is assumed to be rated at 500 kW, while the DER is rated at 200 kW. First it has been assumed that the DSTATCOM is not connected in the system and the microgrid supplies a balanced and rectifier load. The electromagnetic torque produced by the diesel generator is shown in Fig. 5.8 (a). It can be seen that the torque ripple is more than 0.1 per unit (pu). However when the DSTATCOM is connected to the system, the torque ripple reduces to below 0.01 pu. This is shown in Fig. 5.8 (b).

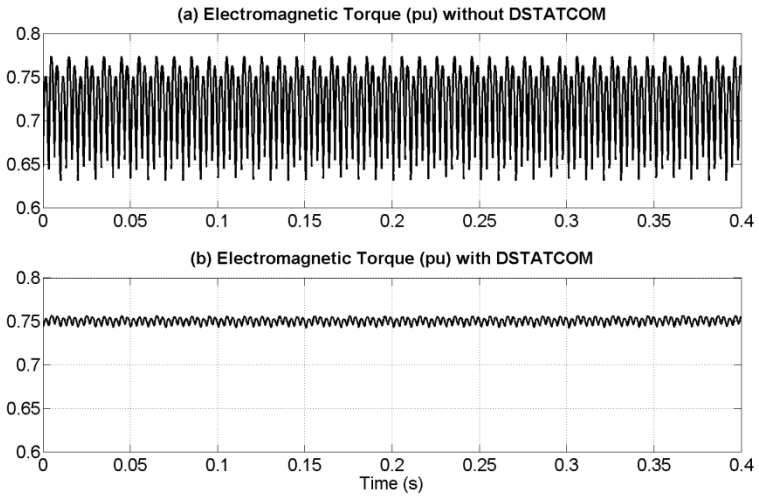

Fig. 5.8. Electromagnetic DGEN torque with and without the DSTATCOM.

In this study, the frequency variation limit from the 50 Hz is considered ± 0.5 Hz. The total capacity of the microgrid is 700 kW. The power consumption in the microgrid will be zero when the frequency of the microgrid is 50.5 Hz and will be 700 kW when the frequency of the microgrid is 49.5 Hz according to considered frequency variation limit. Therefore, for each 70 kW variation from the half the rated power of 700 kW, the frequency variation is 0.1 Hz. For example, a DG rated at 500 kW will supply 250 kW power at 50 Hz. When frequency is 50.1 Hz, it supplies 200 kW power and when frequency is 49.9 Hz, it supplies 300 kW power. Since the frequency of the microgrid can vary between 49.5 to 50.5 Hz, the frequency based DSTATCOM can hold the load bus voltage constant irrespective of load type.

The steady state load current and current supplied by the DGEN are shown in Fig. 5.9 (a) and (b) respectively. The power supplied by the DGEN and the DER are shown in Fig. 5.10. The DGEN supplies 370 kW, which is 2.5 times the 148 kW power supplied by the DER. The estimate system frequency of 49.76 Hz, as shown in Fig. 5.11, matches with calculated frequency from the droop as discussed above. The dc capacitor voltage is held constant at 16 kV, as shown in Fig. 5.12. The output angle of the PI controller (5.2) is shown in Fig. 5.13.

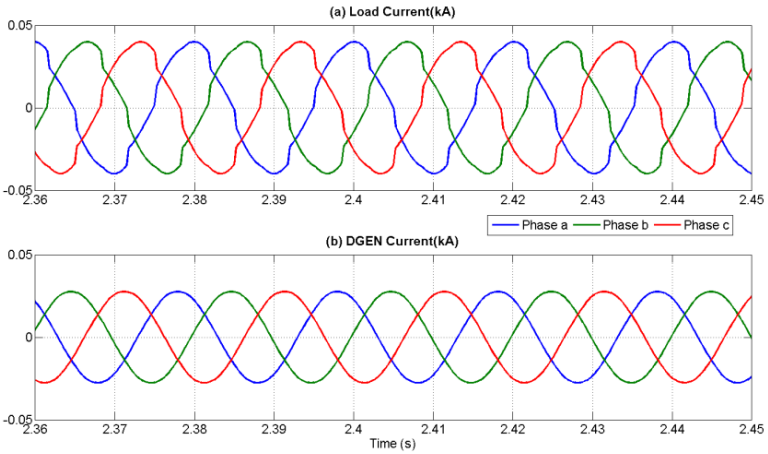

Fig. 5.9. Load current and DGEN current in microgrid.

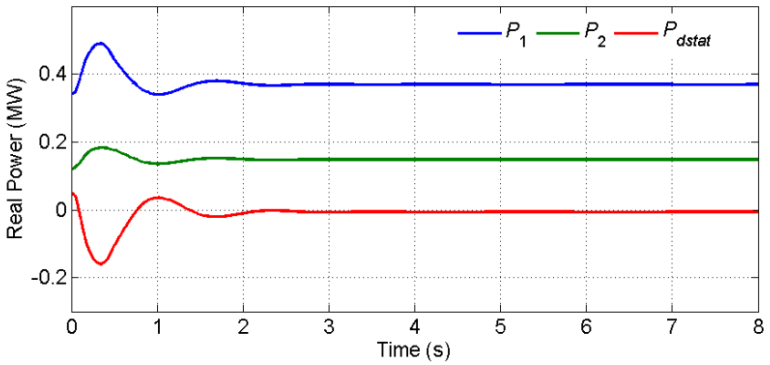

Fig. 5.10. The Real power of the DGs and DSTATCOM.

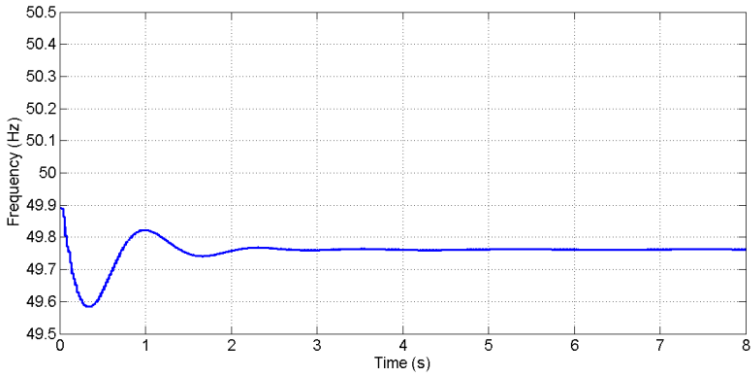

Fig. 5.11. Microgrid frequency.

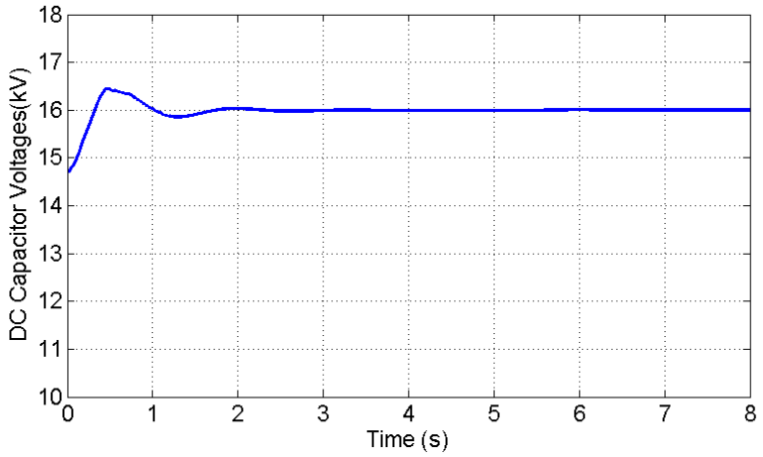

Fig. 5.12. The dc capacitor voltage.

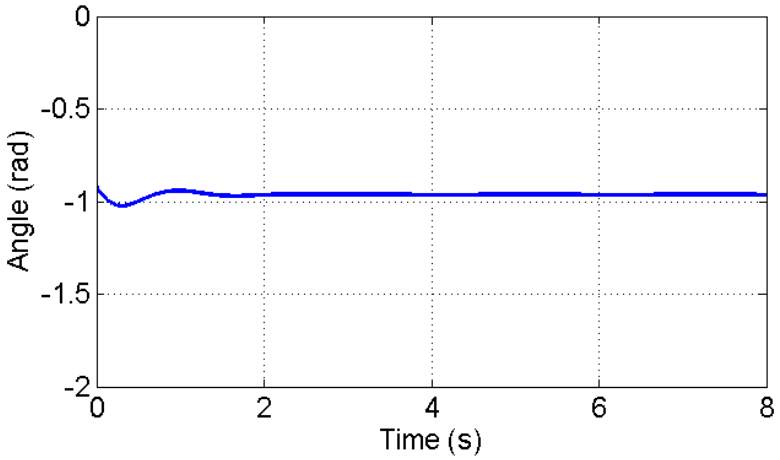

Fig. 5.13. Angle of PI controller output (5.2).

5.3.2. Operation of the DSTATCOM at Set Reference Frequency with Isochronous Controller

The microgrid as shown in Fig. 5.1 operates in frequency droop control, given by

$$\omega = \omega^* + m_f \times (0.5 \times P^* - P) \tag{5.10}$$

$$V = V_r + n_f \times (Q^* - Q) \tag{5.11}$$

where ω and ω^* are the instantaneous and rated frequency of the system. Note that in the ω–P droop equation, droop gain m_f is chosen according to the considered value of frequency variation f_d (± 0.5 Hz) as discussed in Chapter 2, Section 2.2.3.

5.3.2.1. ISOCHRONOUS CONTROLLER

Note that in the frequency droop, given in (5.10), half the rated power is used such that the frequency can vary ± 0.5 Hz from the fundamental frequency of 50 Hz. However, the DSTATCOM is restricted to operate at the actual frequency of the system as discussed in section 5.2. However it is desirable that the DSTACOM operates at the fundamental frequency of 50 Hz. In this case, ω in (5.1) can be chosen as 100π and the angle controller of (5.2) can be applied directly. To achieve this, it is required to recover the droop frequency through an isochronous controller such that available DGs in microgrid operate at the set reference frequency of 50 Hz.

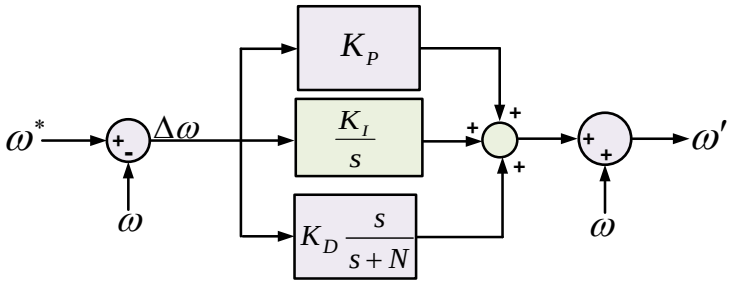

Fig. 5.14. Schematic diagram of the isochronous controller.

The schematic diagram of the isochronous controller is shown in Fig. 5.14, which is essentially a PID controller. The frequency obtained from the droop control for each DG, is first compared with the reference (synchronous frequency). The error is then passed through a PID controller. The controller output is added with the droop frequency to obtain ω'. This frequency is then used to control the DG. It has been discussed already in Chapter 3 Section 3.3.1.

5.4. SIMULATION STUDIES

For simulation studies, the microgrid and the DSTATCOM parameters are listed in Table. 5.1 and Table. 5. 2 respectively. The DGEN has a rating of 500 kW and the DER has a rating of 200 kW. The balanced *R-L* load and rectifier load are considered to validate the performance of the DSTATCOM in the microgrid which is operated in a frequency droop control with isochronous controller.

CASE (A): MG OPERATION WITH DSTATCOM AND RECTIFIER LOAD

In this case, both the rectifier load and the DSTATCOM are connected at the beginning (cold start). The total load demand is 500 kW. The real power flow in the microgrid is shown in Fig. 5.15 (a). It can be seen that power supplied by the DGEN and DER is in the ratio of 2.5:1, while the DSTATCOM absorbs negligible power. It is to be noted that the load power will contain distortion due to the presence of harmonics. However only the average power is shown here and hence the distortions are not visible. The microgrid frequency with isochronous controller is shown in Fig. 5.15 (b). The frequency of the microgrid should be 49.76 Hz if it operates in frequency droop control from (5.10). However, it can be seen from Fig. 5.15 (b) that the frequency of the microgrid is merged to 50 Hz due to isochronous controller with frequency droop control. The isochronous controller parameters are given in Table 5.3.

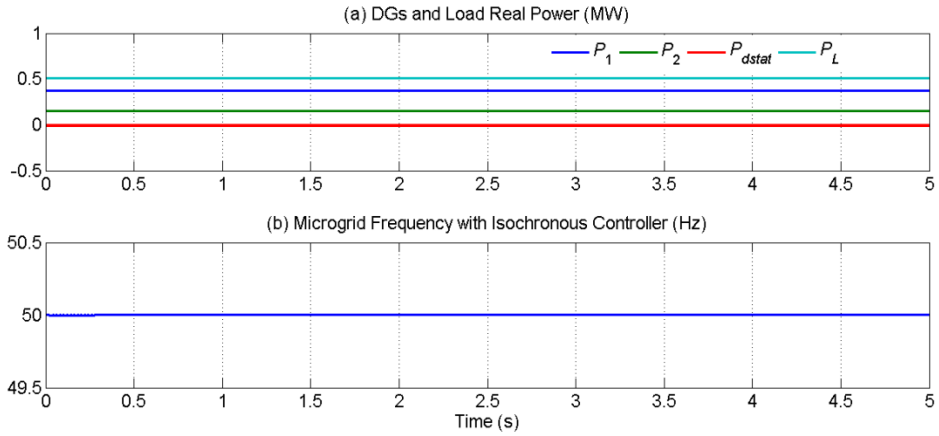

Fig. 5.15. Real Power and microgrid frequency with isochronous controller.

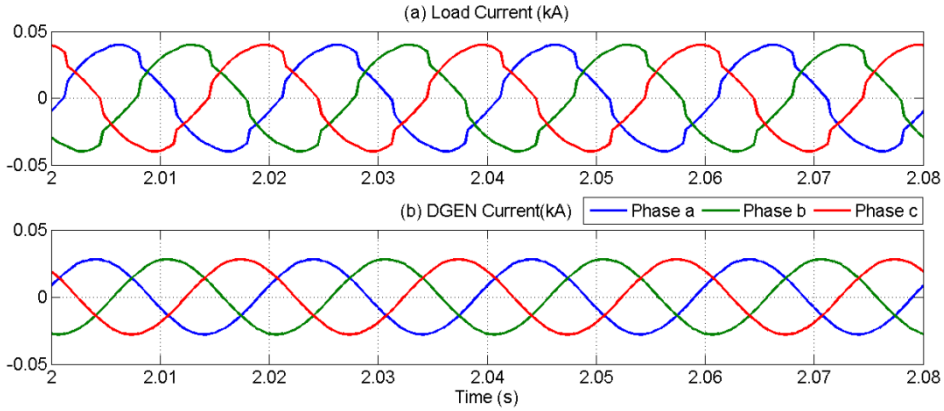

Fig. 5.16. Three phase load and DGEN currents.

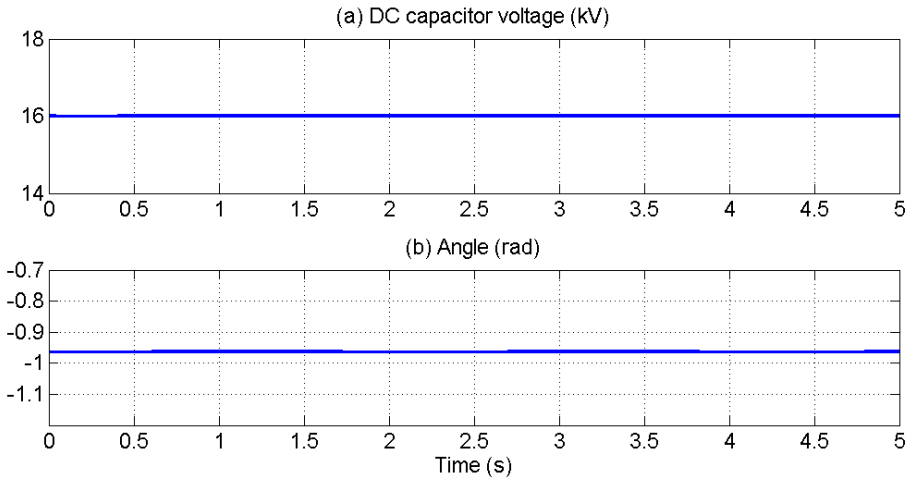

Fig. 5.17. The dc link capacitor voltage and angle controller (5.2) output angle.

The three phase load currents are shown in Fig. 5.16 (a), which contain the harmonic components in them. The currents supplied by the DGEN are sinusoidal due to the voltage correction by the DSTATCOM as can be seen in Fig. 5.16 (b).The dc link capacitor voltage is shown in Fig. 5.17 (a). It can be seen that it settles to the desired voltage of 16 kV within 2 s. The output of angle controller is shown in Fig. 5.17 (b).

CASE-(B): MG OPERATION DURING A LOAD CHANGE

With the system operating in the steady state, the linear *R-L* load is suddenly increased by 50 kW at 1 s. From the plots given in Fig. 5.18 (a), it can be seen that both the DGs increase their power output in the specified ratio, while the power from/to the DSTATCOM remains unchanged. The DG frequencies come back to their steady state values within 0.5 s as shown in Fig. 5.18 (b). The three phase load current and DGEN current are shown in Fig. 5.19 (a) and Fig. 5.19 (b) respectively. The angle controller is effective as dc capacitor voltage and the angle settle within 2 s, as can be seen in Fig. 5.20.

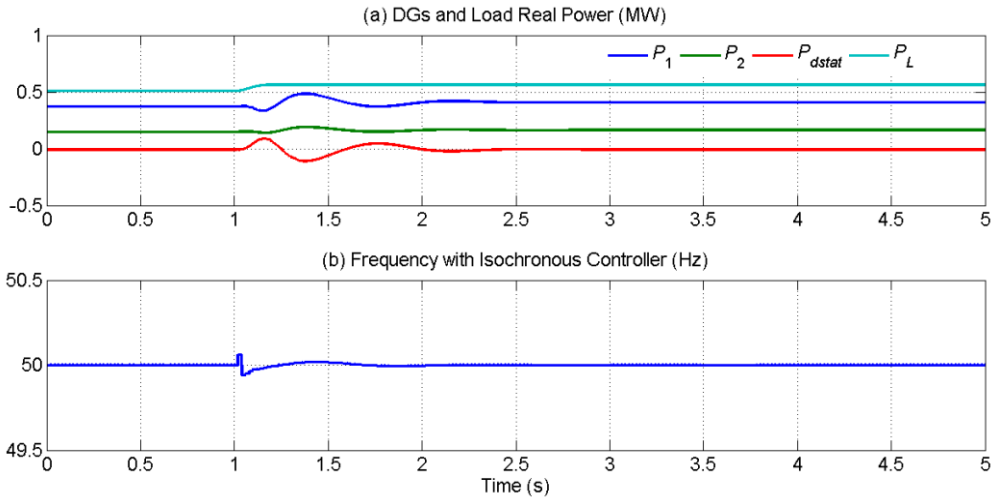

Fig. 5.18. The real power sharing and microgrid frequency with load variation in the microgrid.

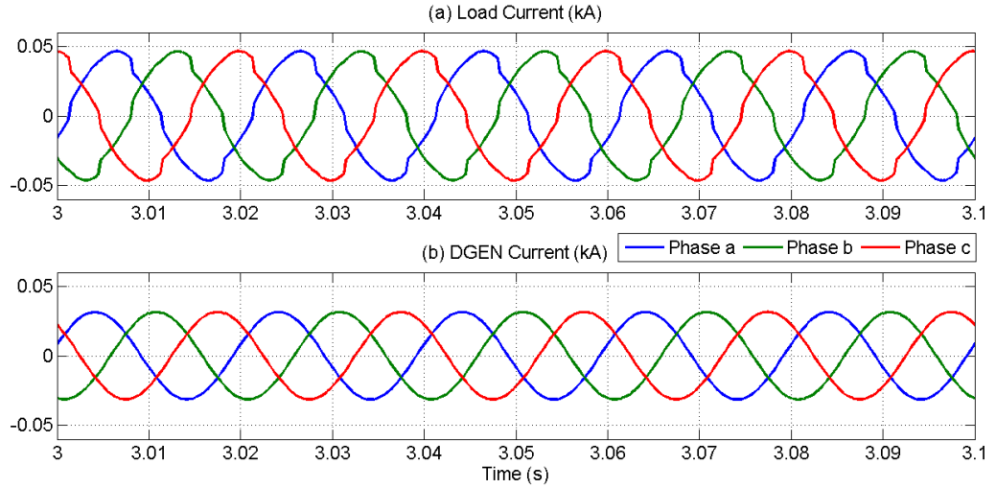

Fig. 5.19. The three phase load current and DGEN current after load changes.

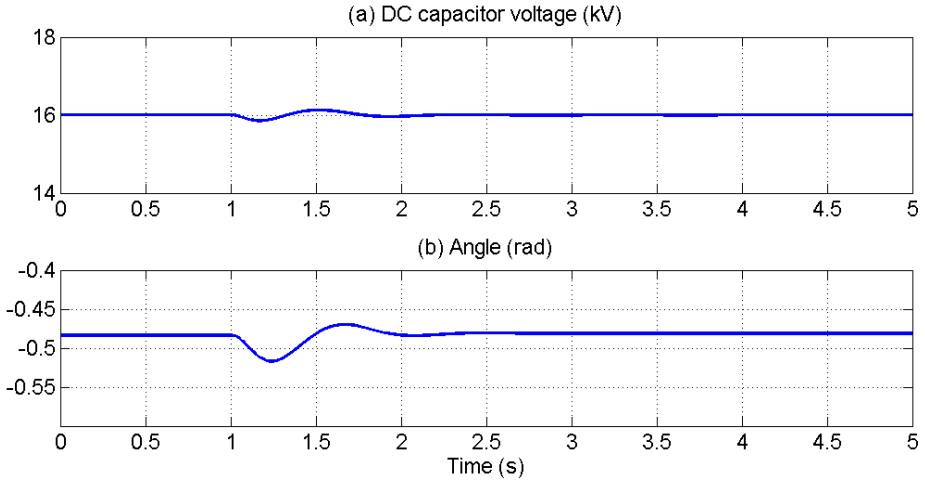

Fig. 5.20. The dc capacitor voltage and angle controller (5.2) output angle with load variation.

Table. 5.1. Parameters of the microgrid.

System Quantities	**Values**
Feeder impedance	R_{f1} = 1.21 Ω, L_{f1} = 38.5 mH R_{f2} = 2.42 Ω, L_{f2} = 77.0 mH
DGEN Rating	500 kW
DER Rating	200 kW
Load-1	R_{La}=272 Ω, L_{La} = 419 mH R_{Lb}=272 Ω, L_{Lb} = 419 mH R_{Lc}=272 Ω, L_{Lc} = 419 mH
Non-Linear Load	Full bridge rectifier with a load of 1500 Ω and 100 mH.
Droop Coefficient (Frequency–Voltage)	
m_{f1}	0.0126 rad/MWs
m_{f2}	0.0314 rad/kWs
n_{f1}	0.02 kV/MVAr
n_{f2}	0.05 kV/MVAr

Table. 5. 2. Parameters of the DSTATCOM.

Parameters	**Values**
R_f	0.001 Ω
C_f	50 μF
L_f	33 mH
V_{dcref}	16 kV
C_{dc}	5000 μF
PI controller parameters	
Proportional gain	-0.1×10^{-3}
Integral gain	-1.0×10^{-3}

Table. 5. 3. The parameters of isochronous controller (Fig. 5.14).

System data	**Value**
Proportional gain (K_P)	0.1
Integral gain (K_I)	10
Differentiator gain (K_D)	0.004
Constant coefficient (N)	200

5.5. CONCLUSION

If a DSTATCOM is connected in a microgrid for load voltage regulation and harmonic mitigation, it has been shown in this chapter that the DSTATCOM should be operated at the actual frequency of the microgrid. Two methods are discussed to synthesize the DSTATCOM voltages at the actual frequency of the microgrid. In the first method, the actual frequency is estimated from simple frequency estimation technique based on the symmetrical component theory and DSTATCOM voltages are synthesised at the measured actual frequency of the microgrid. In other method the isochronous controller is used to merge the microgrid frequency at 50 Hz with corresponding to the load variation. Therefore, microgrid frequency retains at the set reference frequency 50 Hz and DSTATCOM voltages are synthesised at the frequency of 50 Hz. A few case studies are presented to validate the proposed methods.

CHAPTER 6

INTERCONNECTION OF MICROGRIDS FOR MUTUAL SUPPORT DURING CONTINGENCIES

Installation of microgrids can be beneficial in remote areas where there is no existing high voltage line or where drawing such lines is not economically feasible. A microgrid in such areas is expected to operate in islanded mode. However as discussed in Chapter 4, such islanded operation will require storage to prevent either load shedding or system collapse or both.

In such scenarios, when there are two microgrids in close proximity, they can be connected together. It is preferable to interconnect them through a back to back (BTB) converter such that each can nominally operate independent of other. However during an emergency overloading in one microgrid (MG), the other can provide support with its surplus available power [66].

In this chapter such a collaborative arrangement between two neighboring microgrids has been considered. It has been assumed that these microgrids operate in autonomous modes. Furthermore, one of the two microgrids contains inertial generators and hence operates in conventional frequency droop control. The other microgrid has only converter interfaced DGs and hence operates in an angle droop [19, 28]. Therefore these two microgrids cannot be simply connected by a tie-line. Even though these two neighboring microgrids can nominally operate independent of each other, they however exchange their excess available power during stress in one of them. This requires the precise calculation of excess power in the microgrid that needs to supply power to other microgrid. This also requires overload detection to get support from the other. These strategies are different for each microgrid since they employ different droop control strategies. The back-to-back converter system facilitates the bidirectional power flow between the microgrids. The microgrids do not communicate with each other directly. BTB converter system actually controls the power flow between the microgrids during any contingency. It determines the overloading (if any) and the level of available surplus power in the microgrids based on the local measurement and received data from each microgrid. The benefit of the

interconnection is in the avoidance of unnecessary load shedding. A load shedding may still be required if the cumulative generation capacity of the two microgrids is less than their cumulative load demand.

6.1. System Structure

System structure is considered as shown in Fig. 6.1. There are two microgrids – A and B. These two are connected together through a back-to-back voltage source converter (VSC). Microgrid-A (MG-A) contains dispatchable DGs, which operate in frequency droop control. On the other hand, Microgrid-B (MG-B) contains only converter interfaced DGs, which operate in modified angle droop control. These two microgrids are connected through BTB converter, which consists of two VSCs connected through a common dc capacitor (C_{dc}). Each VSC contains H-bridges that are supplied from common dc bus. The output of each H-bridge is connected with LCL (T) filter to link with the microgrid. The detailed structure and control of VSCs are discussed in Appendix A. The nominal operation of this BTB converter system is discussed next.

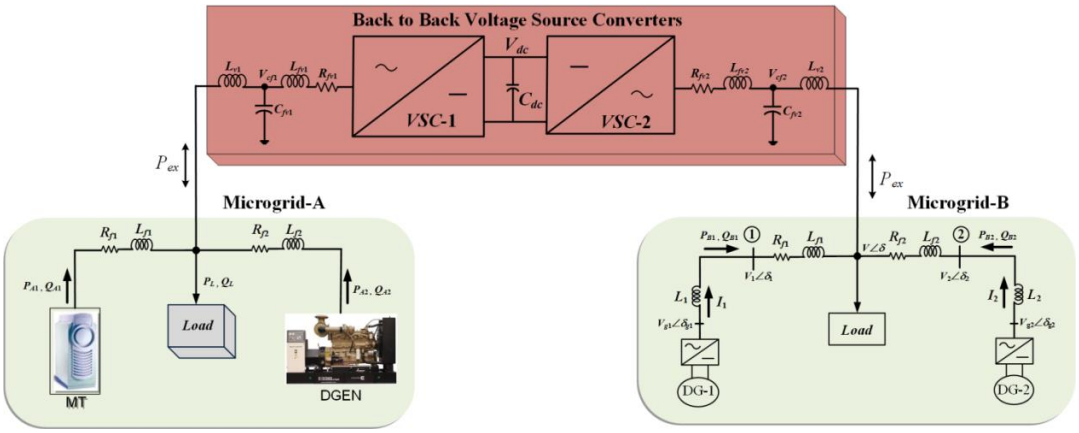

Fig. 6.1. Interconnection of two microgrids.

6.2. Operation of Back-to-Back Converters

The BTB converter system contains two VSCs – VSC-1 and VSC-2. VSC-1, connected to MG-A, holds the dc capacitor voltage (V_{dc}) constant by drawing power from MG-A through angle control. VSC-2, which is connected to MG-B, controls the power flow in either direction. For this, it needs the information of operating status of all DGs in microgrid (e.g. the ON/OFF status of their coupling circuit breakers). Thus, a low-cost, low-bandwidth communication system is required.

Nominally, BTB converter does not need to transfer power in either direction. It is assumed that in this scenario both MGs have sufficient reserve power to supply their local demand. In this case switches of VSC-2 are blocked. Note that each VSC will have its associated losses. Therefore the switches of VSC-2 are blocked to save power. The switches are de-blocked only when power transfer in either direction is required. However, VSC-1 remains active since it needs to hold the voltage across the dc link capacitor constant. If the switches of VSC-1 are blocked as well, then the dc capacitor needs to be charged when power transfer is required. This is the time at which one of the MGs is stressed. Large capacitor charging transient will further weaken the interconnection and make both MGs unstable.

VSC-1 is connected with MG-A, in which the frequency can drift from the nominal frequency of 50 Hz. Therefore, it needs to be synchronized with the MG frequency. This is implemented by the synchronization procedure, as discussed in Chapter 3 Section 3.3.2. VSC-2 is connected with MG-B which always operates at 50 Hz. Hence no synchronization is required for this VSC.

6.3. OPERATION AND CONTROL OF MG-A

6.3.1. NOMINAL OPERATION

The DGs in MG-A are controlled in a frequency droop,

$$\omega = \omega_r + m_f \times \left(0.5P_A^* - P_A\right) \tag{6.1}$$

$$V = V_r + n_f \times (Q_A^* - Q_A) \tag{6.2}$$

where ω_r and ω are the rated and instantaneous frequency of the system respectively. The rated and actual real power are denoted by P_A^* and P_A respectively. Q_A^* and Q_A are the rated and actual reactive power respectively. m_f, n_f are the droop coefficients of the frequency and voltage droop lines.

Note that it has been assumed that all the DGs in this microgrid are dispatchable. The frequency deviation (f_d) is limited to ± 0.3 Hz from base frequency, while the voltage deviation from the base voltage is set at ± 5% for MG-A.

6.3.2. SURPLUS POWER CALCULATION

Surplus power of a microgrid can be defined as power difference between load demand and the total generation capacity of the microgrid. Consider the frequency droop of (6.1). From this we get

$$0.5P_A^* - P_A = \frac{\omega - \omega_r}{m_f}$$

Assume that the minimum frequency is ω_m rad/s (which is equivalent to 49.7 Hz). At this frequency, DG must supply the maximum rated power i.e., $P_A = P_A^*$. Then the value of m_f can be calculated from (6.1) as

$$m_f = 2\frac{\omega_r - \omega_m}{P_A^*} \tag{6.3}$$

Now the surplus power of a DG is calculated from (6.1) as

$$P_A^* - P_A = \frac{\omega - \omega_r}{m_f} + 0.5P_A^* \tag{6.4}$$

Substituting the value of m_f from (6.3) into (6.4), we get

$$P_A^* - P_A = \left[\frac{\omega - \omega_r}{\omega_r - \omega_m} + 1\right]\frac{P_A^*}{2} \tag{6.5}$$

The solution of the above equation gives

$$P_A^* - P_A = \frac{\omega - \omega_m}{\omega_r - \omega_m} \times \frac{P_A^*}{2} = \frac{\omega - \omega_m}{m_f} \tag{6.6}$$

Assume that there are n DGs operating in MG-A. Since the minimum frequency of all the DGs is the same, the surplus powers of these DGs are then given by

$$P_{surpAk} = P_{Ak}^* - P_{Ak} = \frac{\omega_k - \omega_m}{m_{fk}}; \quad k = 1,....,n \tag{6.7}$$

Therefore the total power surplus in the microgrid is given by

$$P_{surpA} = \sum_{k=1}^{n} P_{surpAk} \tag{6.8}$$

Now assume that DGs are cumulatively supplying a total power of P_L, then all the DGs share this power as per their droop gains such that the frequency is constant throughout the microgrid. The surplus power can be calculated from (6.8), knowing the value of droop gains and the microgrid frequency. Now suppose one of the DGs (say DG-*m*) gets disconnected. This means that the load is increased by $P_L + P_m$. This will then be supplied by the rest of the DGs and a drop in the frequency will occur. The surplus power will then be calculated based on

$$P_{surpA} = \sum_{\substack{k=1 \\ k \neq m}}^{n} P_{surpAk} \tag{6.9}$$

$$P_{surpAk} = P_{Ak}^{*} - P_{Ak} = \frac{\omega_k - \omega_m}{m_{fk}}; \quad k = 1, \cdots, n, k \neq m \tag{6.10}$$

Thus from (6.9), the total surplus power of the MG can be calculated with any addition or removal of the DG.

The schematic diagram of MG-A is shown in Fig. 6.1. This consists of a diesel generator (DGEN) and a micro-turbine (MT). The system data used are given in Table. 6.1 in which DG-1 (MT) and DG-2 (DGEN) have ratings of 250 kW and 500 kW respectively. The droop coefficient parameters of DGs are 0.015 rad/kW-s and 0.0075 rad/kW-s respectively. The nominal frequency of the microgrid is assumed to be 49.92 Hz. The surplus powers for DG-1 and DG-2 respectively are 92.15 kW and 184.30 kW, while the total power surplus in the microgrid is 276.45 kW, as shown in Fig. 6.2.

Table. 6.1. Parameters of the Microgrid-A

System Quantities	**Values**
DG_1 Feeder impedance	R_{f1} = 3.025 Ω, L_{f1} = 57.8 mH
DG_2 Feeder impedance	R_{f2} = 3.025 Ω, L_{f2} = 57.8 mH
DG Rated Power	MT: 250 kW, DGEN: 500 kW
Droop Coefficient (Frequency–Voltage)	
m_{f1}	0.015 rad/MWs
m_{f2}	0.0075 rad/MWs
n_{f1}	0.04 kV/MVAr
n_{f2}	0.02 kV/MVAr

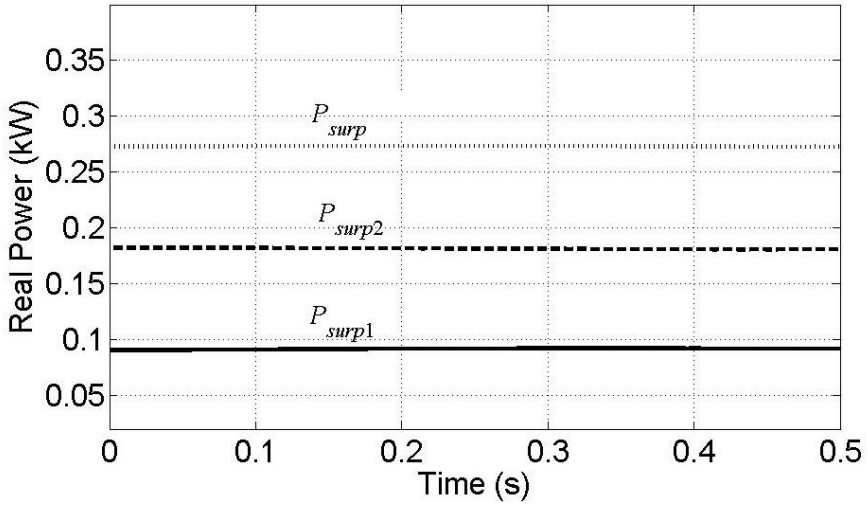

Fig. 6.2. Surplus power of DGs in MG-A.

6.3.3. OVERLOAD POWER CALCULATION

Since MG-A operates in the frequency droop, the frequency is used as the overload detection signal. Once, system frequency hits to the lower limit of the frequency band (i.e., 49.7 Hz), the overload signal triggers on, indicating that the peak load demand is higher than the total cumulative rating of the DGs. When this occurs, the inertial DGs (DGENs) start releasing their stored kinetic energy (KE) to supply the excess power requirement. Therefore the frequency of the DGEN that is calculated from the droop control will start reducing. On the other hand, since the MTs do not have any significant KE, then they will supply their maximum amount of power. Therefore the MG-A frequency will drop below 49.7 Hz. Note that if this condition persists for a longer period of time, the system will collapse once the stored KE of the

DGENs diminishes as shown in Chapter 4, Section 4.2. Hence power must be drawn from MG-B to prevent this.

Suppose MG-A contains *m* DGs. From (6.1), the overload power of the DGs are calculated as

$$P_{Ak} = 0.5 \times P_{Ak}^{*} - \left(\frac{\omega_k - \omega_r}{m_{fk}} \right); \quad k = 1,..., m \tag{6.11}$$

Therefore the total overload power is given as

$$P_{ov} = \sum_{k=1}^{m} P_{Ak} - P_{Ak}^{*} \tag{6.12}$$

For example, assume that the total load demand increases suddenly to 820 kW when the system is operating stably in the steady state. The DGEN droop controller frequency output is shown in Fig. 6.3. It is evident that the frequency starts reducing and reaches a steady value as overload persists in the system. The overload power is calculated using the DGEN droop frequency from (6.11) and (6.12) as

$$P_{A2} = 0.5 \times 0.5 - \left(\frac{311.708 - 314.159}{7.5} \right)$$
$$P_{ov} = 0.5767 - 0.5 = 0.0767\, MW$$

Note that the excess power demand is 70 kW. However the overload power calculated above is slightly above this value to cater for the line losses. The DGs in a microgrid should not only supply the load demand but the I^2R losses as well.

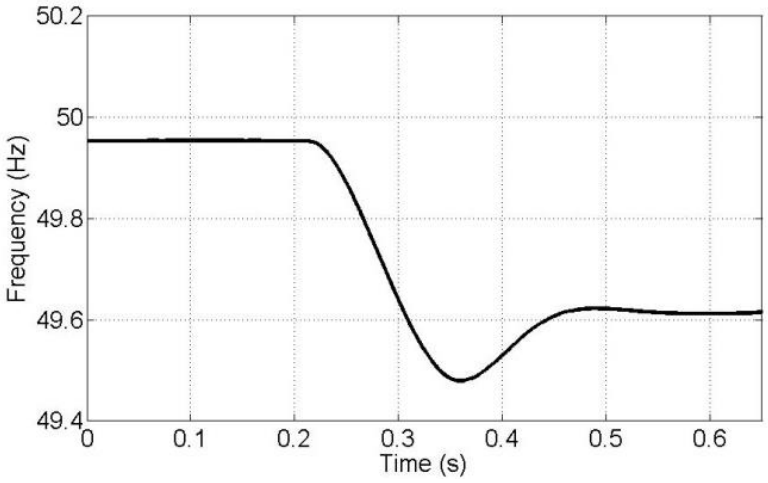

Fig. 6.3. DGEN frequency during overload.

6.3.4. VSC-1 CONTROL

VSC-1 control scheme is shown in Fig. 6.4. It contains a T-filter to suppress switching frequency harmonics. Assume that it is connected at point T of the MG-A. The reference voltage across the capacitor (V_{fv1}) of the VSC-1 ($V_{cf1\text{ref},abc}$) is needed to synthesize at the same frequency of the MG-A. Also the angle of the reference voltage ($V_{cf1\text{ref},abc}$) should be such that the DC capacitor voltage is held constant. Therefore this angle is set through a PI controller as given in (3.9). The VSC reference voltage is synthesized using synchronisation algorithm as discussed in Chapter 3, Section 3.3.2. Once the voltage references are synthesized [121], these are tracked through the switching controller.

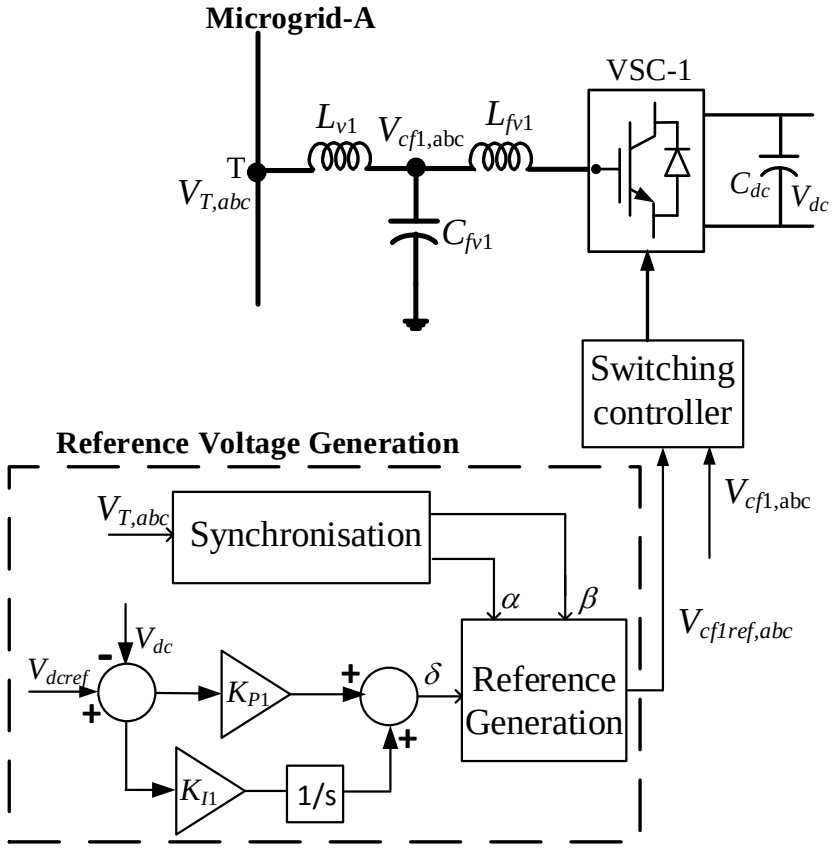

Fig. 6.4. VSC-1 control scheme.

6.4. OPERATION AND CONTROL OF MG-B

6.4.1. NOMINAL OPERATION

Microgrid-B consists of only converter interfaced DGs as shown in Fig. 6.1. Since the converters can track a voltage reference almost instantaneously [92], it has been shown in [28] that an angle droop can have faster and superior performance than

a frequency droop. However, the angle droop control is mentioned in [28] shows that power sharing ratio depends on the output impedance of the converters. Therefore, to share the power amongst DGs independent from the output inductance of the DG, modified angle droop control is used in MG-B as discussed in detail in Chapter 2, Section 2.2.2.

In modified droop control, the angle droop equations are used to synthesize the bus voltages as

$$\delta = \delta^* + m_a \times \left(P_B^* - P_B\right) \tag{6.13}$$

$$V = V^* + n_a \times \left(Q_B^* - Q_B\right) \tag{6.14}$$

where δ^* and δ are the rated and instantaneous angle of the terminal voltage respectively. The rated real power and instantaneous real power are denoted by P_B^* and P_B respectively. Q_B^* and Q_B are the rated and instantaneous reactive power respectively. m_a, n_a are the droop coefficients of the angle and voltage droop lines.

Once, the quantities voltage magnitude (V_{gi}) and angle (δ_{gi}) are calculated as discussed in Chapter 2, Section 2.2.2, then instantaneous three phase reference voltage are obtained as

$$\begin{aligned} v_{DGia} &= \sqrt{2}V_{gi}\sin\left(\omega t + \delta_{gi}\right) \\ v_{DGib} &= \sqrt{2}V_{gi}\sin\left(\omega t + \delta_{gi} - 120°\right) \\ v_{DGic} &= \sqrt{2}V_{gi}\sin\left(\omega t + \delta_{gi} + 120°\right) \end{aligned} \tag{6.15}$$

DG-*i* (*i*=1,2..*n*) has to synthesis these three voltages (6.15) at its output terminal. The converter structure of the DGs are considered same as discussed in Appendix A.

6.4.2. SURPLUS POWER CALCULATION AND OVERLOAD DETECTION

Microgrid-B operates in angle droop control therefore the surplus power depends on voltage angle. It can be calculated from the droop angle which is given in (6.13). If the reference angle is chosen as 0°, (6.13) can be written for i^{th} DG as

$$P_{surpBi} = P_{Bi}^* - P_{Bi} = \frac{\delta_i}{m_{ai}} \tag{6.16}$$

Therefore, the total power surplus is the sum total of all DGs in this microgrid. If one of the DGs is switched off, the surplus power is calculated in the similar fashion as given in (6.9).

The advantage of the angle droop is that it does not require any extensive detection method for any overloading condition. In an autonomous microgrid, an angle droop control scheme can be designed by choosing the reference angle as zero for all the DGs. Therefore, as it can be surmised from (6.13) that, when overloading occurs, the droop angles become negative. This can be used as a trigger signal. Therefore, the overload has to be detected as soon as the angles reach zero. Hence the lower threshold for the angles is chosen zero. This is used for deblocking VSC-2.

Note that for both surplus power calculation and overload detection in this scheme, the droop angles are required at the BTB converter. Furthermore the operating status of the DGs will be required for surplus power calculation. Therefore a communication medium will be required for this purpose.

6.4.3. VSC-2 CONTROL FOR POWER TRANSFER FROM MG-B TO MG-A

In this case, the overload occurs in MG-A. The overload detection and power calculation is discussed in Section 6.3.3. The control scheme of VSC-2 is shown in Fig. 6.5. The main aim is to make power exchange from MG-B to MG-A (P_{ex}) equal to overload power (P_{ov}). This is accomplished by a PI controller that controls the angle of the voltage v_{cf2} across the capacitor (C_{vf2}). This angle is computed as

$$\delta_{cf\,2} = K_P\left(P_{ov} - P_{ex}\right) + K_I \int \left(P_{ov} - P_{ex}\right) dt \tag{6.17}$$

The main aim of this controller is to deflect the angle δ_{cf2} from the angle of the voltage ($V_{B,a}$) in such a way that the required amount of power flows from MG-B to MG-A.

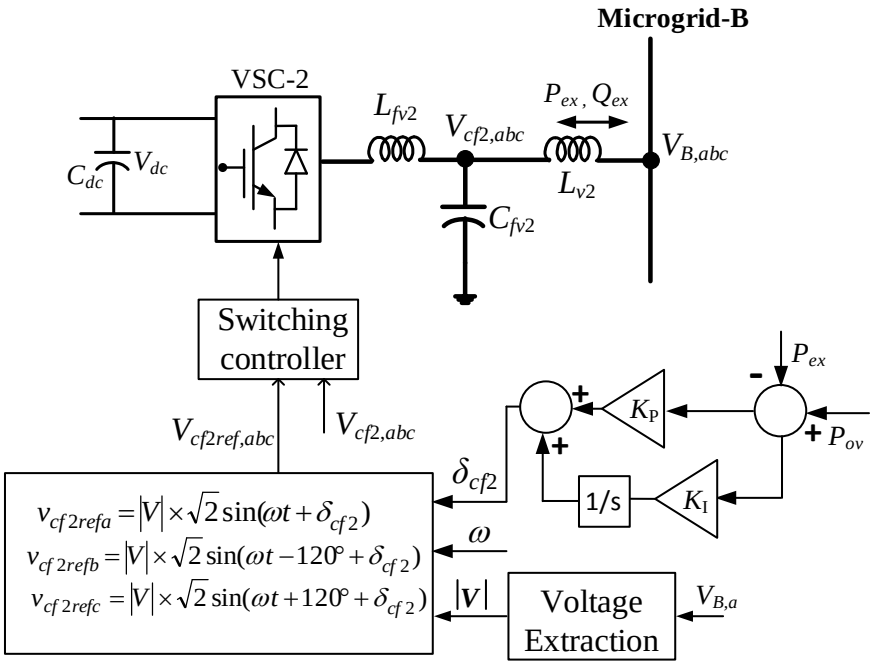

Fig. 6.5. VSC-2 control scheme.

6.4.4. VSC-2 CONTROL FOR POWER TRANSFER FROM MG-A TO MG-B

In this mode, the overload occurs in MG-B. Here it is assumed that the power drawn from MG-A will be shared with the DGs of MG-B. However, MG-A can only supply the available excess amount of power, as discussed in Section 6.3.2. Therefore, its droop coefficients are determined dynamically. Assume that MG-B has *n* number of DGs. Then we define a constant Θ as

$$\Theta = P_{B1}^{*} m_{a1} = P_{B2}^{*} m_{a2} = \cdots = P_{Bn}^{*} m_{an} \tag{6.18}$$

This constant now dictates what the droop gain of an incoming DG will be, given its rated power. Now when MG-B needs power from MG-A, VSC-2 can draw power from MG-A using the same angle droop constant. Hence the droop gain based on the surplus power is given as

$$m_{asurp} = \frac{\Theta}{P_{surp}} \tag{6.19}$$

In this case the converter output reference voltage is computed from the angle droop control as discussed in Section 6.4.1. This control scheme is shown in Fig. 6.6, where $V_{cf2ref,abc}$ is calculated from angle droop controller.

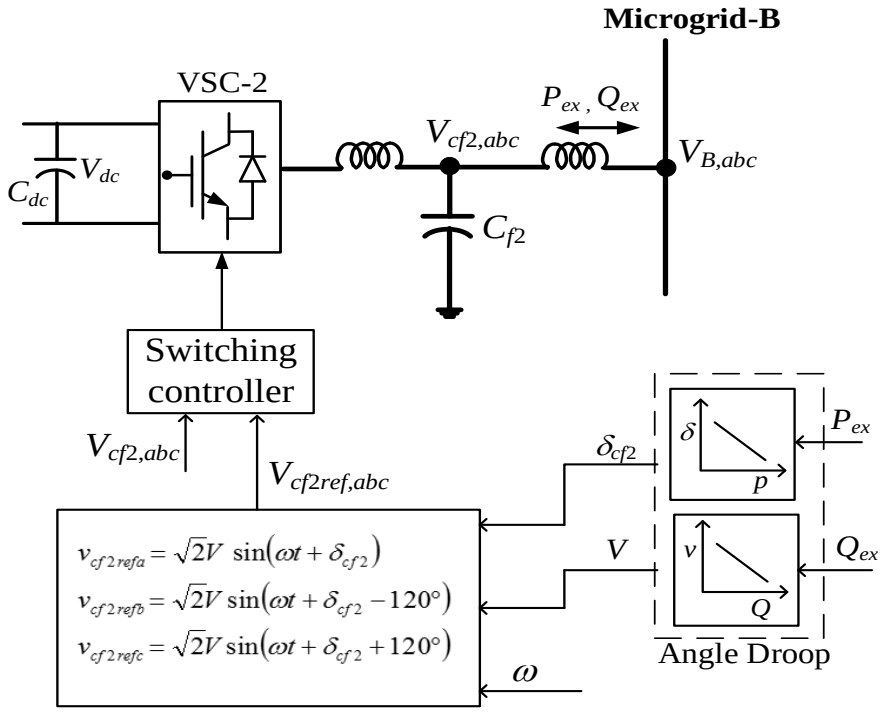

Fig. 6.6. VSC-2 control scheme.

6.5. THE OVERALL VSC CONTROL STRATEGY

The overall VSCs control strategy is shown in Fig. 6.7. VSC-1, which is connected with MG-A, operates at same frequency of the microgrid while holding the DC capacitor voltage constant. This is synchronized with the microgrid through the algorithm presented in Chapter 3, Section 3.3.2. VSC-2 is connected to MG-B and operates at a fix frequency of 50 Hz. This converter controls the power flow from MG-A to MG-B or vice versa.

The mode of operation of VSC-2 depends on the overload triggering signal. In the nominal mode of operation, both microgrids have sufficient amount of power to support their own local loads. When MG-A is overloaded and MG-B has sufficient power, $Trig_{ovA}$ will be equal to one and $Trig_{ovB}$ should be zero. In this case, the exact amount of power shortfall will be supplied by MG-B to MG-A. On the other hand, when MG-B is overloaded, $Trig_{ovB}$ will be equal to one. If MG-A has sufficient power during this time, $Trig_{ovA}$ should be zero and MG-A will supply MG-B using the same angle droop used by the DGs in MG-B.

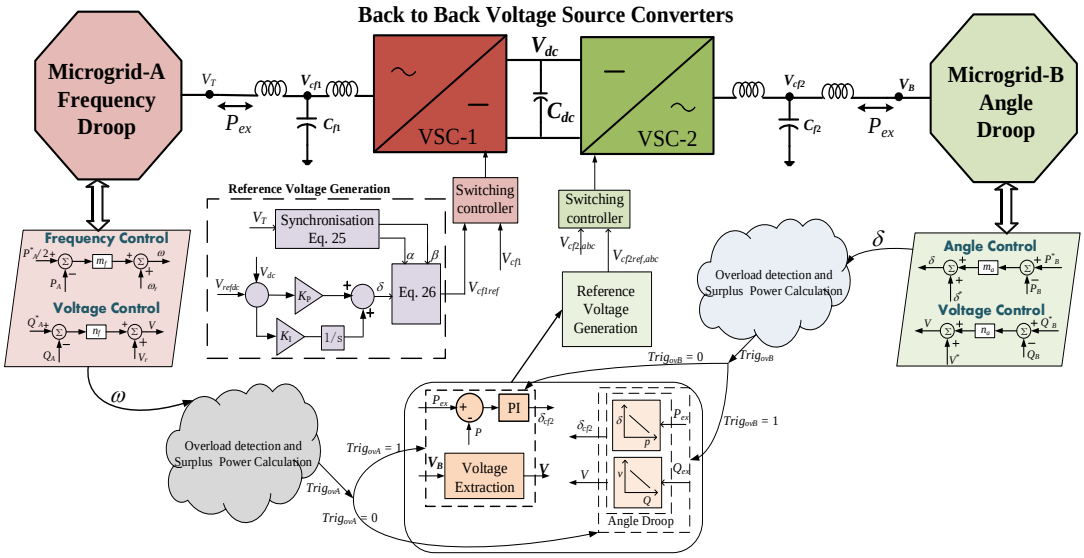

Fig. 6.7. The overall control scheme for VSCs.

6.6. SIMULATION STUDIES

6.6.1. NOMINAL OPERATION

The system structure shown in Fig. 6.1 is considered. The parameters of the MG-A, MG-B and VSCs are listed in Table. 6.1, Table 6.2 and Table 6.3 respectively. The total local load demand in MG-A is 450 kW and MG-B is 200 kW. The powers supplied by the DGs, along with the load power in MG-A are shown in Fig. 6.8. The frequencies of the DGs in this microgrid are shown in Fig. 6.8 (b). Since the load demand is more than the half of rated power, the frequency is expected to be below 50 Hz.

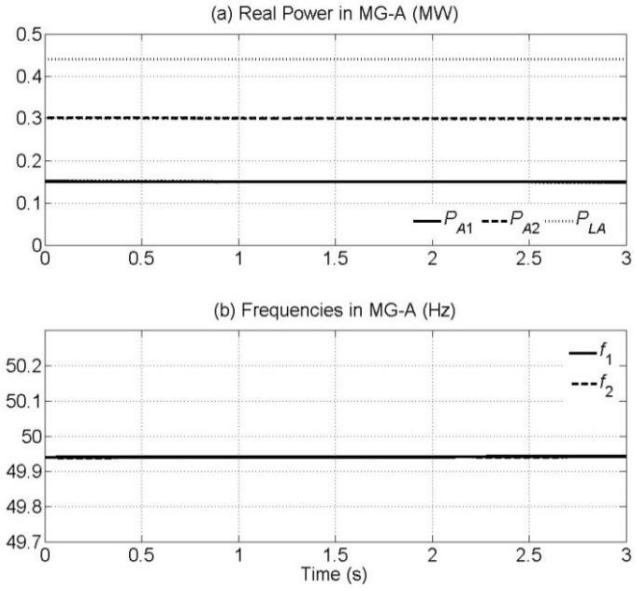

Fig. 6.8. Power and frequency in MG-A during nominal operation.

In MG-B, power shared by the two DGs and the power consumed by the load are shown in Fig. 6.9, where the load is suddenly reduced to 150 kW. However the power supplied by the DG-1 is remained twice the amount that supplied by DG-2. The power drawn through VSC-2 is zero, while the dc capacitor voltage V_{dc} is held constant at 2.5 kV by VSC-1, as shown in Fig. 6.10.

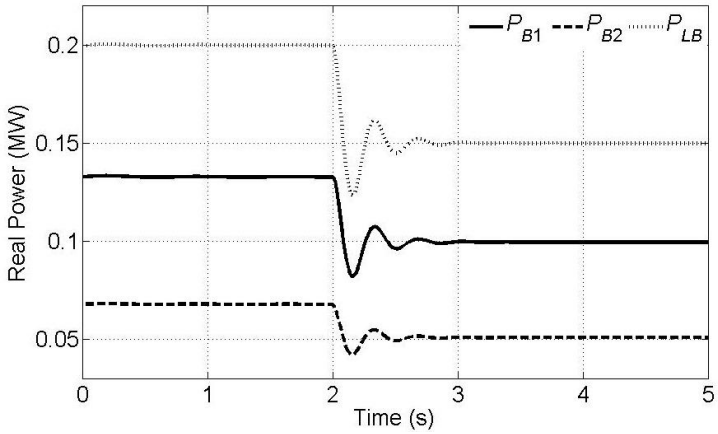

Fig. 6.9. Real power sharing in MG-B through angle droop control.

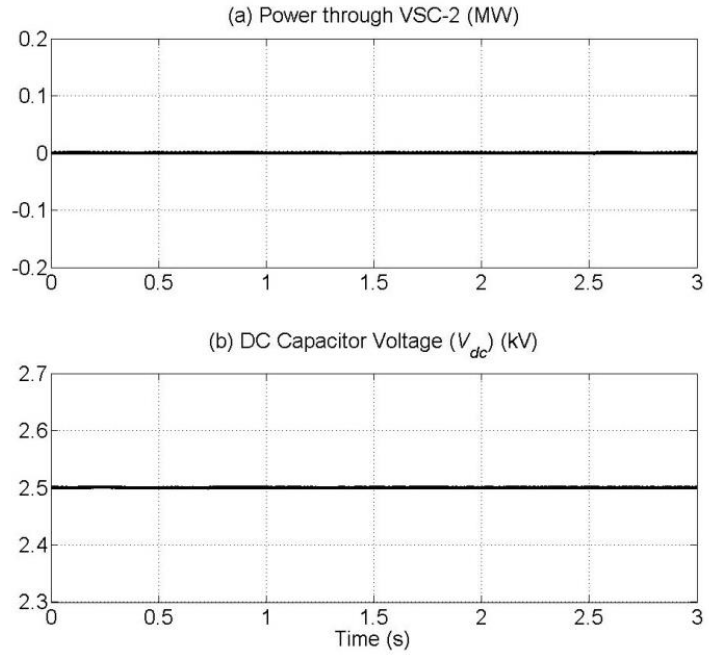

Fig. 6.10. Power exchange and dc capacitor voltage during nominal operation.

6.6.2. MG-A OVERLOADED

In this case, the local load of MG-A is increased to 820 kW at 1 s, which exceeds the total maximum available power in this MG. The overload power requirement, calculated from (6.12), is given to VSC-2 controller. Therefore this amount of power is drawn from MG-B. The load and DGs powers for MG-A and MG-

B are shown in Fig. 6.11 and Fig. 6.12 respectively. It can be seen that DGs in MG-A reach their maximum limit. However, the power supplied by the DGs in MG-B increases, even though the load consumption in this microgrid remains constant.

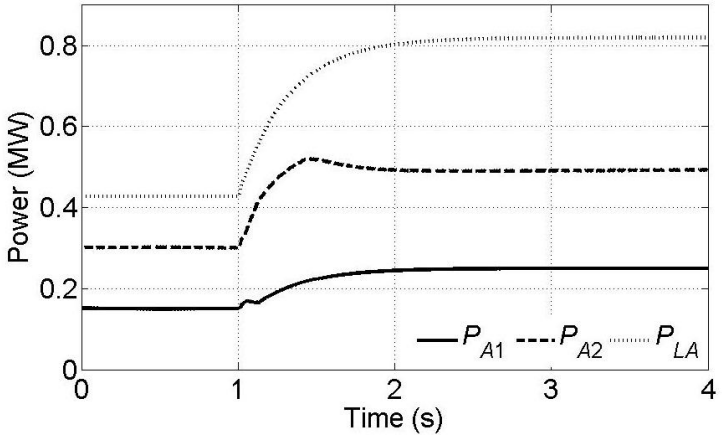

Fig. 6.11. Power in MG-A during an overload in MG-A.

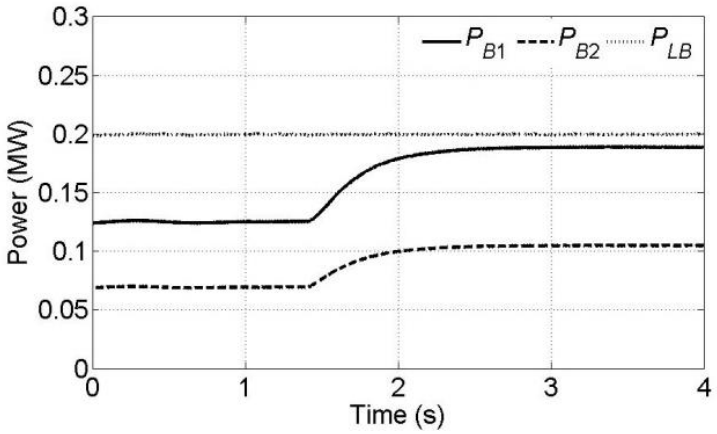

Fig. 6.12. Power in MG-B during an overload in MG-A.

The power flow through VSC-2 is shown in Fig. 6.13 (a). It is negative indicating that a power is flowing from MG-B to MG-A. The dc capacitor voltage is shown in Fig. 6.13 (b). It can be seen that it remains constant at 2.5 kV barring some initial transients.

The overload power drawn from MG-B also depends on its available surplus power which can be calculated from (6.16). This available surplus power must be higher than the overload power to support MG-A. In case, the overload power which need to draw from MG-B is higher than the available surplus power then load shedding will be required which is not considered in this thesis.

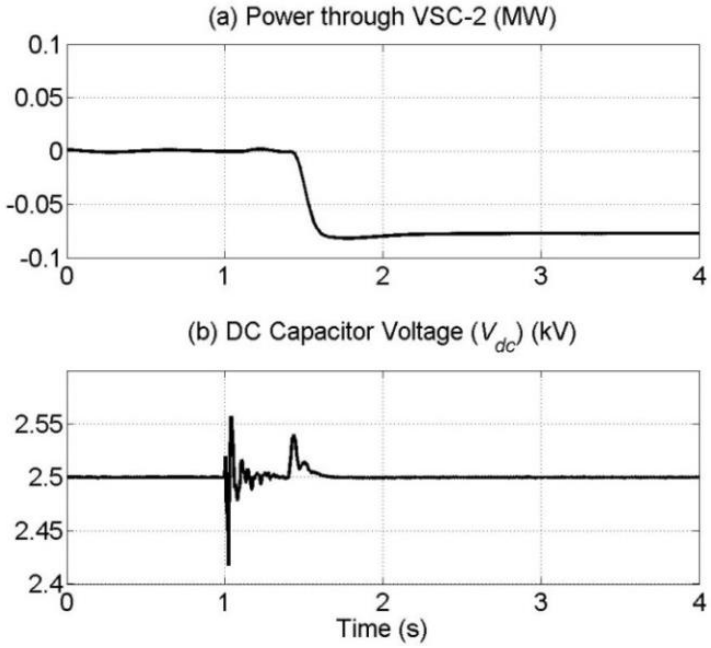

Fig. 6.13. Power through VSC-2 and dc capacitor voltage during an overload in MG-A.

6.6.3. MG-B OVERLOADED

With the system operating in the steady state, the power demand rises to 290 kW in MG-B. Since this is still within the supply capacity of the DGs, they continue to supply the demand according to their ratio, as shown in Fig. 6.14 (a). The droop angles are close to zero but higher than zero, as can be seen from Fig. 6.14 (b). However, if the load demand increases to 350 kW that is beyond the total capacity of the DGs, the droop angles become negative and voltage drop catastrophically, as shown in Fig. 6.15. To avoid this, when the droop angles reach a pre-set lower threshold zero, VSC-2 is switched on.

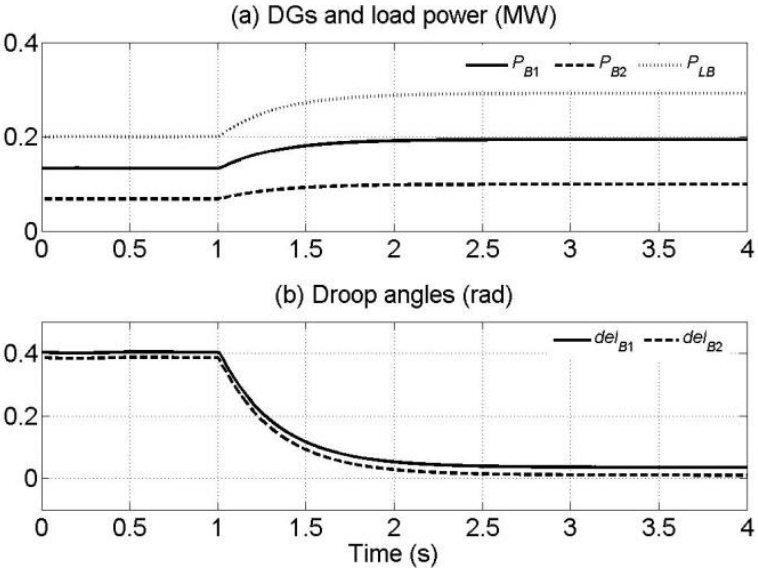

Fig. 6.14. Illustration of near overload in MG-B.

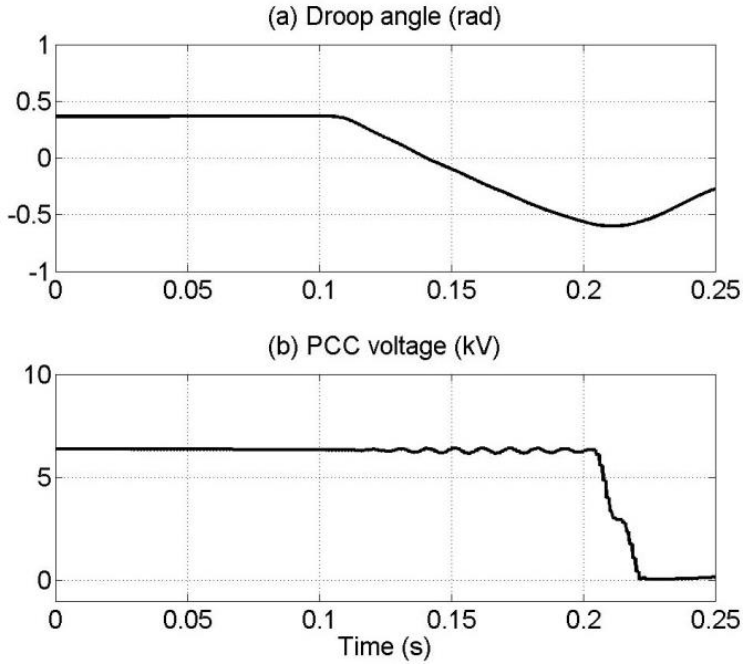

Fig. 6.15. Illustration of overload in MG-B.

In this case, let us assume load demand in MG-B is increased to 320 kW which is higher than the total power generation capacity of the DGs in this MG. Therefore, the angle of DGs nearly reaches zero and this triggers the overloading signal to ON state. This signal is used to de-block the switches of VSC-2. Then VSC-2 starts drawing power in same angle droop control with DGs of MG-B according to available surplus power and rest of the load power supplied from the DGs of the MG-B as shown in Fig. 6.16 (a). The angles of the DGs are shown in Fig. 6.16 (b).

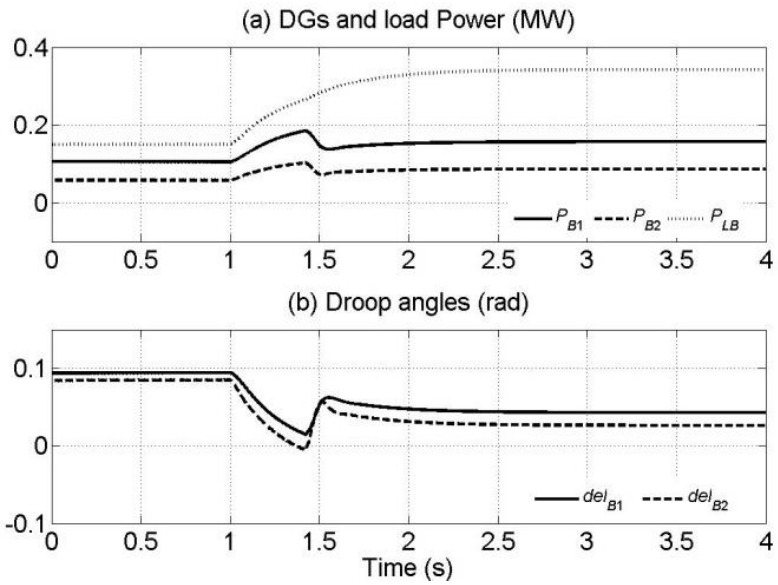

Fig. 6.16. DGs power and frequency in MG-B during overload in MG-B.

The power supplied by the DGs in MG-A are shown in Fig. 6.17 (a). It can be seen that power supplied by DGs increases, even though its local load requirement does not change. The frequency of the DGs also reduces as shown in Fig. 6.17 (b). The power supply through the VSC-2 is shown in Fig. 6.18 (a). It is positive indicating that a power is flowing from MG-A to MG-B. The dc capacitor voltage V_{dc} is held constant at 2.5 kV barring some initial transients as shown in Fig. 6.18 (b).

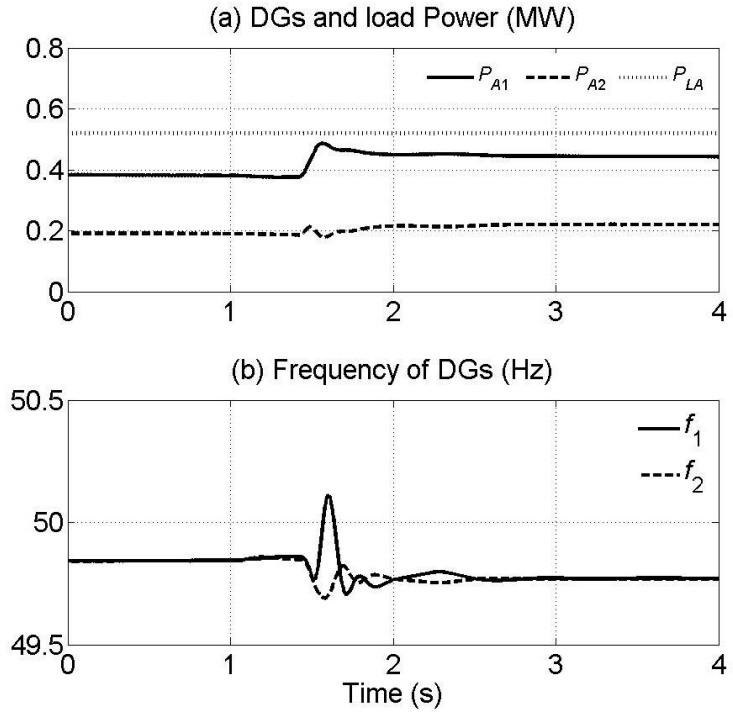

Fig. 6.17. DGs power and frequency in MG-A during overload in MG-B.

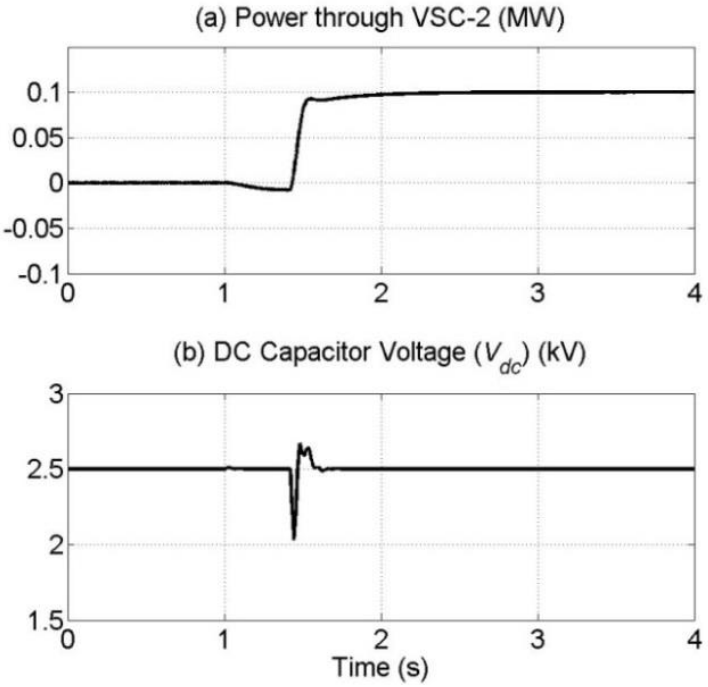

Fig. 6.18. Power exchange and dc capacitor voltage during overload in MG-B.

Table. 6.2. Parameters of the microgrid-B.

System Quantities	**Values**
DG_1 Feeder impedance	R_{f1} = 3.025 Ω, L_{f1} = 57.8 mH
DG_2 Feeder impedance	R_{f2} = 3.025 Ω, L_{f2} = 57.8 mH
DGs Rated Power	DG-1: 200 kW, DG-2: 100 kW
Output Inductor	$L_1 = L_2$ = 10 mH
Droop Coefficient (Angle–Voltage)	
m_{a1}	2.0 rad/MW
m_{a2}	1.0 rad/MW
n_{a1}	1.0 kV/MVAr
n_{a2}	0.5 kV/MVAr

Table. 6.3. Parameters of VSCs.

Parameters	**Values**
$R_{fvi,\ i=1,2}$	0.1 Ω
$C_{fvi,\ v=1,2}$	50 μF
$L_{vi\ i=1,2}$	15 mH for VSC-1 and 10 mH for VSC-2
V_{dcref}	2.5 kV
Transformer	0.1 MVA, 3/11 kV, leakage inductance ($L_{fvi,\ i=1,2}$) of 5%

Table. 6.4. Parameters of PI controller (VSC-1).

System data	Value
Proportional gain (K_{p1})	-0.2
Integral gain (K_{I1})	-5

Table. 6.5. Parameters of PI controller (VSC-2).

System data	Value
Proportional gain (K_p)	-0.5
Integral gain (K_I)	-20

6.7. CONCLUSION

In this chapter, a new interconnection strategy is presented for two neighboring microgrids, operating in autonomous mode. It has been shown how a microgrid, operating in frequency droop control can be joined together through a BTB VSC system to a microgrid operating in angle droop. The operation of BTB converter plays an important role to support the microgrid during contingency. The overloading detection and excess power calculation methods for the microgrid operating under frequency droop control are discussed. The overloading in the angle droop control is detected through the angle of any converter output voltage and available excess power is calculated based on droop angles. Extensive digital computer simulation results are provided to validate the proposals.

CHAPTER 7

CONCEPT OF POWER EXCHANGE HIGHWAY FOR CLUSTER OF MICROGRIDS

The interconnection of the number of microgrids can make distribution system more reliable and efficient [66]. It can enable utilities to make more efficient use of their existing assets through peak shaving and service quality control. The interconnection of the microgrids through highways for power exchange can rapidly escalate the microgrid capabilities [81]. If only two microgrids are connected to each other then they can be connected directly through a back to back converter as discussed in Chapter-6. In [123], a hybrid microgrid (MG) structure composed of three single phase back to back converters which shares the load among different phases is presented. So far a large majority of published work only have considered interconnection of two microgrids. If there are three microgrids, they can be connected in the triangular arrangement as shown in Fig. 7.1.

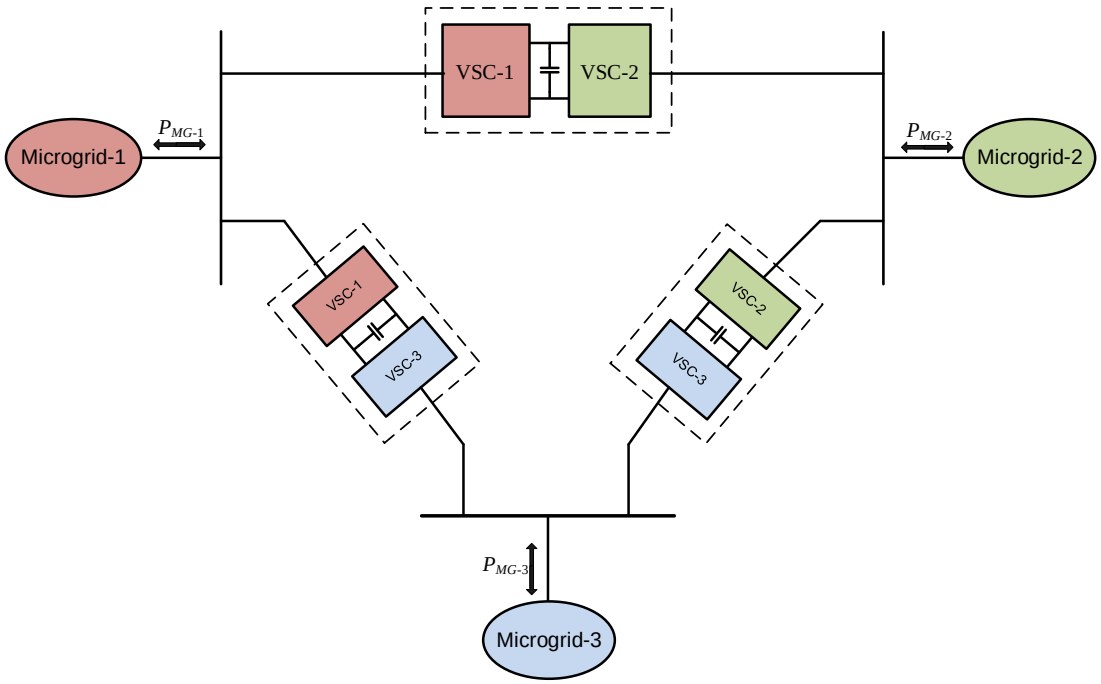

Fig. 7.1. Interconnection of three microgrids.

In this figure, each microgrid is connected through a back to back converter to exchange power between them during any contingency. The operation of the back to back converter can be the same as discussed in Chaper-6 for two interconnected

microgrids. However, there may be several microgrids that need to be interconnected. Thus direct back to back connection is not always feasible.

7.1. SYSTEM STRUCTURE

When several MGs are to be connected together, they need a common platform for power exchange. The schematic diagram of the proposed topology is shown in Fig. 7.2. In this, the power between the microgrids is exchanged only through the power exchange highway (PEH). To isolate a MG from power exchange highway, each microgrid is interconnected through a back to back (BTB) converter. The DGs available in microgrids operate in frequency droop to supply their loads. The BTB consists of two voltage source converters (VSC-1 and VSC-2) which are connected through a common dc capacitor. VSC-1 is connected with the microgrid and operates at the same frequency of the microgrid. It holds the dc link capacitor voltage constant. VSC-2 operates in dynamic frequency droop to control power exchange in between microgrids through PEH.

As shown in Fig. 7.2, a total *N* numbers of microgrids are connected to PEH through BTB converter. The PEH only has to exchange power in between MGs. Thus it can be either three phases or single phase. In this thesis, only three phase type of PEH is considered. Since the PEH is isolated from a MG, the voltage and frequency of PEH can differ from these of any MG. Furthermore, these MGs also can operate at different frequencies base on their local loads.

The main purpose of the topology is to provide support to microgrids during contingency in any one of them. It increases the functionality of a microgrid and extends its maturity. It can increase the total effective capacity of individual microgrid to support peak load. During peak load demand, the excess power can be supplied by other microgrids effectively and instantly using this topology. The microgrids can have different types of DGs such as inertial, a converter interfaced DG (non-inertial). It has been assumed that all DGs operate in frequency droop independently. They will be joined together at PEH through another power-frequency droop. Note that the PEH is only required to flow power between microgrids – no local load is connected to PEH. It is well known that power flow in ac circuits mainly depends on the relative angle difference. Voltage magnitude does

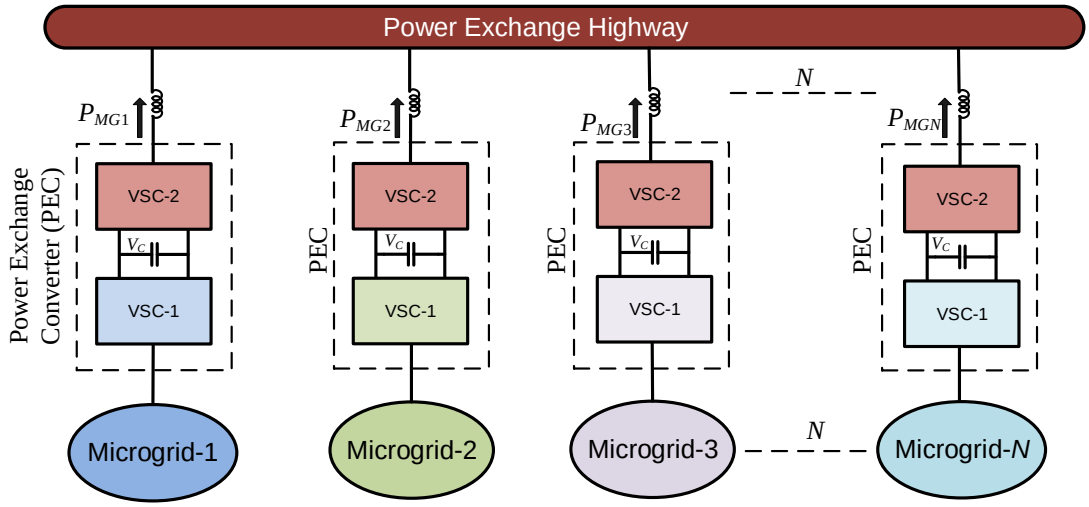

Fig. 7.2. Topology of microgrids interconnection.

not have any significant role in the power flow. Therefore, for PEH, no voltage magnitude-reactive power droop needs to be employed.

7.2. Operation and Control of Microgrid

7.2.1. Nominal Operation

The generalized topology of the microgrid is shown in Fig. 7.3 where, DGs are controlled through a frequency droop [92], given by

$$f = f_r + m_M \times \left(0.5 \times P_M^* - P_M\right) \tag{7.1}$$

$$V = V_r + n \times (Q^* - Q) \tag{7.2}$$

where f_r and f are the rated and instantaneous frequency of DG respectively and the subscript M denotes microgrid.

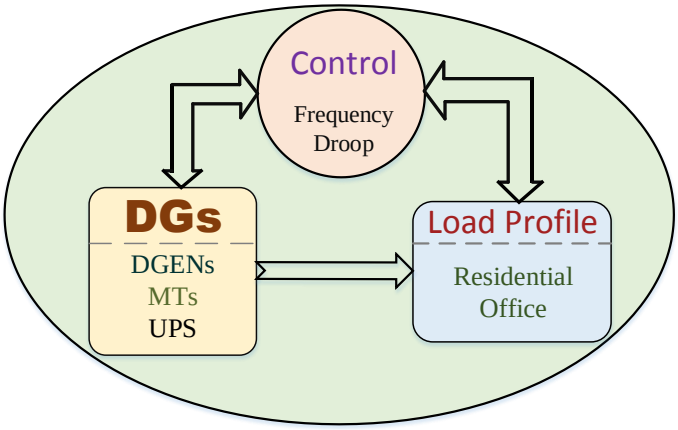

Fig. 7.3. The microgrid topology.

The dispatchable types of DGs are considered in all MGs. These DGs can be diesel generator (DGEN) and converter interfaced type (microturbine (MT), UPS etc.). To operate converter interfaced DG at same response rate of inertial DG, pseudo inertia is used as discussed in Chapter 2 and the detail model of the DGEN and MT are also discussed in the same Chapter. The frequency deviation in MGs is considered within $\pm f_d$ (0.5 Hz) from standard frequency 50 Hz and the voltage magnitude deviation from base voltage is set at ± 5%. The droop coefficients of DGs are calculated based on the above stipulations.

7.2.2. SURPLUS POWER

Surplus power (P_{ee}) is the excess available power in a microgrid that can be used to support other microgrids, if required. The surplus power is calculated following the procedure discussed in Chapter 6, Section 6.3.2. A simpler calculation of surplus power is proposed in this chapter, which only depends on the estimated microgrid frequency and total generation capacity of the microgrid at a given time.

The difference of total capacity of a MG (P_M^*) and power supplied (P_M) by it can be defined as the surplus power. It is assumed that each microgrid should keep 20% of its total generation as a reserve power to support its own peak load demand. Therefore only 80% of its maximum generation can be used for surplus power calculation. If a microgrid operates at frequency f, then from (7.1), we get

$$P_{ee} = 0.8 \times P_M^* - P_M = \frac{f - f_m}{m_M} \tag{7.3}$$

where f is actual frequency of MG and f_m is set as 49.7 Hz, which is the microgrid frequency when it supplies 80% of power P_M^*. The calculation of droop gain is given in terms of rad/s.MW by (2.22) in Chapter 2. It can be directly written in term of frequency as

$$m_M = \frac{f_{max} - f_{min}}{P_M^*} \tag{7.4}$$

where f_{max} is the maximum frequency (50.5 Hz) and f_{min} is the minimum frequency (49.5 Hz) the MG can have.

Substituting the value of m_M from (7.4) into (7.3), we get

$$P_{ee} = \frac{f - f_m}{f_{\max} - f_{\min}} \times P_M^* \tag{7.5}$$

Define, $f_{max} - f_{min} = 2f_d$, we get

$$P_{ee} = \frac{f - f_m}{2 \times f_d} \times P_M^* \tag{7.6}$$

From (7.6), the surplus power of the MG can be calculated based on the actual frequency and the total capacity of the microgrid in presence of plug and play DGs as mentioned in Chapter 6, this requires the status of all DGs.

7.2.3. POWER BALANCING DURING CONTINGENCY

From (7.1) it can be seen that once MG frequency hits to the lower limit of the frequency band, the MG supplies its total maximum capacity power (P_M^*) to the load (P_L) which implies ΔP ($P_M^* - P_L$) will be zero. Once the peak load demand of the MG increases more than its total capacity ($\Delta P<0$), frequency of the microgrid drops below the lower limit and available inertial DGs in the microgrid start releasing their stored kinetic energy (KE) in their rotor to support the microgrid. If this condition persists for a longer period of time, the system will collapse once the stored KE of inertial DGs diminish. However, this power can be drawn from other microgrids (if the surplus power available in them) through the PEH to counter the overload. The drawing of this exact amount of power is tantamount to a reduction of load such that ΔP becomes 0. At this point, the microgrid frequency becomes 49.5 Hz. Thus the basic aim is to get

the frequency back to 49.5 Hz by drawing power from the other microgrids through the PEH.

Hence, the overload power is computed in such a way that MG frequency is maintained at lower limit of frequency droop and drawn from the other microgrids. To achieve this, a PI controller is used, the output of which is overload power. This is given by

$$P_{ov} = K_{P1}(f_{\min} - f) + K_{I1}\int (f_{\min} - f)\, dt \tag{7.7}$$

where f_{min} is the lower limit of the frequency and f is actual frequency of MG. K_{P1} and K_{I1} are the proportional and integral gain of the controller respectively.

The overload power estimated from (7.7) can be supplied from the other microgrids, which are connected through PEH. How this estimated overload power can be shared by the others MGs according to their available surplus power is explained in Section 7.4.

The block diagram of the overload prevention scheme is shown in Fig. 7.4. The microgrid frequency f is compared with a fixed frequency of 49.5 Hz. If this is greater than 0, then a trigger signal (T_{rg}) is activated. Otherwise the trigger signal remains zero. If T_{rg} = 1, then the input to the PI controller is e_f (49.5- f). When the T_{rg} changes from 1 to 0, a one shot Schmitt trigger is used to generate a pulse that will reset the integrator. In input to the PI controller is then changed to 0 such that no overload power is required from PEH.

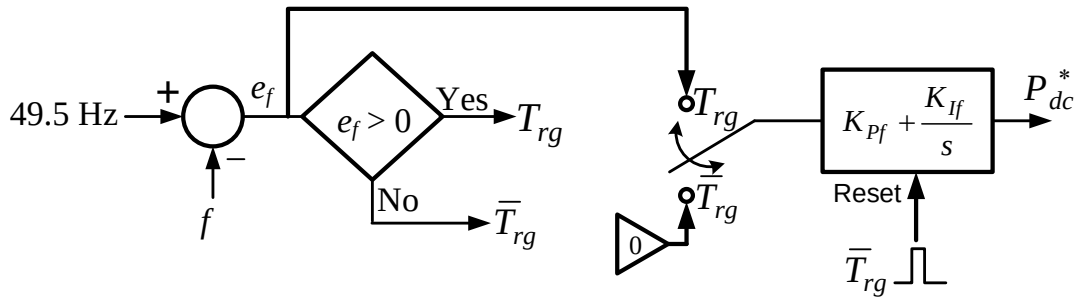

Fig. 7.4. Schematic diagram of the overload prevention scheme.

7.3. OPERATION OF POWER EXCHANGE CONVERTERS (PECS)

The BTB converter, connection an MG with the PEH, is termed as a power exchange converter (PEC) as its sole purpose is to exchange power between the MG and PEH. The control system block diagram of PEC is shown in Fig. 7.5. VSC-1 holds the dc link capacitor voltage (V_{dc}) constant by drawing power from the MG. The MG operates in frequency droop therefore from (7.1) its frequency can drift from 50 Hz according to available local load. Hence, VSC-1 is synchronized with the MG frequency to operate at same frequency of MG as discussed in Chapter 3. The control strategy of the VSC-1 is illustrated in Fig. 7.5. The angle (δ) of reference voltage of VSC-1 is calculated from a PI controller that maintains the dc capacitor voltage constant and the reference voltage is synthesized by phase shifting terminal voltage of the microgrid by angle (δ).

VSC-2 operates in a dynamic frequency droop to share available surplus power (belonging to its MG) with the other microgrid through PEH, which is discussed in details in the next section. Nominally PEC does not need to transfer any power through PEH. This implies that all MGs have sufficient generation to supply its local load. However, VSC-1 and VSC-2 both remain active since VSC-1 has to maintain the dc capacitor voltage constant and VSC-2 has to supply the overload power instantly. If VSC-1 starts charging the dc capacitor voltage when power transfer is required then large capacitor charging transient can cause a large transient in the PEH, which may cause a failure in the overloaded MG.

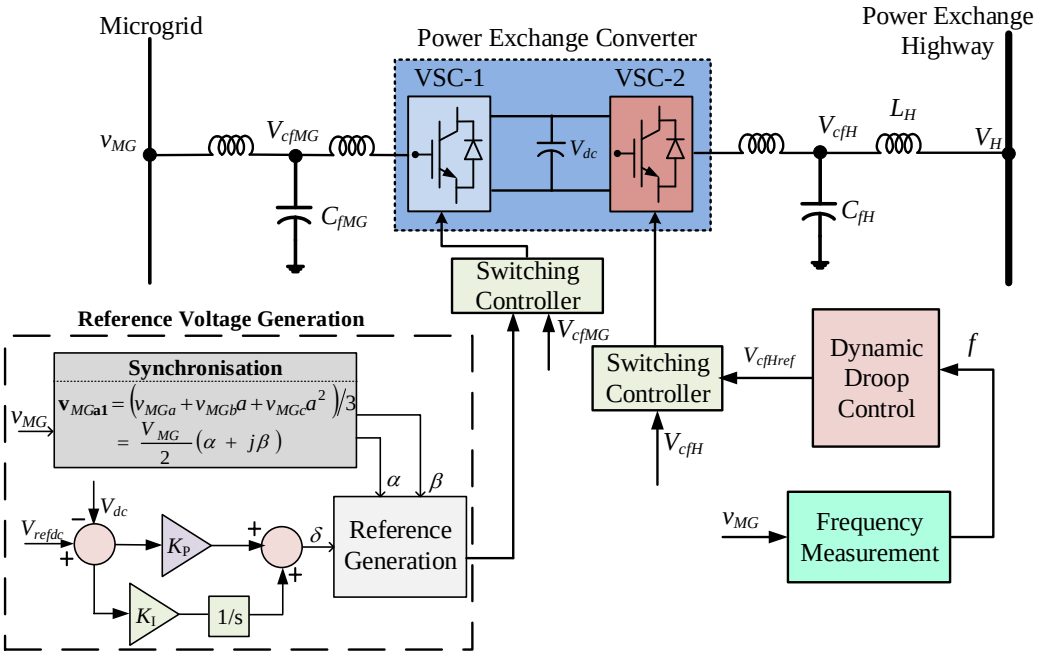

Fig. 7.5. Control scheme of Power Exchange Converter.

VSC-2 switches can remain blocked during nominal operation and can be deblocked when a contingency occurs in any of the MGs. This might require extensive communication between the MGs [101] and can cause delay. To avoid this, VSC-2 is kept ON all the time such that it operates like a DG in a microgrid. A DG in an MG supplies power based on its rating, as determined by its fixed droop gain. However the PEC in an MG, connected to PEH, cannot have a fixed droop gain since its power supplies depend on the surplus power available in the MG. Therefore PEH droop has to be dynamically adjusted as discussed below.

7.4. DYNAMIC DROOP CONTROL

The dynamic droop is used to control power flow through the PEH, where the power flow depends on the overload power required by a microgrid and the available surplus power in the other microgrids. It has been discussed in Section 7.2.2 that the surplus power of a microgrid depends on its frequency. Therefore it changes when the local load of a microgrid varies. Thus the surplus power can be considered as the present capacity of a microgrid that can be used to support others.

Therefore, droop coefficients of the converters connected to the PEH need to be calculated dynamically. Note that the droop coefficient of any DG depends on its

rated capacity. Generally the ratings of dispatchable DGs are constants and hence their droop coefficients are also constant. The dynamic droop, on the other hand, varies with the maximum level of power that an MG can supply. It is given by

$$f_H = f_{Hr} + m_H \times \left(P_H^* - P_H\right) \tag{7.8}$$

where P_H^* is the available surplus power in microgrid connected to PEH, P_H is actual power supplied by converter to PEH and m_H is the dynamic droop coefficient, which is calculated from frequency range and P_H^* as

$$m_H = \frac{(f_{Hmax} - f_{Hmin})}{P_H^*} \tag{7.9}$$

Note that f_H in (7.8) is 50 Hz when $P_H^* = P_H$, which is equal to f_{Hmin} and frequency deviation (f_{Hd}) is 0.5 Hz. Therefore f_{Hmax} is 50.5 Hz at which $P_H = 0$. The relation between the droop in PEH and that in an MG is discussed below.

Once an MG starts supplying power to another MG through PEH its frequency decreases. This will cause P_{ee} to in (7.6) to reduce. If the reference power of the dynamic droop is changed for every change in local or external (PEH) load, the droop gains will fluctuate continuously. Therefore P_H^* is computed from P_{ee} – these two quantities are not necessarily the same. It has been mentioned before, every microgrid will always keep 20% of total generation capacity (P_M^*) to supply a suddenly peaking load in the microgrid. Therefore P_H^* in the dynamic droop computation is kept constant until the local load demand of microgrid is changed more than its reserved power (20% of P_M^*).

Hence, the estimation of dynamic droop coefficient (m_H) and reference power (P_H^*) depends on the corresponding microgrid frequency and the dynamic droop frequency. In Fig. 7.6, the droop lines of PEC and microgrid are shown. It can be seen that when no power flows in the PEH, frequency of the PEC is at its maximum limit of 50.5 Hz. Now consider case when P_{H1} amount of power flows from PEC to PEH, while the MG is supplying P_1 amount of power such that its frequency is f_1. Now if the local load increases such that this MG has to supply P_2 amount of power, the frequency changes to f_2. This change is solely caused by the change in the local load and power flowing from the MG to PEH remains unaltered. Therefore the frequency of the dynamic PEH droop will remain constant at f_{H1} (see Fig. 7.6).

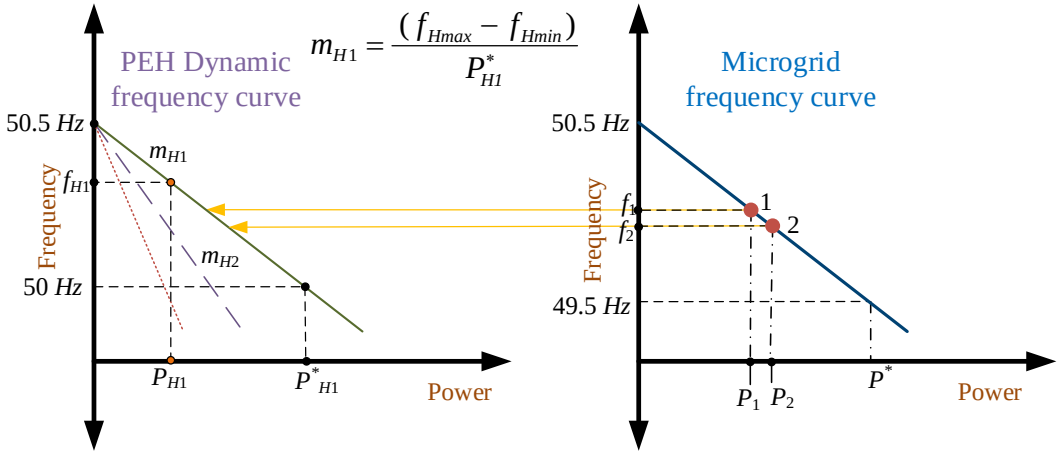

Fig. 7.6. Droop line for PEH when MG frequency variation is less than 0.2 Hz due to local load change in MG.

Note that the power variation in MG can be calculated from its frequency. Since the frequency variation is limited to be within ± 0.5 Hz, each 0.1 Hz variation in the MG frequency corresponds to 10% variation in P_M^*. Therefore, if the MG frequency reduction is less than 0.2 Hz due to local load variation, as indicated by no change in f_{H1}, the dynamic droop line will not change and the droop gain will remain constant at m_{H1}.

However the MG frequency can vary with both the variation in local load and power flow in PEH. An increase (decrease) in the supplied power by the MG is equal to that in PEC output indicates that there is no change in the power consumption level of the MG local load. This can also be determined by the microgrid and the dynamic droop frequencies. Consider the droop lines of Fig. 7.7. It can be seen that the MG frequency changes from f_1 to f_2 as a consequence of the change in the PEH droop from f_{H1} to f_{H2}. From (7.1), the power variation in the MG is

$$\Delta P_M = \frac{(f_1 - f_2)}{m_M} \tag{7.10}$$

Now since f_{max} = 50.5 Hz and f_{min} = 49.5 Hz, from (7.4), we get

$$m_M = \frac{1}{P_M^*} \tag{7.11}$$

Combining (7.10) and (7.11), we get

$$\Delta P_M = (f_1 - f_2) \times P_M^* \tag{7.12}$$

In a similar way, the frequency variation in PEH is given by

$$\Delta P_H = 2(f_{H1} - f_{H2}) \times P_H^* \tag{7.13}$$

Therefore when $\Delta P_M = \Delta P_H$, it can be surmised that the entire power change is due to an increase in the power flow through PEC.

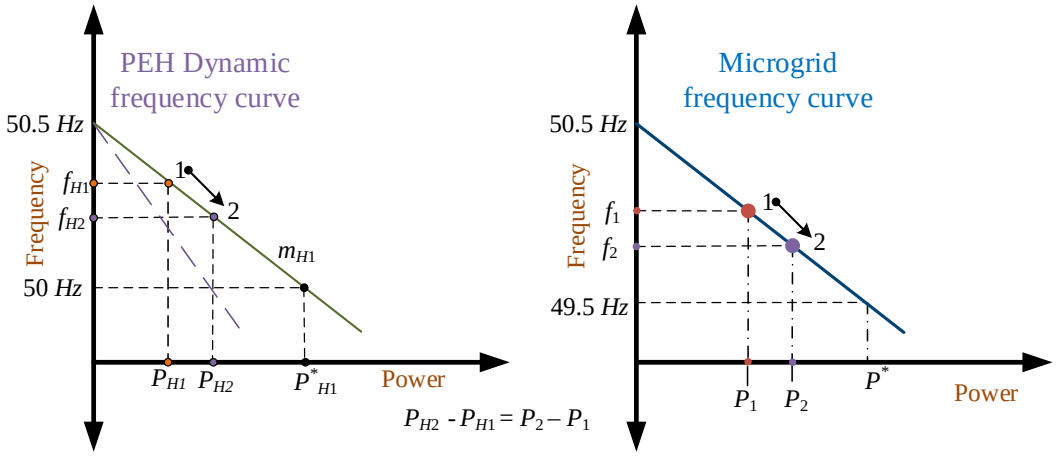

Fig. 7.7. Droop lines for the PEH and the MG.

It has been mentioned that an MG should have 20% reserve available power to cater to the peaks in its local load. Therefore we can write

$$0.8P_M^* \geq P_M + P_H^*$$

Now consider the case when P_M changes by more than 20% of P_M^*. For example consider the case when the rating (P_M^*) of a microgrid is 1 MW and it is supplying P_M = 250 kW. Then we can choose P_H^* as 550 kW. Now suddenly the local load increases to 450 kW. This implies that P_H^* has to be reduced to 350 kW. On the other hand, if the local load increases by 50 kW, there is no need to change P_H^* since there still will be a reserve of 150 kW.

Thus, if the local load changes more than the 20% of the total capacity of the microgrid, then P_H^* is estimated from currently available P_{ee}, which is

$$P_{ee} = P_H^* = 0.8 \times P_M^* - (P_M - P_H) \tag{7.14}$$

where P_M is calculated from (7.1) using the value of MG frequency and P_H is calculated from (7.8) using the value of the PEH frequency. Substituting the value of P^*_H from (7.14) to (7.9), the value of m_H also can be estimated.

In Fig. 7.8, it can be seen that the power (P_H) supplied from PEC remained same and the power supplied by the microgrid is changed from point 1 to 2 which is more than the 20% of the total capacity of the microgrid. Therefore the reference power is changed from P^*_{H1} to P^*_{H2} and dynamic droop coefficient is changed from m_{H1} to m_{H2}.

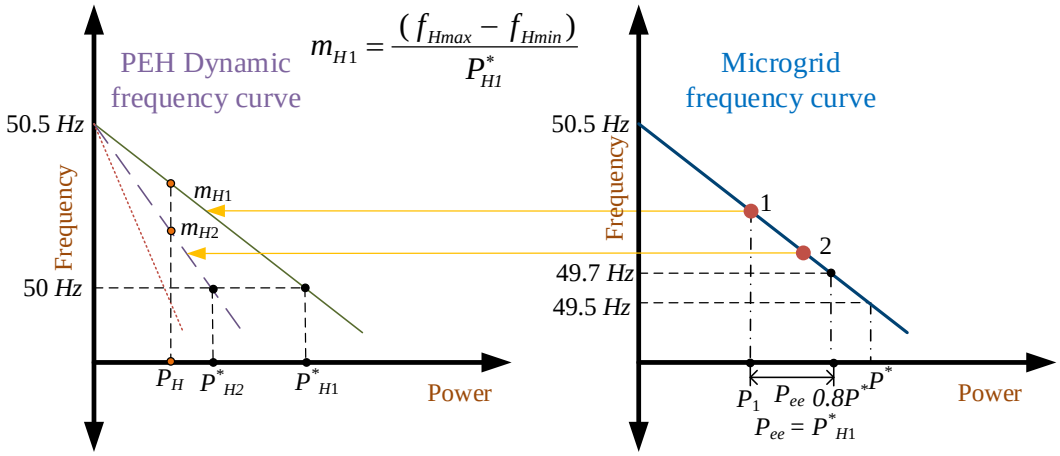

Fig. 7.8. Droop line selection for PEH.

In Fig. 7.9, a cluster of microgrids is shown with their control schemes, where only two microgrids are shown. It can be generalized to *n* number of microgrids. Let us assume, one of the microgrids has power shortage due to overload. Therefore, the other microgrid, which is assumed to have available surplus power, will start supplying power through the PEH. The PEC operates in dynamic droop control. The overload power (P_{ov}) is estimated from (7.7). If this amount of power is drawn from the other microgrid, the frequency can be maintained at the lower limit of (f_{min}). Then P_{ov} is taken as the reference power for the PEC (VSC-2) of the overloaded MG. It needs to extract this amount of power from the other MGs. Therefore, it is accomplished by a PI controller that controls the angle of the output voltage of PEC (VSC-2), given by

$$\delta = K_{P2}(P_{ov} - P_H) + K_{I2}\int (P_{ov} - P_H)\, dt \tag{7.15}$$

The main aim of this controller is to deflect the angle δ from the angle of the voltage (v_H) in such a way that the required amount of power flows from the PEH. To operate at the same frequency of the PEH, VSC-2 reference voltage is generated in such that it is synchronized with v_H at angle difference δ. It works as a constant P load for the PEH.

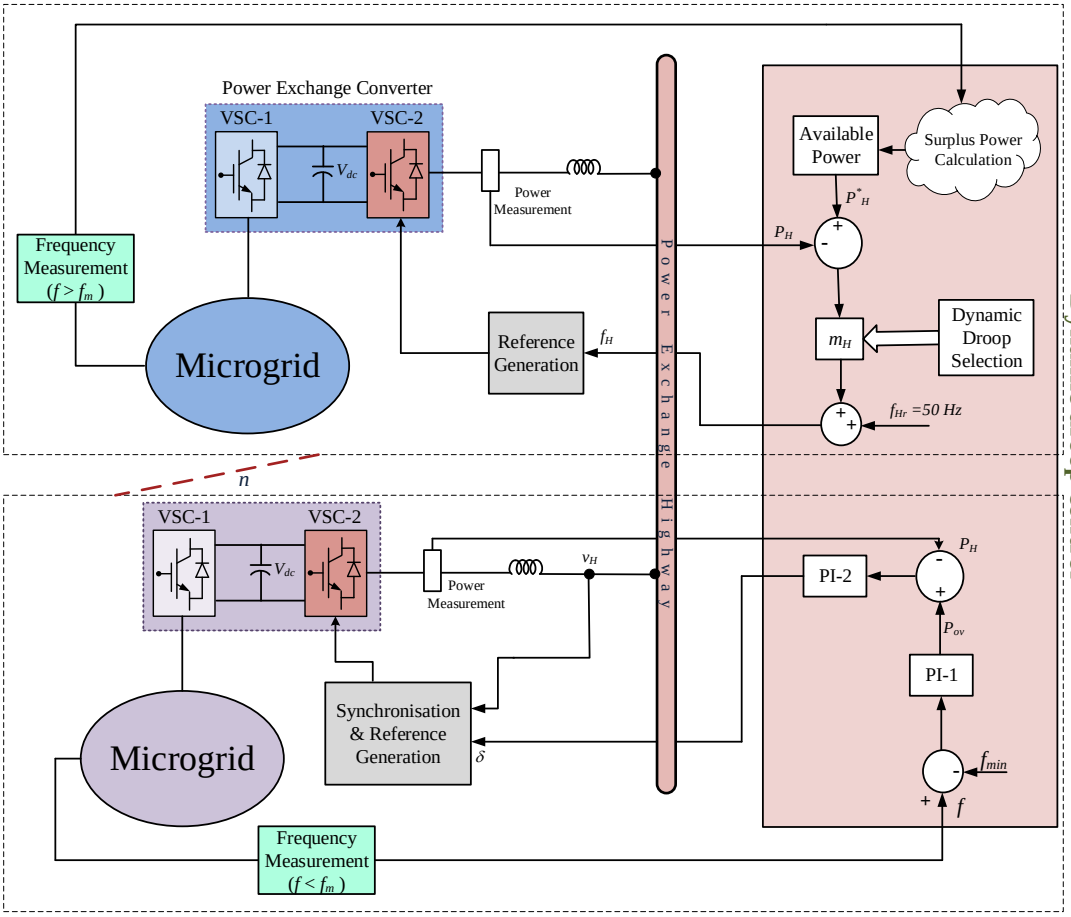

Fig. 7.9. Dynamic droop control in cluster of microgrids

The other MGs operate in dynamic droop to share this overload power according to available surplus power. The available maximum power in MGs is calculated from (7.6), which is equivalent to P_H^*. The dynamic droop coefficient (m_H) is selected according to reference power (P_H^*). With these parameters, the frequency of the PEC (VSC-2) is calculated from (7.8).

7.5. SIMULATION STUDIES

The proposed control strategy is validated in PSCAD. The parameters of the MGs are given in Table 7.1, Table 7.2 and Table 7.3. Various test conditions are chosen for studies. The results are discussed below.

7.5.1. FREQUENCY BASED OVERLOAD PREVENTION

This example verifies the Section 7.2.3. Let us consider a microgrid contains two DGENs each with a rating of 500 kW. In the steady state, the local load of MG is 850 kW. The load demand is increased to 1050 kW which is higher than the total capacity of the MG. This MG is connected with the PEH through PEC. The overload power is estimated in such a way that frequency of the MG is maintained at the lower limit through the PI controller. Results are shown in Fig. 7.10 and Fig. 7.11. It can be seen from Fig. 7.10 (a) that microgrid frequency is brought back to 49.5 Hz and the estimated overload power from PI controller also settle to a steady state value, as shown in Fig. 7.10 (b). Both these settle within 6 s. The power flow in microgrid is shown in Fig. 7.11, where it can be seen that the DGENs supply their rated power in steady state and overload power is extracted from the PEH.

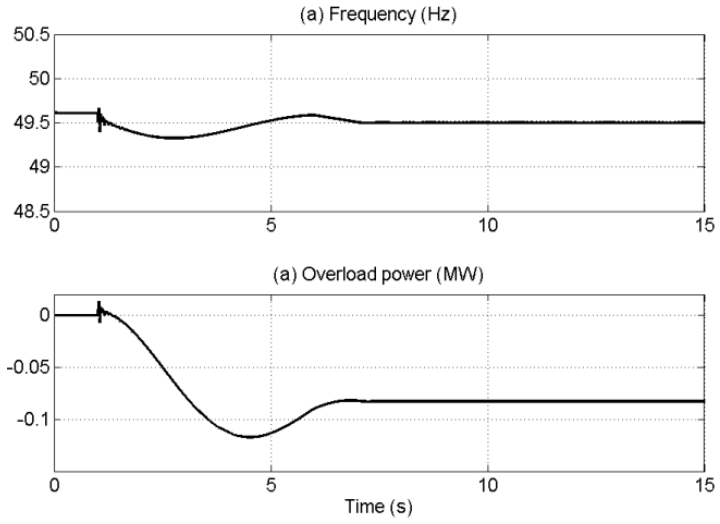

Fig. 7.10. MG frequency and overload power balancing through PEC.

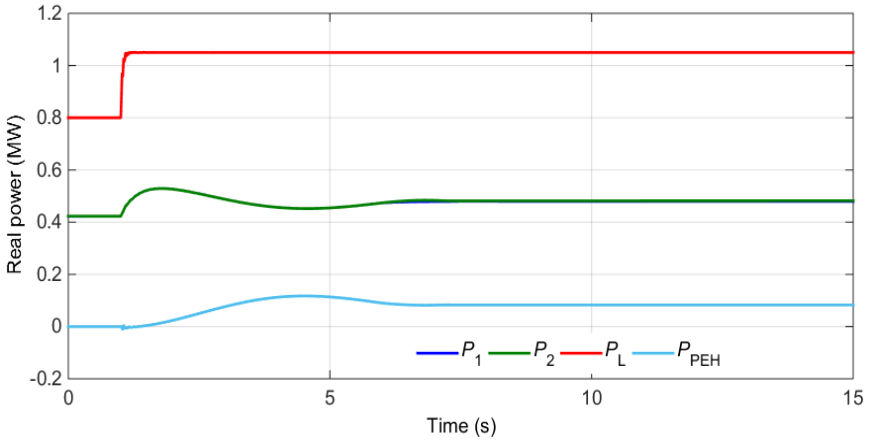

Fig. 7.11. Power flow in MG during contingency.

7.5.2. MICROGRIDS CLUSTER OPERATION

Two different case studies are considered. These are

Case (A) No power exchange through PEH

Case (B) Power exchange through PEH for power balancing during contingency

CASE (A): NO POWER EXCHANGE THROUGH PEH

In this case, all microgrids have sufficient amount of available power to support their local loads. Therefore, there is no need of power exchange in between MGs through PEH. Let us assume that three MGs are considered in structure shown in Fig. 7.2, which are connected through PEH. Each MG has different capacity as parameters of DGs in MG are given in Table 7.1, Table 7.2 and Table 7.3. MG-1 has total capacity of power 750 kW and consists of local load of 300 kW. Similarly, the total capacity of MG-2 and MG-3 are 600 kW and 1000 kW respectively. In steady state the local loads of MG-2 and MG-3 are 280 kW and 850 kW respectively. Therefore, the power exchange from PEH is zero as can be seen from Fig. 7.12 (a). The frequency of each microgrid is shown in Fig. 7.12 (b), it can be seen that each MG is operating independently at different frequency to support its local load. The frequency of the VSC-2 connected to PEH is at upper limit of the dynamic frequency droop (50.5 Hz), shown in Fig. 7.12 (b). It illustrates that there is no power exchange through PEH.

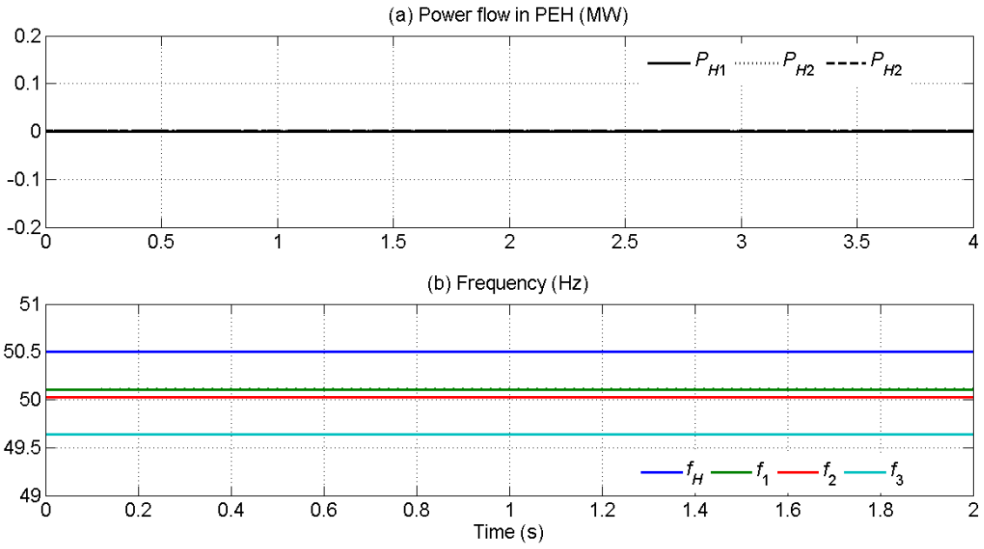

Fig. 7.12. Power flow in PEH and Frequencies in PEH and MGs

Table. 7.1. Parameters of Microgrid-1.

System Quantities	**Values**
DG_1 Feeder impedance	R_{f1} = 3.025 Ω, L_{f1} = 57.8 mH
DG_2 Feeder impedance	R_{f2} = 3.025 Ω, L_{f2} = 57.8 mH
DG Rated Power	DG-1: 250 kW, DG-2: 500 kW
Droop Coefficient (Frequency–Voltage)	
m_{f1}	0.0251 rad/MWs
m_{f2}	0.0126 rad/MWs
n_{f1}	0.004 kV/MVAr
n_{f2}	0.002 kV/MVAr

Table. 7.2. Parameters of Microgrid-2.

System Quantities	**Values**
DG_1 Feeder impedance	R_{f1} = 1.21 Ω, L_{f1} = 38.5 mH
DG_2 Feeder impedance	R_{f2} = 2.42 Ω, L_{f2} = 77.0 mH
DG Rated Power	DG-1: 200 kW, DG-2: 400 kW
Droop Coefficient (Frequency–Voltage)	
m_{f1}	0.0314 rad/MWs
m_{f2}	0.0157 rad/MWs
n_{f1}	0.002 kV/MVAr
n_{f2}	0.001 kV/MVAr

Table. 7.3. Parameters of Microgrid-3.

System Quantities	**Values**
DG_1 Feeder impedance	R_{f1} = 3.025 Ω, L_{f1} = 57.8 mH
DG_2 Feeder impedance	R_{f1} = 3.025 Ω, L_{f1} = 57.8 mH
DG Rated Power	DG-1: 500 kW, DG-2: 500 kW
Droop Coefficient (Frequency–Voltage)	
m_{f1}	0.0126 rad/MWs
m_{f2}	0.0126 rad/MWs
n_{f1}	0.04 kV/MVAr
n_{f2}	0.04 kV/MVAr

CASE (B): POWER BALANCING IN MG-3

Let us assume that the local load demand in MG-3 is increased to 1065 kW which is greater than the total capacity of the MG-3 and other MGs having same rating as mentioned in case A. Therefore, the frequency of MG-3 reduces and hits to the lower limit of frequency droop. Hence, overload power estimator activates to extract the power from the other microgrids in the same manner as shown in Section 7.5.1. The dynamic frequency droop controls the power sharing based on the available surplus power in other MGs. At this time the surplus power in MG-1 and MG-2 are 300 kW and 200 kW respectively. It can be seen in Fig. 7.13 (a) that PEC-3 extracts 75 kW power from PEC-1 and PEC-2, which is shared by them. The frequency of the dynamic droop is shown in Fig. 7.13 (b), which is 50.5 Hz when there is no power flow through PEH and it reduces to 50.42 Hz according to the power flow in PEH.

The power flow in the microgrids connected to the PEH through the PEC is shown in Fig. 7.14. In nominal situation, MG-1 consists of two DGs with rating of 250 kW and 500 kW and the local load is 300 kW. The power flow in MG-1 is shown in Fig. 7.14 (a.1). It can be seen that power from MG-1 increases as it starts supplying power to MG-3. The frequency of the MG-1 also reduces according to power as can be seen in Fig. 7.14 (a.2). VSC-1 connected with the MG-1 holds the dc capacitor voltage at constant value of 2.5 kV, baring some transients during power flow change in the PEC, as shown in Fig. 7.14 (a.3).

In nominal situation, MG-2 consists of two DGs with rating of 200 kW and 400 kW and the local load is 280 kW. The power flow in MG-2 and the frequency of

DGs are shown in Fig. 7.14 (b.1) and Fig. 7.14 (b.2) respectively. The dc link capacitor voltage of the VSC-1 connected with MG-2 is shown in Fig. 7.14 (b.3). In nominal situation, MG-3 contains two DGs which are the same rating of 500 kW and its local load is 850 kW. When the power increases to 1075 kW, the DGENs supply at the maximum capacity (Fig. 7.14 (c.1)). Frequency is held at 49.5 Hz (Fig. 7.14 (c.2)) and the dc capacitor voltage remains 2.5 kV (Fig. 7.14 (c.3)).

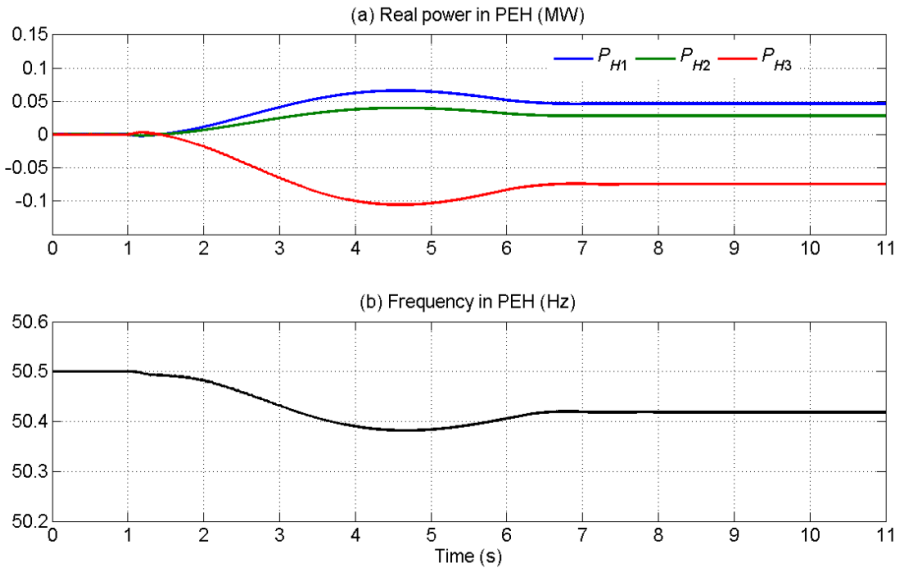

Fig. 7.13. Power flow and frequency in PEH.

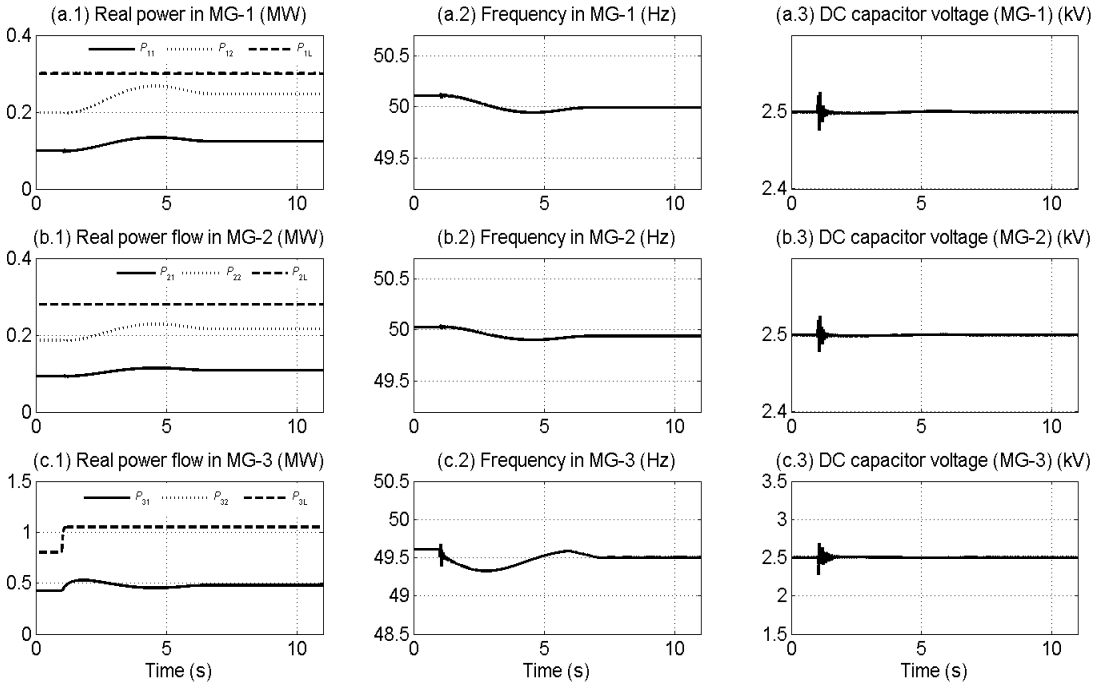

Fig. 7.14. The power flow and frequencies in microgrids with VSC-1 (PEC) dc capacitor voltage.

7.5.3. MG NON PARTICIPATION IN POWER SHARING

A MG may not participate in power sharing through PEH, especially when there is no sufficient reserve in it. The following conditions are set based on which an MG may not participate in power sharing.

- The reference power of dynamic droop is less than 20% of the total capacity of the microgrid and the dynamic droop frequency is higher than half of the maximum limit of frequency (f_{Hmax}). It means others have well sufficient power to support any overloaded microgrid and the microgrid does not have sufficient reserve.
- If frequency of the microgrid (f) is less than 50 Hz and load has increased more than 10% of reserve power. This will result in frequency drop of 0.1 Hz and a more in the MG. In either case the MG has to plug out.

A simple way of plugging out is to halt the power flow. Refer to Fig. 7.5, where inductor L_H connects the VSC-2 output voltage (V_{cfH}) to PEH voltage (V_H). If the reference for V_{cfH} is chosen as V_H, there will be no power flowing through L_H. In this way VSC-2 remains in the circuit supply zero power, but ready for any contingency in its own MG. The results are shown in Fig. 7.15. In this case four MGs are connected through PEH. It can be seen in Fig. 7.15 (a) that MG-4 is overloaded and consuming 120 kW power from other three microgrids. At 1 s, MG-1 stops participating in power sharing through PEH and power supplied by other microgrids are increased to support MG-4. The frequency of the PEH is reduced as MG-1 stopped power supplying to PEH as shown in Fig. 7.15 (b).

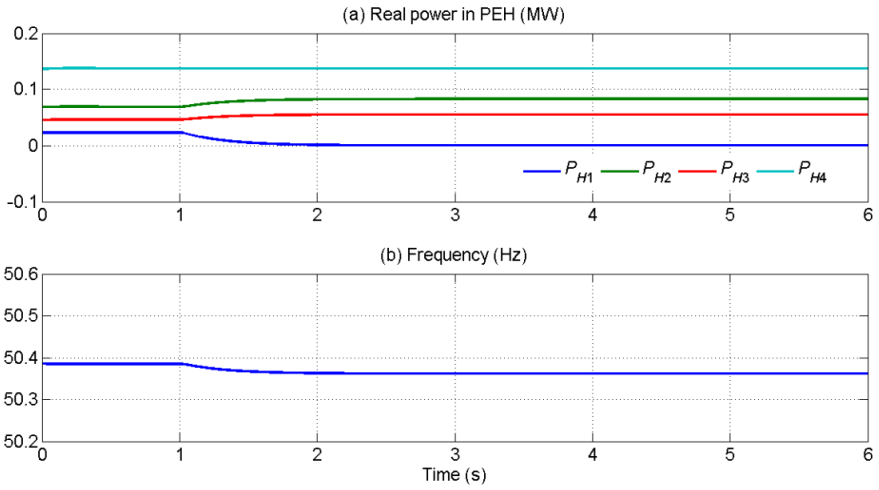

Fig. 7.15. Power flow in PEH during non-participation of MG in power sharing and PEH frequency.

7.6. CONCLUSION

In this chapter, a topology of the cluster of microgrids interconnection is proposed. The power exchange highway concept is used to interconnect the microgrids and to support any microgrid during contingency. In this chapter, mainly control strategy of power sharing amongst microgrids which are connected through the power exchange highway is focused. Each microgrid operates in independent frequency droop control. To isolate these microgrids, back to back converter is connected between PEH and microgrid. This BTB converter is termed in this chapter as power exchange converter. The dynamic droop control is discussed to control the power flow in PEH.

Few issues of proposed topology in this chapter such as how long the MG can support to the overloaded microgrid and MGs connection/disconnection in PEH, can be decided based on the MG frequency which represent its available surplus power. A situation, when two and more microgrids need power during contingency and other microgrids also do not have surplus power at same time then load shedding has to be considered. These issues are beyond the scope of this thesis. Few extensive digital computer simulation results are provided to validate the proposed control strategy of microgrids cluster interconnection.

CHAPTER 8

CONCLUSIONS

The general conclusion of the thesis and scope of future work are presented in this chapter. The conclusion are based on the work carried out and reported in the earlier chapters.

8.1. GENERAL CONCLUSIONS

These are listed below.

1. When a microgrid contains inertial and non-inertial generators, the difference in their time constants can lead to large transient oscillations. To avoid this, the response speed of converter interfaced generators can be made slower using the pseudo inertia concept that imitates a governor action, as well as includes a swing equation. The governor and swing equation parameters can be tailored to respond in harmony with inertial rotary generators.
2. A modification of the angle droop, which considers the bus voltages rather than converter output voltages, can overcome the main drawback of this technique, which is the dependence on the converter output inductances for power sharing.
3. For the interconnection of non-dispatchable DGs with an islanded microgrid that is operating in a frequency droop, two strategies can be employed. One of these strategies includes a synchronisation algorithm, which requires only the instantaneous measurements of PCC bus voltages. In the other strategy, an isochronous controller can be integrated with frequency droop control such that the system operating frequency always remains at 50 Hz.
4. A DSTATCOM can be used in a microgrid for power quality improvement. However the DSTATCOM must operate at the microgrid frequency. When an isochronous controller is used, the DSTATCOM can operate at 50 Hz. Alternatively microgrid operating frequency needs to be estimated, based on which the DSTATCOM must synthesize its voltages.

5. Energy storage devices (e.g. BESSs) are required to prevent collapse in an islanded microgrid due to an overload. To improve the lifetime of the BESSs, they must operate in a fashion such that only the amount of overload power is supplied. The modified angle droop can facilitate this even when a microgrid contains rotary generators and operates in frequency droop.
6. Two microgrids that are in close proximity can be interconnected for mutual support during any contingency. To maintain the integrity of operation of these two microgrids, they must be connected by an interlinking back to back converter system. To control the power flow during contingency in any of the two microgrids, the overload power estimation and available surplus power computation are required. The interlinking converter then regulates the bidirectional power flow based on these quantities.
7. A cluster of microgrids can be interconnected through common ac feeder, which has been termed as a power exchange highway (PEH), to support during contingency in any microgrid. Each microgrid in such a cluster must be connected through an interlinking converter with the power exchange highway such that each microgrid can operate independent of all other microgrids. To control the power flow amongst microgrids, an outer layer droop control is required. Since the available surplus power in a microgrid is not a constant quantity and varies with the changes with the microgrid local load, the droop gains of the outer layer should be dynamically selected. The interlinking converter then facilitates a bidirectional power flow between a microgrid and the power exchange highway.

8.2. SCOPE FOR FUTURE WORK

Some scopes of future work can be identified as given below.

1. The pseudo inertia concept only slows down the speed of response of a converter interfaced DG and cannot supply any electrical power during overload power due to lack of stored kinetic energy. However the DC bus of the converter can be equipped with ultra-capacitors, which do not discharge rapidly. This needs to be thoroughly investigated.

2. In cluster of microgrids, the power exchange highway can be three-phase AC, single-phase AC or even DC. The converter configuration, rating and power flow control scheme for the single-phase AC or even DC power exchange highway can be investigated.
3. In this thesis, mainly the control strategy for the power flow control amongst cluster of microgrid is focused. This strategy only considers the surplus available power in each microgrid. The cost factor has not been considered. The outer layer droop control can be modified to include the cost power supply from each microgrid independently.
4. A supervisory control scheme and communication infrastructure will be needed for including the cost in the outer layer. They can also be investigated.

APPENDIX A

The voltage source converter structure and control used in this thesis are presented in this appendix which is already published by other authors. These converter structures have been used in converter interfaced DGs and back to back converters. Depending on the requirement, the LCL and LC type of filter is used. The control strategies of the converter adopted in this thesis are output feedback controller and state feedback controller according to requirements.

A.1. CONVERTER STRUCTURE AND POLE SHIFT SWITCHING CONTROL

The structure of the voltage source converter (VSC) is shown in Fig. 2.7. It contains three H-bridges that are supplied from the common dc bus. The output of each H-bridge is connected to a T-filter consisting of an inductor (L_1), a capacitor (C_f) in the secondary side of the single-phase transformer. The secondary sides of the transformers are connected in wye. The transformers provide galvanic isolation and voltage boosting. The resistance R_f represents the switching and transformer losses, while the inductance L_f represents the leakage reactance of the transformers. Note that the inductor L_1 is taken as the output inductor of VSC. In droop control, the desired instantaneous output voltage of VSC is obtained from droop equations. The aim of the VSC switching control is to establish this desired voltage across the capacitor C_f. The pole shift controller is used to achieve VSC switching control [124]. The filter parameters of VSC are given in Table. A.1.

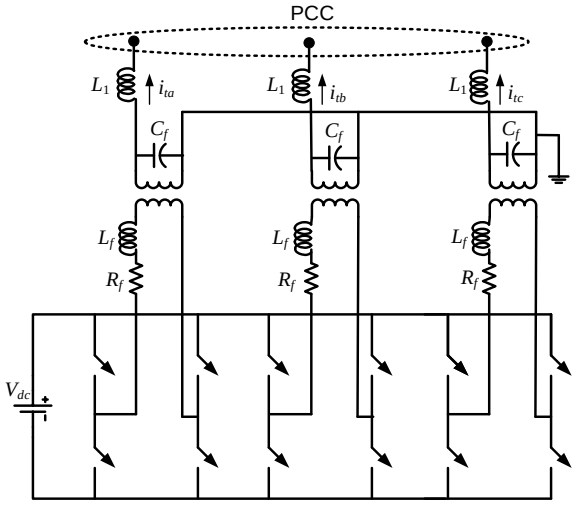

Fig. A.1. The structure of VSC.

Table. A.1. VSC filter parameters (Fig. A.1).

Parameters	**Values**
R_f	1 Ω
C_f	50 μF
L_1	25 mH
V_{dcref}	2.5 kV
Transformer	1 MVA, 3/11 kV, leakage inductance (L_f) of 2.5%

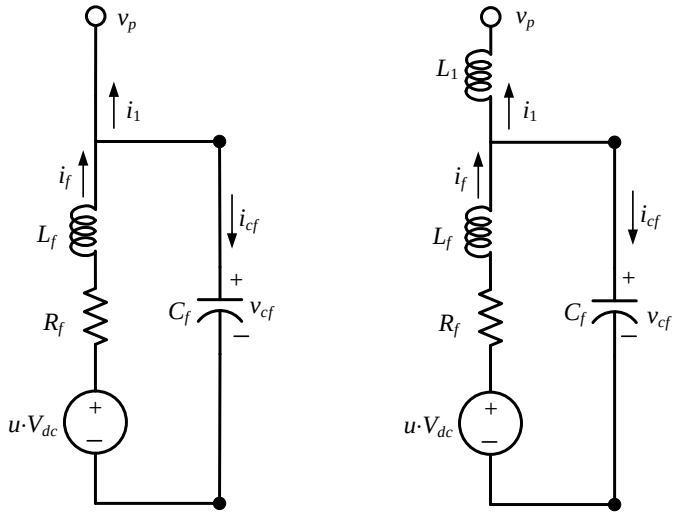

(a) LC type output filter (b) LCL type output filter

Fig. A.2. Single phase converter equivalent circuit.

From the equivalent circuit of Fig. A.2 (a), a state vector is defined as $\mathbf{x}(t) = [v_{cf}(t)\ i_f(t)]$. Then the state-space equation of one phase of the VSC is expressed as

$$\dot{x}_1(t) = Ax_1(t) + B_1 u_c(t) \tag{A.1}$$

While the state space equation for Fig. A.2 (b) can be given as

$$\dot{x}_2(t) = Ax_2(t) + B_2 u_c(t) + B_2 v_p(t) \tag{A.2}$$

where u_c is the continuous time version of switching function u. Based on the feedback control law, u_c is computed.

Let the VSC output given in (A.1) is v_{cf}. The instantaneous three phase reference voltages (v^*) are generated with the voltage magnitude value V and voltage

angle ϕ. Therefore, input-output relationship of VSC [124] can be written in discrete form as

$$\frac{v_{cf}(z)}{u_c(z)} = \frac{M(z^{-1})}{N(z^{-1})} \tag{A.3}$$

The switching control u_c is computed from

$$u_c(z) = \frac{S(z^{-1})}{R(z^{-1})}\left\{v^*(z) - v_{cf}(z)\right\} \tag{A.4}$$

The closed transfer function is

$$\frac{v_{cf}(z)}{v^*(z)} = \frac{M(z^{-1})S(z^{-1})}{N(z^{-1})R(z^{-1}) + M(z^{-1})S(z^{-1})} \tag{A.5}$$

Based on the pole placement strategy [125] the polynomial coefficients S and R can be chosen. Once u_c is computed, switching function u can be generated as

$$\begin{aligned} &\textit{if} \quad u_c > h \quad \textit{then} \;\; u = +1 \\ &\textit{elseif} \quad u_c < h \quad \textit{then} \;\; u = -1 \end{aligned}$$

where h is a small number.

A.2. CONVERTER STRUCTURE AND STATE FEEDBACK CONTROLLER

This VSC is a transformer-less three-phase three-leg neutral-clamped VSC, with the schematic diagram of Fig. A.3. In this figure, each switch represents an insulated gate bipolar transistor (IGBT) along with a snubber circuit and an anti-parallel diode. The dc link of the VSC is composed of two series-connected dc capacitors (C_{dc}), each with a dc voltage of $V_{dc}/2$, where their common node is connected to the system neutral to provide a path for the circulation of the zero-sequence component of the load current. An LC filter (L_f-C_f) is connected at the output of each phase of the VSC to suppress the high frequency switching harmonics of the current and voltage output of VSC. The resistance R_f represents the converter losses.

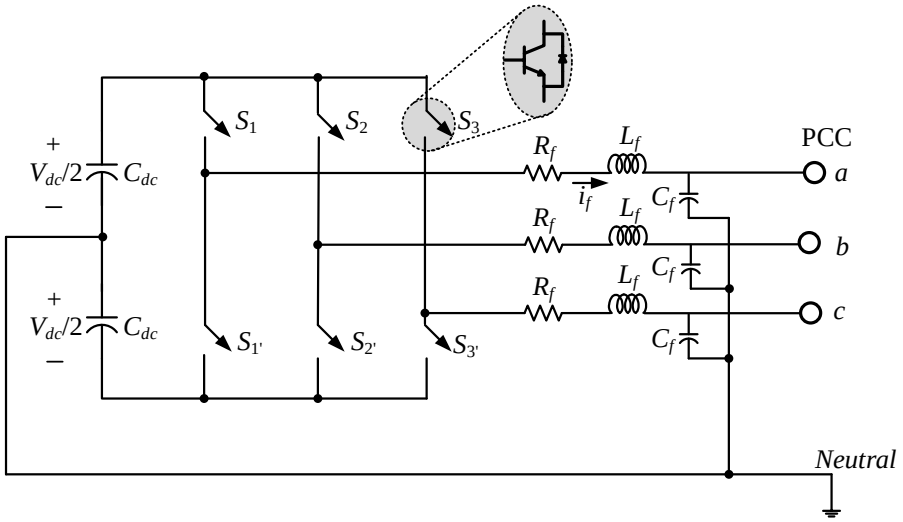

Fig. A.3. The VSC structure.

In a state feedback controller, to generate the switching signal for the converter the chosen states are compared with their reference values. The two state variables, v_{cf}^* is the reference capacitor voltage, while it is rather difficult to form the reference i_f^*. Fortunately the current i_f is only required for feedback stabilization – its contribution to reference tracking is not required. We can therefore stipulate that i_f should only contain low frequency components and its high frequency components should be forced to zero [121]. Therefore, the high frequency components of i_f are extracted by passing it through a high-pass filter (HPF), with a cutoff frequency of α, which is compared to zero and is used for u_c computation. The HPF is given by

$$\frac{i_{fHPF}}{i_f} = \frac{s}{s+\alpha} \tag{A.6}$$

A discrete-time linear quadratic regulator (DLQR) is used for the switching control, in per phase basis. The control law is shown in Fig. A.4.

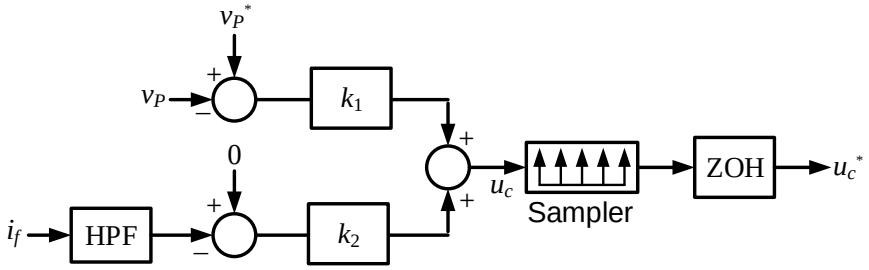

Fig. A.4. VSC feedback control law.

In Fig. A.4, k_1 and k_2 are feedback gains, obtained using DLQR procedure. The resulting control signal u_c is sampled by a sampler and held by a zero order hold (ZOH) circuit to obtain u_c^*. The VSC switching control scheme is shown in Fig. A.5. This consists of a triangular carrier waveform (v_{tri}) that varies from – 1 to + 1 with a duty ratio of 0.5. The control output u_c is sampled twice in each cycle – at negative and positive peaks of the carrier waveform. The switching signals are generated from the comparison of the carrier waveform and the sampled output, as shown in Fig. A.5. Note that the switches S_1 and $S_{1'}$ are complimentary as shown in this figure.

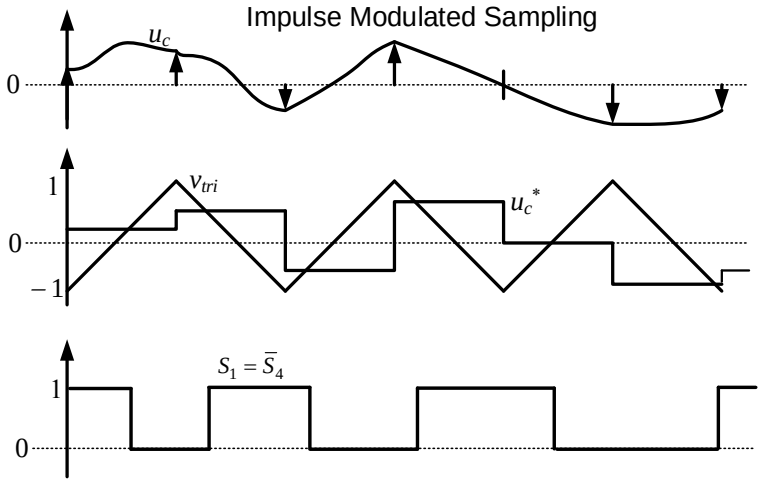

Fig. A.5. PWM switching control of VSC.

Table. A.2. VSC filter parameters (Fig. A.3).

Parameters	**Values**
R_f	0.001 Ω
C_f	50 μF
L_1	33 mH
V_{dcref}	16 kV

APPENDIX B

B.1. FREQUENCY ESTIMATION TECHNIQUE

Let us consider a three phase voltage

$$\begin{aligned} v_{au} &= V_m \sin(\omega_1 t + \phi) \\ v_{bu} &= V_m \sin(\omega_1 t - 120° + \phi) \\ v_{cu} &= V_m \sin(\omega_1 t + 120° + \phi) \end{aligned} \tag{B.1}$$

where V_m is the peak voltage magnitude, ω_1 is unknown frequency and ϕ is phase angle of voltage.

The positive sequence of the considered voltage in (B.1) is

$$V_u = v_{au} + a\, v_{bu} + a^2\, v_{cu} = |V_u| \angle \delta_u \tag{B.2}$$

where $a = e^{j120°}$

Let us assume, $\omega_1 = \omega = 100\pi$ rad/s, $\phi = 0$ and peak voltage 1 p.u. From (B.2), vector is

$$|V_u| \angle \delta_u = 1.5 \angle -90^o \text{ ; t = 0, 0.02s, 0.04 s…} \tag{B.3}$$

This vector starts its rotation at $t = n \times 0.02$ s, $n = 0, 1, 2, \ldots$ from point A as shown in Fig. B.1. It completes its one rotation (360°) in 50 Hz ($t = (n + 1) \times 0.02$ s). The rotation per Hz is 360/50 = 7.2°. If frequency of this vector is less than 50 Hz it takes more than $(n + 1) \times 0.02$ s to complete one rotation. Therefore, in $(n + 1) \times 0.02$ s it reaches to point B as shown in Fig. B.1. In the other hand, frequency of vector is higher than 50 Hz it reaches to point C.

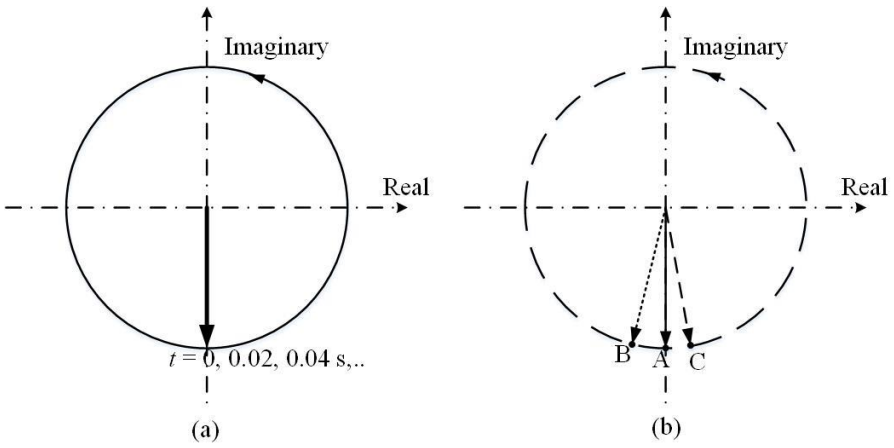

Fig. B.1. Trajectory of a balanced vector rotating at (a) 50 Hz and (b) unknown frequency.

Therefore, frequency (rad/s) can be estimated as

$$\omega_1 = 2\pi \times \left(50 - \frac{\delta_n - \delta_{n+1}}{7.2} \right) \tag{B.4}$$

Thus, accurate frequency of MG is estimated from (B.4)

REFERENCES

[1] S. Chowdhury, S. P. Chowdhury, and P. Crossley, *Microgrids and Active Distribution Networks*, UK: Institution of Engineering and Technology, 2009, pp. 57-76.

[2] J. A. P. Lopes, C. L. Moreira, and A. G. Madureira, "Defining Control Strategies for MicroGrids Islanded Operation", *IEEE Transactions on Power Systems*, vol.21, no.2, pp. 916-924, 2006.

[3] D. Pudjianto, C. Ramsay, and G. Strbac, "Virtual power plant and system integration of distributed energy resources," in *Renewable Power Generation IET*, vol.1, no.1, pp.10-16, 2007.

[4] Md R. Islam, and A. Gabbar Hossam, "Study of microgrid safety and protection strategies with control system infrastructures," *Smart Grid and Renewable Energy*, vol.3, no.1, pp.1-9, 2012.

[5] P. Piagi, and R. H. Lasseter, "Autonomous Control of Microgrds," in Proc. *IEEE Power Engineering Society General Meeting*, Montreal, June 2006.

[6] F. Katiraei, M. R. Iravani, and P. W. Lehn, "Micro-grid autonomous operation during and subsequent to islanding process," *IEEE Transactions on Power Delivery*, vol.20, no.1, pp.248-257, Jan. 2005.

[7] P. Agrawal, "Overview of DOE Microgrid Activities", Symposium on Microgrid, Montreal, June 23, 2006 [Online]. Available: http://der.lbl.gov/2006microgrids_files/USA/Presentation_7_Part1_Poonum-agrawal.pdf.

[8] M. Shahabi, M. R. Haghifam, M. Mohamadian, and S.A, Nabavi-Niaki, "Dynamic Behavior Improvement in a Microgrid with Multiple DG Units Using a Power Sharing Approach," *IEEE Bucharest Power Tech Conference* , pp.1-8, 2009.

[9] K. D. Brabandere, B. Bolsens, J. V. D Keybus, A Woyte, J Driesen, and R Belmans, "A Voltage and Frequency Droop Control Method for Parallel Inverters," *IEEE Trans. Power Electronics*, vol. 22, pp. 1107 - 1115, 2007.

[10] F. Katiraei, and M. R. Iravani, “Power management strategies for a microgrid with multiple distributed generation units,” *IEEE Trans. Power Syst.*, vol. 21, no. 4, pp. 1821 - 1831, Nov. 2006.

[11] L. Zhang, L. Harnefors, and H. P. Nee, “Power-Synchronization Control of Grid-Connected Voltage-Source Converters,” *IEEE Trans. on Power Systems*, vol. 25, pp. 809 - 820, 2010.

[12] M. C. Chandorkar, D. M. Divan, and R. Adapa, “Control of parallel connected inverters in standalone ac supply systems,” *IEEE Trans. Ind. Appl.*, vol. 29, no. 1, pp. 136 - 143, Jan./Feb. 1993.

[13] R. H. Lasseter, “Control of distributed resources,” in L H. Fink, C.D. Vournas (Eds.), Proceedings: *Bulk Power Systems Dynamics and Control*, *Organized by IREP and National Technical University of Athens*, Santorini, Greece, pp. 323-329, Aug. 1998.

[14] C. K. Sao, and P. W. Lehn, “Autonomous load sharing of voltage source converters,” *IEEE Transactions on Power Delivery,* vol.20, no.2, pp.1009-1016, April 2005.

[15] F. Katiraei, R. Iravani, N. Hatziargyriou, and A. Dimeas, “Microgrids management,” *Power and Energy Magazine, IEEE* , vol.6, no.3, pp.54-65, May-June 2008.

[16] K. De Brabandere, B. Bolsens, J. Van den Keybus, A. Woyte, J. Driesen, and R. Belmans, “A Voltage and Frequency Droop Control Method for Parallel Inverters,” *IEEE Transactions Power Electronics*, vol.22, no.4, pp.1107-1115, July 2007.

[17] J. M. Guerrero, L. Hang, and J. Uceda, “Control of distributed uninterruptible power supply systems,” *IEEE Trans. Ind. Electron.*, vol.55, no.8, pp.2845-2859, Aug.2008.

[18] J. C. Vasquez, J. M. Guerrero, A. Luna, P. Rodríguez, and R. Teodorescu, “Adaptive droop control applied to voltage-source inverters operating in grid-connected and islanded modes,” *IEEE Trans. Ind. Electron.*, vol. 56, no. 10, pp. 4088-4096, Oct. 2009.

[19] R. Majumder, A. Ghosh, G. Ledwich, and F. Zare, “Power Management and Power Flow Control with Back-to-Back Converters in a Utility Connected

Microgrid," *IEEE Transactions on Power System*, vol. 25, no. 2, pp. 821-834, May 2010.

[20] P. Arboleya, D. Diaz, and J. M. Guerrero, "An improved control scheme based in droop characteristic for microgrid converters," in *Proc. Electric power systems research*, pp.1215-1221, 2010.

[21] E. Rokrok, and M. E. H. Golshan, "Adaptive voltage droop scheme for voltage source converters in an islanded multi-bus microgrid," *IET generation, trans. distrib.*, vol.4, no.5, pp.562-578, May.2010.

[22] W. Yao, M. Chen, and J. Matas, "Design and analysis of the droop control method for parallel inverters considering the impact of the complex impedance on the power sharing," *IEEE Trans. Ind. Electron.*, vol.58, no.2, pp576-588, Feb.2011.

[23] J. He, and Y. W. Li, "An Enhanced Microgrid Load Demand Sharing Strategy," *IEEE Transactions on Power Electronics*, vol.27, no.9, pp. 3984-3995, Sept. 2012.

[24] E. Planas, A. G. Muro, J. Andreu, I. Kortabarria, and I. M. Alegria, "General aspects, hierarchical controls and droop methods in microgrids : A review," *Renewable and Sustainable Energy Reviews*, vol. 17, pp. 147–159, January 2013.

[25] C.T. Lee, C. C. Chu, and P. T. Cheng, "A New Droop Control Method for the Autonomous Operation of Distributed Energy Resource Interface Converters," *IEEE Transactions on Power Electronics*, vol.28, no.4, pp.1980-1993, April 2013.

[26] N. Pogaku, M. Prodanovic, and T. C. Green, "Modeling, Analysis and Testing of Autonomous Operation of an Inverter-Based Microgrid," *IEEE Transactions in Power Electronic*, vol.22, no.2, pp.613-625, March 2007.

[27] Y. W. Li, and C. N. Kao, "An accurate power control strategy for power-Electronic-interfaced distributed generation units operating in a low-voltage multibus microgrid," *IEEE Trans. Power Electron.*, vol.24, no.12, pp.2977-2988, Dec.2009.

[28] R. Majumder, B. Chaudhuri, A.Ghosh, R. Majumder, G. Ledwich, and F. Zare, "Improvement of Stability and Load Sharing in an Autonomous Microgrid Using Supplementary Droop Control Loop," *IEEE Transactions on Power Systems*, vol.25, no.2, pp.796 -808, May 2010.

[29] R. Majumder, A. Ghosh, G. Ledwich, and F. Zare, "Angle droop versus frequency droop in a voltage source converter based autonomous microgrid," in *Power and Energy Society General Meeting, IEEE*, pp. 1-8, July-2009.

[30] R. Majumder, F. Shahnia, A. Ghosh, G. Ledwich, M. Wishart, and F. Zare, "Operation and Control of a Microgrid Containing Inertial and Non-Inertial Micro Sources," in *TENCON IEEE Region 10 Conference*, pp. 1-6, 2009.

[31] Alfred Engler, and Nikos Soultanis, "Droop control in LV-Grids," in *International Conference on Future Power System*, pp. 1-6, 2005.

[32] H. Gu, X. Guo, and W. Wu, "Accurate Power Sharing Control for Inverter-Dominated Autonomous Microgrid," in *International Conference on Power Electronics and Motion Control Conference (IPEMC)*, pp.368-372 , 2012.

[33] T. L. Vandoorn, B. Meersman, and J. De Kooning, "Automatic power sharing modification of P/V droop controllers in low-voltage resistive microgrids," *IEEE Trans. Power Del.*, vol.27, no.4, pp.2318-2325, Oct. 2012.

[34] Q. Zhong, "Robust Droop Controller for Accurate Proportional Load Sharing among Inverters Operated in Parallel," *IEEE Transactions on Industrial Electronics*, pp. 1-10, 2011.

[35] R. Majumder, G. Ledwich, A. Ghosh, S. Chakrabarti, and F. Zare,"Droop Control of Converter-Interfaced Microsources in Rural Distributed Generation," *IEEE Transactions on Power Delivery*, vol. 25, no.4, pp. 2768-2778, 2010.

[36] R. Hunter, and G. Elliot, *Wind-Diesel Systems, A Guide to the Technology and its Implementation*. Cambridge, U.K.: Cambridge Univ. Press, 2005.

[37] S. Hier, *Grid Integration of Wind Energy Conversion Systems*, John Wiley and sons, June 2014.

[38] C. Abbey, F. Katiraei, C. Brothers, L. B. Dignard, and G. Joos, "Integration of distributed generation and wind energy in Canada," *IEEE, Power Engineering Society General Meeting*, 2006.

[39] N.H. Lipman, "Overview of wind/diesel systems" *Renewable Energy* vol.5, no.1, pp.595-617, August 1994.

[40] F. Katiraei, C. Abbey, "Diesel Plant Sizing and Performance Analysis of a Remote Wind-Diesel Microgrid," *IEEE, Power Engineering Society General Meeting*, pp.1-8, June 2007.

[41] M. Fazeli, G. M. Asher, C. Klumpner, Y. Liangzhong, and M. Bazargan, "Novel Integration of Wind Generator-Energy Storage Systems Within Microgrids," *IEEE Transactions on Smart Grid*, vol.3, no.2, pp.728-737, June 2012.

[42] I. D. Margaris, S. A. Papathanassiou, N. D. Hatziargyriou, A.D. Hansen, and P. Sorensen, "Frequency Control in Autonomous Power Systems With High Wind Power Penetration," *IEEE Transactions on Sustainable Energy*, vol.3, no.2, pp.189-199, April 2012.

[43] A. Mohd, E. Ortjohann, W. Sinsukthavorn, M. Lingemann, N. Hamsic, and D. Morton, "Isochronous load sharing and control for inverter-based distributed generation," *International Conference on Clean Electrical Power*, pp.324-329, June 2009.

[44] K. J Bunker, and W. W. Weaver, "Microgrid frequency regulation using wind turbine controls," *Power and Energy Conference at Illinois (PECI)*, pp.1-6, Feb.-Mar. 2014.

[45] K. Strunz, E. Abbasi, and D. Nguyen Huu, "DC Microgrid for Wind and Solar Power Integration," *IEEE Journal of Emerging and Selected Topics in Power Electronics*, vol.2, no.1, pp.115-126, March 2014.

[46] K. M. Abo-Al-Ez, X. Xia, and J. Zhang, "Smart interconnection of a PV/wind DG micro grid with the utility distribution network," *Industrial and Commercial Use of Energy Conference (ICUE)*, pp.1-8, Aug. 2012.

[47] W. Shouxiang, L. Zhixin, W. Lei, M. Shahidehpour, and L. Zuyi, "New Metrics for Assessing the Reliability and Economics of Microgrids in Distribution System," *IEEE Transactions on Power Systems*, vol.28, no.3, pp.2852-2861, Aug. 2013.

[48] R. Karki, and R. Billinton, "Reliability/cost implications of PV and wind energy utilization in small isolated power systems,"IEEE Trans Energy Convers., vol. 16, no. 4, pp. 368–373, Dec. 2001.

[49] R. Yokoyama, T. Niimura, and N. Saito, "Modeling and evaluation of supply reliability of microgrids including PV and wind power," *in Proc. IEEE Power and Energy Soc. General Meeting—Conversion and Delivery of Elect. Energy in the 21st Century*, pp. 1–5, 2008.

[50] Y. M. Atwa, and E. F. El-Saadany, "Reliability evaluation for distribution system with renewable distributed generation during islanded mode of operation," *IEEE Trans. Power Syst.*, vol. 24, no. 2, pp. 572–581, May 2009.

[51] K. Moslehi, and R. Kumar, "A reliability perspective of the smart grid," *IEEE Trans. Smart Grid,* vol.1, no.1, pp.57-64, Jun.2010.

[52] R. Karki, R. Billinton, and A. K. Verma, *Reliability Modeling and Analysis of Smart Power Systems,* Springer New Delhi Heidelberg New York Dordrecht London, pp. 33-66, 2014.

[53] S. Chowdhury, S. P. Chowdhury, and P. Crossley, *Microgrids and Active Distribution Networks,* UK: Institution of Engineering and Technology, pp. 57-76, 2009.

[54] H. Chen, T. N. Cong, W. Yang, C. Tan Y. Li, and Y. Ding, "Progress in electrical energy storage system: A critical review," *Progress in Natural Science, Elsevier,* vol. 19, issue 3, pp. 291-312, March 2009.

[55] W. Cox, Considine, and E. G. Cazalet, "Understanding Microgrids as the Essential Architecture of Smart Energy," *Grid Inerop Forum, Texas*, Dec. 2012.

[56] B. Kroposki, R. Lasseter, T. Ise, S. Morozumi, S. Papatlianassiou, and N. Hatziargyriou, "Making microgrids work," *Power and Energy Magazine, IEEE* , vol.6, no.3, pp. 40-53, May-June 2008.

[57] M. Moorthi, "lithium titanate based batteries for high rate and high cycle life application," *NEI* Corporation. Web http://neicorporation.com/.

[58] R. Lasseter, and M. Erickson, "Integration of Battery-Based Energy Storage Element in the CERTs Microgrid," University of Wisconsin, Madison, Tech. Rep., Oct. 2009.

[59] A. Nanotechnologies Inc., "Application for advanced Batteries in Microgrid Environments," Altair Nanotechnologies Inc., December 2012.

[60] Z. Haihua, T. Bhattacharya, T. Duong, T.S.T. Siew, and A.M. Khambadkone, "Composite Energy Storage System Involving Battery and Ultracapacitor With Dynamic Energy Management in Microgrid Applications," *IEEE Transactions on Power Electronics, ,* vol.26, no.3, pp.923-930, March 2011.

[61] Z. Jianping, G. Zhenyu, R. Yuliang, D. Xinhui, and Y. Xiaohai, "A economic operation optimization for microgrid with battery storage and load transfer," *Systems and Informatics* (ICSAI), pp.186-191, Nov. 2014.

[62] A. G. Tsikalakis, and N. D. Hatziargyriou, "Centralized control for optimizing microgrids operation," *IEEE Trans. Energy Convers*., vol. 23, no. 1, pp. 241 - 248, Mar. 2008.

[63] S. Adhikari, and Li Fangxing, "Coordinated V-f and P-Q Control of Solar Photovoltaic Generators with MPPT and Battery Storage in Microgrids," *IEEE Transactions on Smart Grid,* vol.5, no.3, pp.1270 - 1281, May 2014.

[64] R. Majumder, A. Ghosh, G. Ledwich, and F. Zare, "Enhancing Stability of an Autonomous Microgrid using a gain Scheduled Angle Droop Controller with Derivative Feedback," in *International Journal of Emerging Electric Power Systems,*vol. 10, no. 5, pp. 1-30, 2009.

[65] L. Xu, and D. Chen, "Control and Operation of a DC Microgrid with Variable Generation and Energy Storage," *IEEE Transactions on Power Delivery,* vol.26, no.4, pp.2513-2522, Oct. 2011.

[66] L. Che, M. Khodayar, and M. Shahidehpour, "Only Connect," *Power and Energy Magazine, IEEE,* pp. 70-81, Jan. - Feb. 2014.

[67] A. Bidram, and A. Davoudi, "Hierarchical Structure of Microgrids Control System," *IEEE Transactions* in *Smart Grid,* , vol.3, no.4, pp.1963-1976, Dec. 2012.

[68] N.D. Hatziargyriou, A. Dimeas, A.G. Tsikalakis, J.A.P. Lopes, G. Karniotakis, and J.Oyarzabal, "Management of microgrids in market environment," *International Conference on Future Power Systems,* pp.7-13, Nov. 2005.

[69] A.G. Madureira, J.C. Pereira, N.J. Gil, J.A. Pecas Lopes, G.N. Korres, and N.D. Hatziargyriou, "Advanced control and management functionalities for multi-microgrids," *EUROPEAN Transactions on Electrical Power,* pp.1159-1177, January 2010.

[70] J. M. Guerrero, F. Blaabjerg, T. Zhelev et al, "Distributed generation: toward a new energy paradigm," *IEEE Industrial Electronics Magazine*, pp. 52-64, March 2010.

[71] I. U. Nutkani, P. C. Loh, and F. Blaabjerg, "Power flow control of intertied ac microgrids," *Power Electronics, IET,* vol. 6, no.7, pp. 1329–1338, August 2013.

[72] I. U. Nutkani, P. C. Loh, and F. Blaabjerg, "Distributed Operation of Interlinked AC Microgrids with Dynamic Active and Reactive Power Tuning,"

IEEE Transaction on Industry Applications, vol. 49, no.5, pp. 2188–2196, Sept.-Oct. 2013.

[73] I. U. Nutkani, P. C. Loh, P. Wang, t. K. Jet, and F. Blaabjerg, "Intertied ac-ac microgrids with autonomous power import and export," *International Journal of Electrical Power and Energy systems*, vol. 65, no.7, pp. 385–393, Feb. 2015.

[74] L. Xiong, W. Peng, and P.C. Loh, "A hybrid AC/DC microgrid and its coordination control," *IEEE Trans Smart Grid*, vol. 2, no.2, pp.278–86, 2011.

[75] S. Bala, *Integration of Single-phase Microgrids*. PhD thesis, University of Wisconsin-Madison, 2008.

[76] S. Bala, and G. Venkataramanan, "Autonomous power electronic interfaces between microgrids," *IEEE Energy Conversion Congress and Exposition,* pp.3006-3013, 20-24 Sept. 2009.

[77] E. J. Ng, and R. A. El-Shatshat, "Multi-microgrid control systems (MMCS)," *IEEE Power and Energy Society General Meeting,* pp.1-6, 25-29 July 2010.

[78] A. Kargarian, B. Falahati, F. Yong, and M. Baradar, "Multiobjective optimal power flow algorithm to enhance multi-microgrids performance incorporating IPFC," *IEEE Power and Energy Society General Meeting*, pp.1-6, 22-26 July 2012.

[79] S. Shi, Y. Yan, J. Ming, W. Qianggang, and Z. Niancheng, "Hierarchical coordination control of multi-microgrids system in series and parallel structure," *China International Conference on Electricity Distribution (CICED)*, pp.1-5, 10-14 Sept. 2012.

[80] D. Moore, and D. McDonnell, "Smart grid vision meets distribution utility reality," Elect. Light Power pp. 1-6, Mar. 2007.

[81] H. Farhangi, "The Path of the Smart Grid," *IEEE Power & Energy magazine*, vol.8, no.1, pp. 18-28, Jan.-Feb. 2010.

[82] M. Smith, "Overview of federal R&D on microgrid technologies," in Proc. Kythonos 2008 Symp. Microgrids, June 2, pp. 2–8, 2008.

[83] J. A. Aguado, and V. H. Quintana, "Inter-utilities power-exchange coordination: a market-oriented approach," *IEEE Transactions on Power Systems*, vol.16, no.3, pp. 513-519, Aug 2001.

[84] G. Fahd, and G. B. Sheble, "Optimal power flow emulation of interchange brokerage systems using linear programming," *IEEE Transactions on Power Systems*, vol.7, no.2, pp.497-504, May 1992.

[85] E. Ortjohann, P. Wirasanti, M. Lingemann, W. Sinsukthavorn, S. Jaloudi, and D. Morton, "Multi-level hierarchical control strategy for smart grid using clustering concept," *International Conference on Clean Electrical Power (ICCEP),* pp.648-653, 14-16 June 2011.

[86] J. Wu, and X. Guan, "Coordinated Multi-Microgrids Optimal Control Algorithm for Smart Distribution Management System," *IEEE Transactions on Smart Grid,* vol.4, no.4, pp. 2174-2181, Dec. 2013.

[87] Yu Xunwei, Jiang Zhenhua, and A. Abbasi, "Dynamic modeling and control design of microturbine distributed generation systems," *IEEE International Electric Machines and Drives Conference, IEMDC '09*, pp.1239-1243, May 2009.

[88] S. Krishnamurthy, T. M. Jahns, and R. H. Lasseter, "The operation of diesel gensets in a CERTS microgrid," *Proc. IEEE Power and Energy Society General Meeting Conversion and Delivery of Electrical Energy* in the 21st Century, pp. 1-8, 2008.

[89] A. R. Bergen, *Power system analysis*, Prentice-Hall, New Jersey, 1986 ISBN: 0136878644.

[90] M. G. Simões, B. Palle, S. Chakraborty, and C. Uriarte, "Electrical Model Development and Validation for Distributed Resources," *NREL/SR*-581-41109, 2007.

[91] P. M. Anderson, and A. A. Fouad, *Power System Control and Stability*, 1st ed., Iowa State University Press, 1977, ISBN: 0813812453.

[92] P. Kundur, *Power System Stability and Control*, McGraw-Hill, New York, 1994.

[93] IEEE Std 421.5 - 2005, *IEEE Recommended Practice for Excitation System Models for Power System Stability Studies*, 2006.

[94] H. Yasin, A. A. EI-Zeftawy, M. N. Serag, and A. A. Gado, "Design of a controller for operating Diesel Generator to supply isolated loads," *Power Systems Conference, MEPCON* Eleventh International Middle East, pp.487-491, Dec. 2006.

[95] D. N. Gaonkara, and R. N. Patel, "Modeling and simulation of microturbine based distributed generation system," *IEEE Power India Conference,* pp.1-5, 2006.

[96] R. H. Lasseter, "Dynamic models for micro-turbines and fuel cells," *Power Engineering Society Summer Meeting*, vol.2, pp. 761-766, 2001.

[97] S. R. Guda, C. Wang, and M. H. Nehrir, "A Simulink-based microturbine model for distributed generation studies," *Power Symposium, Proceedings of the 37th Annual North American* , pp.269-274, Oct. 2005.

[98] Li Gang, Li Gengyin, Wei Yue, Ming Zhou, and K. L. Lo, "Modeling and simulation of a microturbine generation system based on PSCAD/EMTDC," *5th International Conference on Critical Infrastructure (CRIS)*, pp.1-6, Sept. 2010.

[99] A. K. Saha, S. Chowdhury, S. P. Chowdhury, and P. A. Crossley, "Modelling and simulation of microturbine in islanded and grid-connected mode as distributed energy resource," *Power and Energy Society General Meeting - Conversion and Delivery of Electrical Energy in the 21st Century, IEEE* , pp.1-7, July 2008.

[100] G. J. Kish, and P. W. Lehn, "A micro-turbine model for system studies incorporating validated thermodynamic data," *IEEE Power and Energy Society General Meeting*, Detroit, July 2011.

[101] T. L. Vandoorn, B. Meersman, J. D. M. De Kooning, and L. Vandevelde, "Analogy Between Conventional Grid Control and Islanded Microgrid Control Based on a Global DC-Link Voltage Droop," *IEEE Transactions on Power Delivery, ,* vol.27, no.3, pp.1405–1414, July 2012.

[102] D. J. Glover, S. M Sarma, and J. T. Overbye, *Power System Analysis and Design*, Cengage Learning, Stamford, CT, USA, 2012.

[103] Jinwei He, and Yun Wei Li, "An enhanced microgrid load demand sharing strategy," *IEEE Trans. Power Electronics*, vol. 27, no. 9, pp. 3987–3995, Sep. 2012.

[104] A. Bidram, and A. Davoudi, "Hierarchical Structure of Microgrids Control System," *IEEE Trans. on Smart Grid*, pp. 1-14, May 2012.

[105] J. M. Guerrero, N. Berbel, L.G. de Vicuna, J. Matas, J. Miret, and M. Castilla, "Droop control method for the parallel operation of online uninterruptible power systems using resistive output impedance," *Twenty-First Annual IEEE Applied Power Electronics Conference and Exposition*, pp. 1716 - 1722, March 2006.

[106] R. Majumder, A. Ghosh, G. Ledwich, and F. Zare, "Operation and control of hybrid microgrid with angle droop controller," *TENCON IEEE Region 10 Conference*, pp.509-515, Nov. 2010.

[107] M. Dewadasa, A. Ghosh, and G. Ledwich, "Dynamic response of distributed generators in a hybrid microgrid," *Power and Energy Society General Meeting, IEEE*, pp.1-8, July 2011.

[108] M. R. Patel, *Wind and Solar Power Systems*, USA: CRC Press, 1999, pp. 124-130.

[109] A. A. Jadallah, D. Y. Mahmood, and Z. A. Abdulqader, "Optimal performance of horizontal axis wind turbine for low wind speed regime," *International Journal of Multidisciplinary and Current Research*, vol.2, pp. 159-164, 2014.

[110] K. Kurohane, T. Senjyu, A. Yona, N. Urasaki, T. Goya, and T. Funabashi, "A hybrid smart AC/DC power system," *IEEE Trans. Smart Grid*, vol. 1, no. 2, pp. 199-204, 2010.

[111] A.Keyhani, M.N. Marwali, and M. Dai, *Integration of Green and Renewable Energy in Electric Power Systems*, John Wiley & Sons, USA, 2010, pp.1-2.

[112] B. Wu, Y. Lang, N. Zargari and S. Kouro, *Power Conversion and Control of Wind Energy Systems*, *IEEE* John Wiley and sons, 2011.

[113] W. V. Lyon, "*Transient analysis of alternating-current machinery*," John Wiley, USA, 1954.

[114] A. Elmitwally, and M. Rashed, "Flexible Operation Strategy for an Isolated PV-Diesel Microgrid without Energy Storage," *IEEE Transactions on Energy Conversion*, vol.26, no.1, pp.235-244, March 2011.

[115] K. Yukita, K. Ichiyanagi, Y. Goto, and K. Hirose, "A Study of Electric Power Quality using Storage System in Distributed Generation," 9th International Conference on Electrical Power Quality and Utilization, pp. 1–4, Oct. 2007.

[116] A. Tuladhar, H. Jin, T. Unger, and K. Mauch, "Control of parallel inverters in distributed AC power systems with consideration of line impedance effect," *IEEE Transactions on Industry Applications*, vol.36, no.1, pp.131-138, Jan/Feb 2000.

[117] U. Borup, F. Blaabjerg, and P. N. Enjeti, "Sharing of nonlinear load in parallel-connected three-phase converters," *IEEE Transactions on Industry Applications*, vol.37, no.6, pp.1817-1823, Nov/Dec 2001.

[118] A. H. Samra, and K. M. Islam, “Harmonic effects on synchronous generators voltage regulation,” *IEEE Southeastcon '95. Visualize the Future*, pp.376-380, Mar 1995.

[119] W. Jin-quan, S. Peng-chao, C. Chen-hua, L. Jian-ke, and Y. Tao, “Analysis of Operation of Synchronous Generator under the Distortion of Harmonic Current,” *Asia-Pacific Power and Energy Engineering Conference (APPEEC)*, pp.1-4, March 2012.

[120] M. W. Davis, R Broadwater, and J. Hambric, “Modeling and Testing of Unbalanced Loading and Voltage Regulation,” *NREL* report number NREL/SR-581-41805, July, 2007.

[121] A. Ghosh, and G. Ledwich, “Stability of hysteretic controlled voltage source converters in a power system,” *IEEE PES Innovative Smart Grid Technologies Asia (ISGT)*, pp.1-8, Nov. 2011.

[122] A. Ghosh, and G. Ledwich, “Load compensating DSTATCOM in weak AC Systems,” *IEEE Trans. on Power Delivery*, vol. 18, pp. 1302-1309, Oct. 2003.

[123] Q. Sun, J. Zhou, J.M. Guerrero, and H. Zhang, “Hybrid Three-Phase/Single-Phase Microgrid Architecture with Power Management Capabilities,” *IEEE Transaction on Power Electronics*, vol. 30, no. 10, pp. 5964-5977, 2015.

[124] A. Ghosh, “Performance study of two different compensating devices in a custom power park,” *Proc. IEE – Generation, Transmission & Distribution*, vol. 152, no. 4, pp. 521-528, 2005.

[125] A. Ghosh, A.K. Jindal, and A. Joshi, “Inverter control using output feedback for power compensating devices,” *TENCON Conference on Convergent Technologies for the Asia-Pacific Region*, pp.48-52, Oct. 2003.